

8-2021

Electrical Characterization of Conductive Concrete Containing Graphite Powder

K. I. M. Iqbal

The University of Texas Rio Grande Valley

Follow this and additional works at: <https://scholarworks.utrgv.edu/etd>



Part of the [Civil and Environmental Engineering Commons](#)

Recommended Citation

Iqbal, K. I. M., "Electrical Characterization of Conductive Concrete Containing Graphite Powder" (2021). *Theses and Dissertations*. 895.

<https://scholarworks.utrgv.edu/etd/895>

This Thesis is brought to you for free and open access by ScholarWorks @ UTRGV. It has been accepted for inclusion in Theses and Dissertations by an authorized administrator of ScholarWorks @ UTRGV. For more information, please contact justin.white@utrgv.edu, william.flores01@utrgv.edu.

ELECTRICAL CHARACTERIZATION OF CONDUCTIVE CONCRETE CONTAINING
GRAPHITE POWDER

A Thesis

by

K I M IQBAL

Submitted to the Graduate College of
The University of Texas Rio Grande Valley
In partial fulfillment of the requirements for the degree of

MASTER OF SCIENCE

August 2021

Major Subject: Civil Engineering

ELECTRICAL CHARACTERIZATION OF CONDUCTIVE CONCRETE CONTAINING
GRAPHITE POWDER

A Thesis
by
K I M IQBAL

COMMITTEE MEMBERS

Dr. Philip Park
Chair of Committee

Dr. Jong-min Kim
Committee Member

Dr. Thang Pham
Committee Member

August 2021

Copyright 2021 K I M Iqbal

All Rights Reserved

ABSTRACT

Iqbal, K. I. M., Electrical Characterization of Conductive Concrete Containing Graphite Powder.

Master of Science (MS), August, 2021, 118 pp., 13 tables, 67 figures, 150 references.

Electrically conductive concrete has various potential non-structural functions such as self-sensing, de-icing, and electromagnetic shielding. Since conductive concrete is a composite containing moisture and discrete conductive additives, its electrical properties are very complex. Understanding these properties is the fundamental requirement for developing its non-structural applications. In this research, graphite powder is used as a conductive additive with varying percentages (0% to 30%) by cement paste volume. Both AC impedance analysis and DC measurement are performed in both wet and dry conditions. The results show that the resistivity measured by DC are not consistent because of polarization before/during the measurement. On the other hand, the AC measurements yield consistent results. The resistivity of concrete is lower in wet conditions than in dry conditions. The AC impedance spectroscopy shows that conductive concrete behaves like a circuit made of resistor and capacitor, and the capacitance causes polarization. Various impedance circuits were tested, and the best equivalent circuits for the conductive concrete in dry and wet conditions were proposed based on the simulation results.

DEDICATION

I want to dedicate this thesis to my siblings, especially to my elder brother “Mr. Arman Hossain” who played a significant role throughout my educational career, to my lovely wife “Sharmin Ferdous Emu” whose unconditional love and continuous support helped me completing my Master’s studies smoothly, and to my Supervisor “Dr. Philip Park” for his directions and guidance during my graduate studies at the University of Texas Rio Grande Valley.

ACKNOWLEDGMENTS

I will always remain grateful to Dr. Philip Park for his continuous support, directions, suggestions, and advice throughout my graduate studies. Without his guidance, it wouldn't have been possible for me to finish the research work. I would like to express my sincere gratitude to my thesis committee members Dr. Jong-min Kim and Dr. Thang Pham. The research presented in this thesis was supported by the Department of Civil Engineering and the Graduate College at the University of Texas Rio Grande Valley. Any opinions, findings, conclusions, and recommendations expressed in this paper are those of the authors alone and do not necessarily reflect the views of the sponsoring agencies. The authors acknowledge the contribution provided by Dr. Younho Rew to find an equivalent circuit, Dr. Nazmul Islam for providing AC Impedance devices to continue the research work, and Dr. Paul Y. Choi for his expert opinions throughout the research. The authors also acknowledge Mr. Ryan Weir and Mr. Albert V. Tamashausky at Asbury Carbons Inc. for their material support.

TABLE OF CONTENTS

	Page
ABSTRACT.....	iii
DEDICATION.....	iv
ACKNOWLEDGMENTS.....	v
TABLE OF CONTENTS.....	vi
LIST OF TABLES.....	x
LIST OF FIGURES.....	xii
CHAPTER I. INTRODUCTION.....	1
1.1 Background.....	1
1.2 Objective.....	3
1.3 Methodology.....	4
1.4 Thesis Outlines.....	4
CHAPTER II. LITERATURE REVIEW.....	6
2.1 Introduction.....	6
2.2 Cementitious Materials: From structural to smart applications	6
2.3 Percolation Threshold and Piezoresistivity.....	8

2.4 Imparting conductive additives in concrete and its Application.....	13
CHAPTER III. MATERIALS AND EXPERIMENTAL METHODS.....	19
3.1 Raw Materials.....	19
3.2 Specimen Preparation.....	19
3.3 Electrical Property Measurements and Data Processing	20
CHAPTER IV. INVESTIGATION ON ELECTRICAL PROPERTIES MEASUREMENT	
METHODS.....	26
4.1 Introduction.....	26
4.2 Static/DC Resistivity Measurement.....	28
4.2.1 Continuous Monitoring	28
4.2.2 Discontinuous Measurements.....	33
4.2.3 Effect of Voltage on Static/DC Resistivity.....	34
4.2.4 Summary of Static/DC Measurements.....	36
4.3 AC Impedance Measurement	37
4.3.1 Impedance Spectroscopy Preliminary	37
4.3.2 Impedance Analysis of Conductive Cement Paste.....	39
4.3.3 Repeatability in Measurements and Homogeneity of Mixture observation	
through Impedance Analysis.....	41
4.3.4 Summary of AC Impedance Measurements.....	45
4.4 Conclusion.....	46

CHAPTER V. ELECTRICAL CHARACTERIZATION AND DEGREES OF

SATURATION EFFECTS48

5.1 Introduction48

5.2 Investigating the Effect of Graphite Content50

 5.2.1 Graphite Effects on Dry Specimens51

 5.2.2 Graphite Effects on Wet Specimens55

 5.2.3 Summary of the Effect of Graphite Content.....57

5.3 Determining the Percolation Threshold of Graphite Powder.....58

5.4 Investigating the Effect of Moisture and Degree of Saturation.....60

 5.4.1 Effect of Moisture..61

 5.4.2 Investigating the Effect of Degree of Saturation.....61

 5.4.2.1 Investigating DOS effect through AC Impedance Measurement.....63

 5.4.2.2 Investigating DOS effects through DC Measurements.....67

 5.4.3 Summary of the effect of moisture on Electrical Properties of conductive
 concrete.....69

5.5 Conclusion.....69

CHAPTER VI. ELECTRICAL EQUIVALENT CIRCUIT OF CONDUCTIVE

CONCRETE71

6.1 Introduction.....71

6.2 Fundamental Background on Electrical Equivalent Circuit	72
6.2.1 Resistor	72
6.2.2 Capacitor	73
6.2.3 Simple R-C Circuits.....	74
6.2.4 Simplified Randle Circuit.....	76
6.2.5 Constant Phase Element.....	77
6.2.6 Electrical Equivalent Circuit Models proposed by other Researchers	79
6.3 Electrical Equivalent Circuit for Dry Specimens	84
6.4 Electrical Equivalent Circuit for Wet Specimens	89
6.5 Conclusion.....	100
CHAPTER VII. CONCLUSION AND FUTURE WORK.....	101
7.1 Conclusion.....	101
7.2 Recommendation for Future Work	104
REFERENCES.....	105
BIOGRAPHICAL SKETCH.....	118

LIST OF TABLES

	Page
Table 3.1: Physical Properties of Natural Flake type Graphite Powder (Asbury Carbons Inc.....	19
Table 3.2: Summary of the Specimen used in the experimental program.....	21
Table 3.3: Properties of Electrodes materials.....	23
Table 4.1: Error range for Specimen with Different AC Measurements Trials and Observing the Homogeneity of the mixture (Dry-Impedance)	42
Table 4.2: Error range for Specimen with Different AC Measurements Trials and Observing the Homogeneity of the mixture (Dry-Phase Angle)	43
Table 4.3: Error range for Specimen with Different AC Measurements Trials and Observing the Homogeneity of the mixture (Wet-Impedance)	44
Table 4.4: Error range for Specimen with Different AC Measurements Trials and Observing the Homogeneity of the mixture (Wet-Phase Angle).....	45
Table 5.1: Moisture level and corresponding DOS of Specimens.....	62
Table 6.1: Different Electrical Equivalent Circuit used in other cement-based materials Research.....	80
Table 6.2: Summary of Equivalent Circuit fitting results for Specimens at Dry Conditions.....	88
Table 6.3: Summary of Equivalent Circuit Model-1 and Model-2 fitting results for Specimens at Wet Conditions (fixing components values)	94
Table 6.4: Summary of Equivalent Circuit Model-1 fitting results for Specimens at Wet	

Conditions (without fixing components values)98

Table 6.5: Summary of Equivalent Circuit Model-2 fitting results for Specimens at

Wet Conditions (without fixing components values)99

LIST OF FIGURES

	Page
Figure 2.1: The transition of concrete to multifunctional composites.....	7
Figure 2.2: Electrical resistivity variation with the increase of filler concentration in cement-composite	9
Figure 2.3: Variation of contact electrical resistivity with bond strength at 28 days of curing.....	10
Figure 2.4: Fractional Change in Resistance ($\Delta R/R_0$) vs. compressive strain (a) 28 days of curing (b) 7 days of curing	10
Figure 2.5: Self-sensing comparison of concrete with (a) as received carbon fiber and (b) ozone-treated carbon fiber	11
Figure 2.6: Percolation threshold variation with the length of fiber.....	12
Figure 2.7: Electrical Conductivity vs. Volume fractions of Fiber Content	12
Figure 2.8: Fractional Change in Resistance and Deflection of the specimen under cyclic flexural loading (a) compression side (b) tension side	13

Figure 2.9: Resistance behavior with different deflection levels on concrete specimen	
(a) Compression surface. (b) Tension surface	14
Figure 2.10 SEM photomicrographs illustrating the connection of carbon fibers in	
cement composites (A) $V_f = 1.16\%$, (B) $V_f = 2.21\%$	14
Figure 2.11: Resistivity as a function of the CB volumetric content	15
Figure 2.12: SEM photo of Nickel particle in Cement composite	16
Figure 2.13: Relationship between change in tunneling distance and the fractional change	
in electrical resistivity of NPCC	16
Figure 2.14: The SEM image of treated CNT in composite	17
Figure 2.15: The SEM image of untreated CNT in composite	17
Figure 2.16: Volume resistivity of Carbon nanotube-reinforced composite.....	17
Figure 2.17: The fractional change in resistivity vs. time under cyclic compressive	
loading (0–15 KN)	17
Figure 2.18: SEM image showing the distribution of carbon fibers and graphite particles	18
Figure 2.19: Electrical resistivity change with the graphite content	18
Figure 2.20: The specimen under splitting tensile test	18
Figure 2.21: Results of resistance vs. deformation from the tensile strain stress for the	
specimen with 1.5 vol.%	18

Figure 3.1. Specimen Preparation for Experimental Program: (a) Specimen after applying the conductive silver paste on two opposite sides (b) Attaching copper tape as electrodes(c) Specimen underwater to make it fully saturated (d) Specimen at Oven to make it fully dry (e) Specimen wrapped with plastic foils to control the moisture.22

Figure 3.2: Test Set up for measuring static (DC) resistance through (a) True RMS Digital Multimeter DM-441B (Multimeter-2) (b) Keithley 2400 (C-22) Source Meter (Multimeter-1), and for AC Impedance measurement through (c) Metrohom AUTOLAB PGSTAT302N.....25

Figure 4.1: Static Resistivity measurement of Specimen GP_10 (10%-graphite) through Continuous monitoring for 5 minutes (300 Sec). (a) using Multimeter-1 at 1V in Dry conditions (b) using Multimeter-2 in dry conditions (c) using Multimeter-1 at 1V in wet conditions (d) using Multimeter-2 in wet conditions.....29

Figure 4.2: Static Resistivity measurement of Specimen GP_15 (15%-graphite) through Continuous monitoring for 5 minutes (300 Sec). (a) using Multimeter-1 at 1V in Dry conditions (b) using Multimeter-2 in dry conditions (c) using Multimeter-1 at 1V in wet conditions (d) using Multimeter-2 in wet conditions.....31

Figure 4.3: Static Resistivity measurement of Specimen GP_10 (10%-graphite) through Continuous monitoring for 5 minutes (300 Sec). (a) using Multimeter-1 at 1V in Dry conditions (b) using Multimeter-2 in dry conditions (c) using Multimeter-1 at 1V in wet conditions (d) using Multimeter-2 in wet conditions.....32

Figure 4.4: Static Resistivity measurement of Dry Specimen GP_10 (10%-graphite) ((a) and (d)), GP_15 (15%-graphite) ((b) and (e)), GP_20 (20%-graphite) ((c) and (f)) with

discontinuous monitoring for 2 hrs. at 10 minutes interval. (a), (b), (c) is measured using Multimeter-1 at 1V and (d), (e), (f) is measured using Multimeter-2.....33

Figure 4.5: Static Resistivity measurement of Wet Specimen GP_10 (10%-graphite) ((a) and (d)), GP_15 (15%-graphite) ((b) and (e)), GP_20 (20%-graphite) ((c) and (f)) with discontinuous monitoring for 2 hrs. at 10 minutes interval. (a), (b), (c) is measured using Multimeter-1 at 1V and (d), (e), (f) is measured using Multimeter-2.....34

Figure 4.6: Effect of voltage on continuous static resistivity measurement of conductive cement paste specimen GP_10 (10%-graphite) ((a) and (b)), GP_15 (15%-graphite) ((c) and (d)), GP_20 (20%-graphite) ((e) and (f)). (a), (c), (e) is measured when specimens were at Dry Conditions. (b), (d), (f) is measured when specimens were at Wet Conditions.....36

Figure 4.7: Effect of voltage on discontinuous static resistivity measurement of conductive cement paste specimen GP_10 (1) (a) and GP_10 (2) (b) (10%-graphite) at Dry Conditions.....36

Figure 4.8: (a) Alternating Current (AC) voltage variation with time. (b) A conductive concrete specimen experiencing AC current. (c) A typical Bode plot is showing impedance variation with different AC-frequencies of cement paste. (d) A Typical Nyquist plot shows the variation of real and imaginary impedance....38

Figure 4.9: Impedance responses of Specimen GP_10 (10% graphite by volume of cement paste). Bode plot of Specimen (a) at Dry Conditions and (b) at Wet Conditions. Phase angle variation with AC frequency of Specimen (c) at

Dry Conditions and (d) at Wet Conditions. Nyquist plot of Specimen (e) at Dry Conditions and (f) at Wet Conditions.....	40
Figure 5.1: Impedance variation with AC frequencies of All Specimens at Dry Conditions.....	52
Figure 5.2: Phase angle variation with AC frequencies of All Specimens at Dry Conditions.....	52
Figure 5.3: Nyquist plot showing Real and Imaginary impedance variation of All Specimens at Dry Conditions.....	54
Figure 5.4: Impedance variation with AC frequencies of All Specimens at Dry Conditions.....	55
Figure 5.5: Phase angle variation with AC frequencies of All Specimens at Dry Conditions.....	56
Figure 5.6: Nyquist plot showing Real and Imaginary impedance variation of All Specimens at Dry Conditions.....	57
Figure 5.7: Impedance (Resistivity) variation with graphite content at Dry conditions.....	59
Figure 5.8: Impedance (Resistivity) variation with graphite content at Wet conditions.....	60
Figure 5.9: Bode Plot showing (a) Impedance and (b) Phase Angle variation with different degrees of saturation of Specimen GP_0 (0% graphite).....	63
Figure 5.10: Nyquist Plot showing Imaginary and Real Impedance variation with different degrees of saturation of Specimen GP_0 (0% graphite).....	64
Figure 5.11: (a) Impedance (Bode Plot), (b) Phase Angle, and (c) Imaginary vs. Real Impedance (Nyquist Plot) variation with different degrees of saturation of Specimen GP_15 (15% graphite).....	66
Figure 5.12: (a) Impedance (Bode Plot), (b) Phase Angle, and (c) Imaginary vs. Real Impedance (Nyquist Plot) variation with different degrees of saturation of	

Specimen GP_20 (20% graphite).....	67
Figure 5.13: Static/DC Resistivity variation with different degree of saturation of (a) Specimen GP_0 (0% graphite) (b) Specimen GP_15 (15% graphite) (c) Specimen GP_20 (20% graphite).....	68
Figure 6.1: Three main components of Electrical Equivalent Circuit (a) Resistor (b) Capacitor (c) Inductor.....	72
Figure 6.2: Impedance response of Resistor (100-Ω Resistance) (a) Bode Plot (b) Nyquist Plot.....	73
Figure 6.3: Impedance response of an Ideal Capacitor (a) Bode Plot (b) Nyquist Plot.....	74
Figure 6.4: Series R-C Circuit.....	74
Figure 6.5: Impedance response of a series R-C Circuit (a) Bode Plot (b) Nyquist Plot.....	75
Figure 6.6: Parallel R-C Circuit.....	75
Figure 6.7: Impedance response of a Parallel R-C Circuit (a) Bode Plot (b) Nyquist Plot.....	76
Figure 6.8: A simple Equivalent Circuit/Randle Cell.....	76
Figure 6.9: Typical Nyquist plot of a Randle cell.....	77
Figure 6.10: Influence of CPE in Nyquist Plot.....	78
Figure 6.11: A typical Randle Cell element used to find equivalent circuit for cementitious materials.....	79
Figure 6.12: Proposed Electrical Equivalent Circuit model for conductive cement composite specimens containing graphite powder at dry conditions.....	85
Figure 6.13: Comparison between experimental and equivalent circuit fit of Specimen with 0% graphite at Dry Conditions (a) Bode Plot and Phase Angle (b) Nyquist Plot. (solid lines represent the fitting data and symbols represent the	

experimental data).....	86
Figure 6.14: Comparison between experimental and equivalent circuit fit of Specimen with 10% graphite at Dry Conditions (a) Bode Plot and Phase Angle (b) Nyquist Plot. (solid lines represent the fitting data and symbols represent the experimental data).....	86
Figure 6.15: Comparison between experimental and equivalent circuit fit of Specimen with 15% graphite at Dry Conditions (a) Bode Plot and Phase Angle (b) Nyquist Plot. (solid lines represent the fitting data and symbols represent the experimental data).....	87
Figure 6.16: Comparison between experimental and equivalent circuit fit of Specimen with 20% graphite at Dry Conditions (a) Bode Plot and Phase Angle (b) Nyquist Plot. (solid lines represent the fitting data and symbols represent the experimental data).....	88
Figure 6.17: Electrical Equivalent Circuit model for conductive cement composite specimens containing graphite powder at wet conditions (a) Model-1 (b) Model-2 proposed in this study.....	90
Figure 6.18: Comparison between experimental and equivalent circuit fit of Specimen with 15% graphite at Wet Conditions (fixing dry R_1 , R_2 , Q_2 , R_3 , Q_3 values in the model) (a) Bode Plot (b) Phase Angle (c) Nyquist Plot. (solid lines represent the fitting data and symbols represent the experimental data).....	91
Figure 6.19: Comparison between experimental and equivalent circuit fit of Specimen with 15% graphite at Wet Conditions (without fixing dry R_1 , R_2 , Q_2 , R_3 , Q_3 values in the model) (a) Bode Plot (b) Phase Angle (c) Nyquist Plot.	

(solid lines represent the fitting data and symbols represent the experimental data).....	92
Figure 6.20: Comparison between experimental and equivalent circuit fit of Specimen with 0% graphite at Wet Conditions (without fixing dry R_1 , R_2 , Q_2 , R_3 , Q_3 values in the model) (a) Bode Plot (b) Phase Angle (c) Nyquist Plot.	
(solid lines represent the fitting data and symbols represent the experimental data).....	95
Figure 6.21: Comparison between experimental and equivalent circuit fit of Specimen with 15% graphite at Wet Conditions (without fixing dry R_1 , R_2 , Q_2 , R_3 , Q_3 values in the model) (a) Bode Plot (b) Phase Angle (c) Nyquist Plot.	
(solid lines represent the fitting data and symbols represent the experimental data).....	96
Figure 6.22: Comparison between experimental and equivalent circuit fit of Specimen with 15% graphite at Wet Conditions (without fixing dry R_1 , R_2 , Q_2 , R_3 , Q_3 values in the model) (a) Bode Plot (b) Phase Angle (c) Nyquist Plot.	
(solid lines represent the fitting data and symbols represent the experimental data).....	97

CHAPTER I

INTRODUCTION

1.1 Background

Cement-based concrete is a widely used material in many civil engineering structures for many years. It has been used for different structures such as bridges, highways, buildings, dams, piers, etc. The main function of concrete is to provide enough mechanical abilities to resist forces and transfer the incoming load into a suitable base or ground. Mechanical properties desirable from these materials as structural elements include strength, stiffness, ductility, toughness, capacity for vibration damping, fatigue resistance, creep resistance, and scratch resistance (Chung 2003c).

In addition to these structural properties, it is desirable to have some non-structural functions simultaneously from these materials. These non-structural properties can be achieved if added some additives that can serve both structural functions and some non-structural functions together (Chung 2003c). The materials that served both as structural and non-structural properties simultaneously in a structure are known as multifunctional materials (Chou et al. 2010; Chung 2003c; Ye et al. 2005).

The potential functions of multifunctional concrete include strain sensing, damage sensing, temperature sensing, vibration damping, heating control, electromagnetic shielding ability/ electromagnetic waves reflection and absorption, electrochemical chloride extraction/ corrosion resistance, self-monitoring of freeze-thaw damage, deicing on roads, electrical contacts for

cathodic protection, and thermal insulation capacity (Chen and Chung 1993; Baeza et al. 2010; Chen and Chung 1994; Chen and Chung 1996; Chung 2002c; Chung 2003b; Chung 2004; Pérez et al. 2010; Pu-Woei and Chung 1996; Wen and Chung 2005; Wen and Chung 2006; Wu and Chung 2005; Ye et al. 2005; Zornoza et al. 2010; Baeza et al. 2013; DEL MORAL et al. 2013; Bertolini et al. 2004; Christopher and Sherif 2004; Hou and Chung 1997).

Most of these functions can be enabled when cement-based materials have a certain level of electrical conductivity (Chen and Chung 1995; Chung 2002c; Baeza et al. 2013). The electrical conductivity of cement-based materials has been widely studied because of its numerous applications (Cebeci et al. 2009; Kalaitzidou et al. 2007; Qiu et al. 2007; Sandler et al. 2003; Baeza et al. 2013). Concrete is known to be a nonconductive in dry condition and thermally insulating material. The electrical conductivity of concrete can be enhanced when proper amounts of conductive admixtures were added.

Researchers have studied various additives to improve conductivity of concrete. The most widely used conductive additives include carbon fibers, steel fibers, carbon black, graphite powder, graphene nano-platelets, carbon micro-fiber, nano carbon black, carbon nanotube, carbon nanofibers, etc. (Chen and Chung 1993; Chen and Chung 1995; Wen and Chung 2005; Baeza et al. 2013; Tyson et al. 2011; Kim et al. 2011; Le et al. 2014; Oskouyi et al. 2014). Among these widely used materials, Graphite powder is economically feasible and provides good conductivity in cement concrete.

In this study, flake-type graphite powder (F-516) is used as a conductive additive to investigate the electrical properties of conductive cement paste. The materials will be more conductive when the admixture touches each other to form a continuous conduction path. The volume fraction above which there is a continuous conduction path is known as the percolation

threshold (Chung 2003c). This study will also focus on determining the percolation threshold for graphite powder by volume of cement paste.

The electrical behavior of conductive concrete is very complex. It is challenging to characterize using static resistance measurement since the environmental factors, especially the moisture condition, play a vital role in cementitious concrete. In the presence of a moist condition, the static resistance measurement using direct current (DC) causes electrical polarization, causing variations in measured resistance (Demircilioğlu et al. 2019).

The alternating current (AC) impedance spectroscopy technique is very useful for characterizing complex electrical systems (Gu et al. 1993b; Wen and Chung 2007). It minimizes polarization by alternating current (Wen and Chung 2007) and characterizes the electrical properties with capacitance, inductance, and resistance.

This study will focus on characterizing the electrical properties of conductive cement paste using both DC measurement and AC impedance Spectroscopy. Additionally, an equivalent electrical circuit will be constructed to understand the electrochemical behavior of composite materials.

1.2 Objective

The objective of the research is to investigate the electrical properties of graphite added conductive concrete and characterize its conduction mechanism. Electrical characterization of these multifunctional conductive concrete will be done using the AC impedance spectroscopy.

The specific objectives of the research are:

1. To characterize the electrical properties of conductive concrete using both DC measurement and AC Impedance Spectroscopy under two extreme moisture conditions (fully saturated and completely dry).

2. To investigate the variation of electrical properties with different level of moisture conditions.
3. To determine the percolation threshold for the graphite powder added conductive cement paste.
4. To construct equivalent circuits for both dry and wet conductive concrete.

1.3 Methodology

The research started with a comprehensive literature study related to the electronics, conductive additives, and different applications of conductive concrete. In the second phase of the research, an extensive experimental work was conducted. At first, the cement paste specimens containing the conductive additive (graphite powder) were prepared. After that electrical properties of conductive cement paste were investigated using both DC measurement and AC impedance spectroscopy under the wet and dry condition to assess the moisture effect on the electrical property. Since the differences between two-probe method and four-probe method were almost negligible in the preliminary study, two-probe method was used in this study. Finally, equivalent circuits for both wet and dry specimens were constructed using the measurement results.

1.4 Thesis Outlines

The thesis is divided into seven Chapters. Chapter 1 summarizes the idea of multifunctional concrete, research objectives, and methodology to achieve those objectives. In Chapter 2, a comprehensive literature review including the transition from cementitious materials to smart structures, electrical conduction mechanism, and use of conductive admixture in different research was provided. Chapter 3 introduced experimental program conducted in the research including specimen preparation, testing methods, and equipment.

The findings of the research were described in three following chapters. Chapter 4 discussed electrical properties measurement methods using both DC measurement and AC Impedance Spectroscopy. In Chapter 5 the electrical properties of conductive concrete containing graphite powder were experimentally evaluated. The percolation threshold in using graphite powder were discussed and the effects of moisture were investigated using AC Impedance Spectroscopy. In Chapter 6, electrical equivalent circuit for both dry and wet specimens were proposed and validated by comparing with the experimental data and the simulation results.

The main findings of the research, a brief discussion, and recommendations for future work were summarized in Chapter 7.

CHAPTER II

LITERATURE REVIEW

2.1 Introduction

Concrete is the most widely used construction material, and its primary function is to impart robust mechanical properties to the structure. Although it is poor electrically conductive, adding conductive additives enhances its electrical property, enabling concrete to use other nonstructural functions simultaneously. These materials are multifunctional and can depict structural and nonstructural functions (Ye et al. 2005; Chou et al. 2010; Chung 2003c). Multifunctional concrete reduces the need for some conventional tools such as elastomers for vibration damping, embedded or attached sensors for strain sensing, metal wire mesh for electromagnetic shielding, and foams for thermal insulation, and eventually reducing overall cost (Chung 2003c; Nevers et al. 2011). In this chapter, a brief explanation of recent advances in concrete technology and the transition of traditional concrete to smart concrete materials and its mechanism to evaluate different functions will be discussed.

2.2 Cementitious Materials: From structural to smart applications

Cement is used as a binder in concrete (containing coarse and fine aggregates), cement mortar (containing fine aggregates), or cement paste (containing no aggregate) (Han et al. 2014; Han et al. 2011b; Mehta and Monteiro 2006; Chung 2003c). Concrete is a multi-component material in nature. These components are non-conductive includes cement, water, aggregates,

chemical additives, and mineral additives (Han et al. 2017). Several additives and admixtures have been incorporated in concrete for meeting the requirements of practical applicability, especially for hardening, workability, compressive strength, durability purposes. In recent decades, researchers have been focused on making concrete capable of performing additional functions by adding conductive fibers. This is known as multifunctional cement-based composite and makes concrete smart infrastructure materials (Han et al. 2017). Such functionalities are obtained by adding conductive additives that make the concrete a multiphase material, resulting in functional cement matrixes. In the Figure 2.1, the transition from insulator to conductor of cementitious materials is shown. The distributed filler in the composite form a continuous conductive network that mostly depends on the degree of dispersion of the additives, the volume fractions of fibers, length of fibers, contact electrical resistivity of the interface between the admixture and the cement matrix (Chung 2003c). These continuous functionalized networks allow concrete to perform intrinsically smart properties, including strain and damage sensing and reducing the necessity of extrinsic sensors.

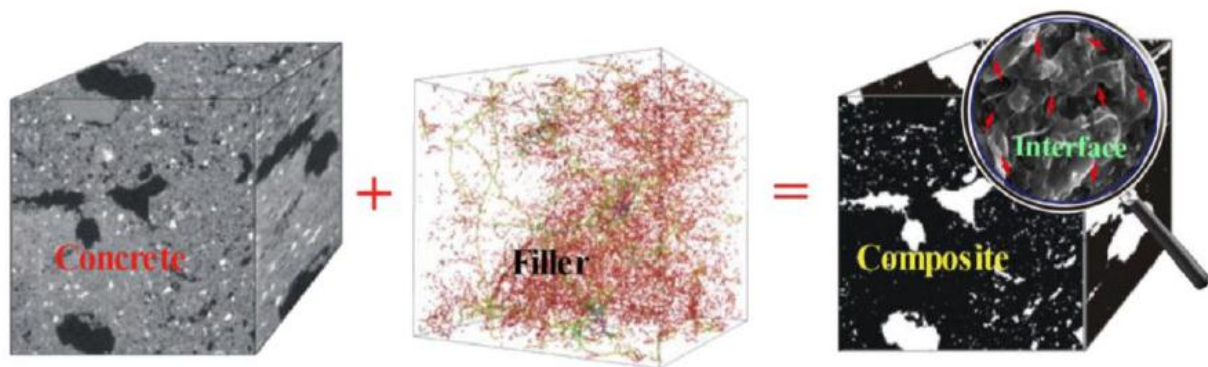


Figure 2.1: The transition of concrete to multifunctional composites (Han et al. 2015).

2.3 Percolation Threshold and Piezoresistivity

Piezoresistivity of a material refers to the ability to change its electrical resistivity when subjected to an external load (Zhu and Chung 2007; Cao et al. 2016). The Gage factor parameter quantifies the piezoresistive material ability, also known as "strain co-efficient" or "strain sensitivity." Stefanescu (2011) defined this parameter by the quotient between the variation of the electrical resistance of a metallic filament and its deformation upon tension/compression along the central axis.

$$GF = \frac{\Delta R \setminus R}{\varepsilon} \quad (1)$$

The cement-based material's resistivity is comparatively higher than any other materials, and it is well known for its insulator behavior. When conductive fillers are added with concrete, it is turned into electrically conductive. The resistivity of conductive composite varies with filler concentration, and the phenomenon is shown in Figure 2.2. The curve is composed of three different sections: the insulation zone (A), the percolation zone (B), the conductive zone (C) (Huang et al. 2008; Al-Saleh and Sundararaj 2009). With the increase of filler concentration, a continuous conductive path is formed in the matrix; hence, electrical resistivity is decreased. The volume fraction above which the admixtures units touch to form a continuous conduction path is known as the percolation threshold (Chung 2003c). It is determined by varying the volume fractions of conductive fillers and observing the variation of electrical resistivity. At the percolation threshold, the electrical conductivity is increased by several orders of magnitude.

This characteristic is explained by the percolation theory (Stauffer and Aharony 1994). It is evident from Figure 2.2 that at a low concentration of fillers, the resistivity is higher. With the increment of filler concentration to the percolation threshold range, the electrical resistivity

decreases. When the fiber concentration is higher than the percolation threshold, the conductivity won't change, but the sensitivity will decrease (Han et al. 2015).

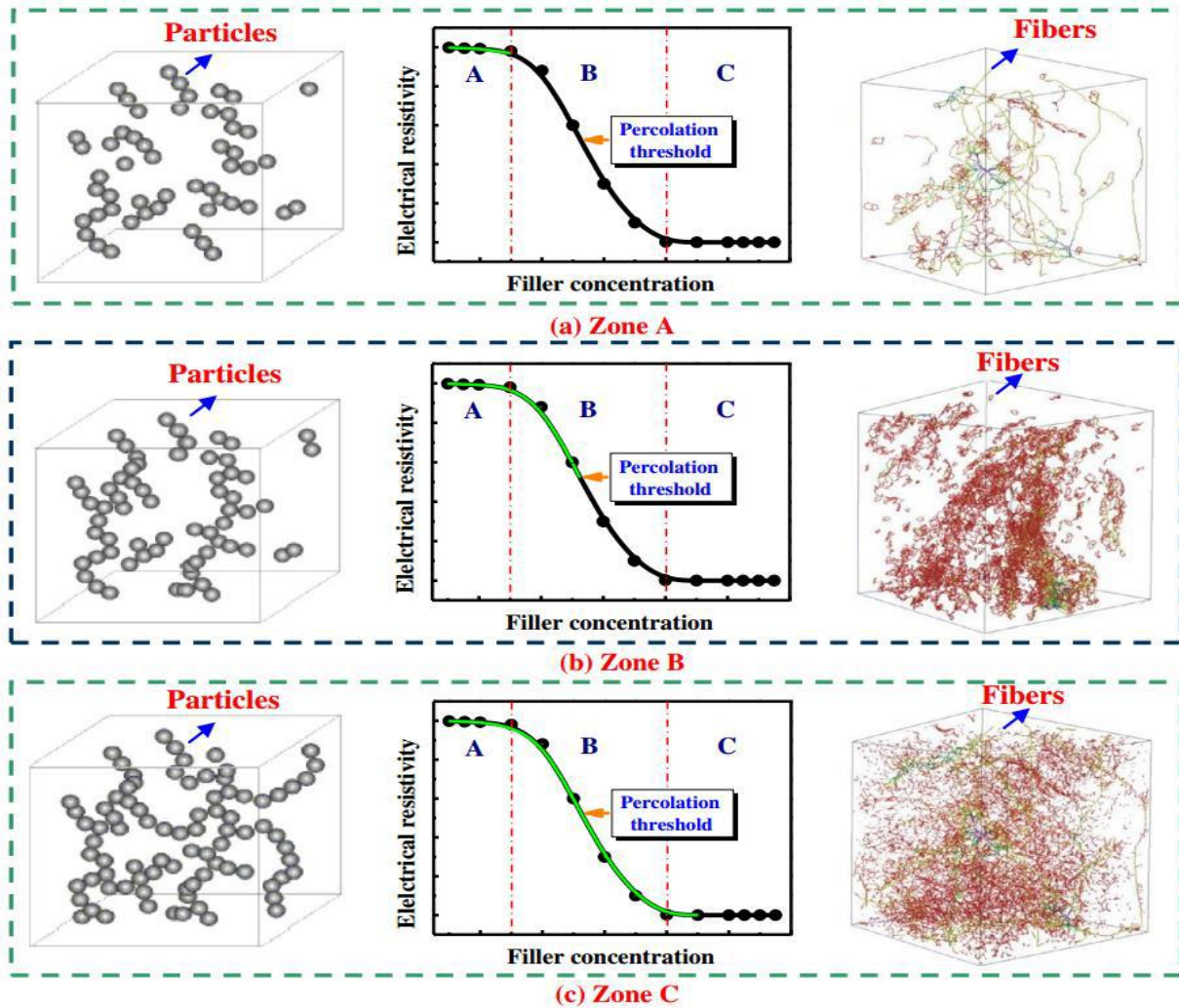


Figure 2.2: Electrical resistivity variation with the increase of filler concentration in cement-composite (Han et al. 2015)

The percolation threshold decreases with the increase of fiber size/aspect ratio and decreases the admixture's unit size (Chung 2003c). Wang et al. (2002) observed that in the case of short carbon fibers in cement, the percolation threshold decreases with fiber length. Several

studies indicated that the piezoresistivity is also dependent on the bond strength of the interface of the matrix, the curing age of the matrix, and the treatment of the fiber contents.

Fu and Chung (1995) observed the contact resistivity between the carbon fiber and cement paste at 28 days of curing using the four-probe method. They found that contact electrical resistivity decrease with increasing bond strength shown in Figure. 04. This study indicated that resistivity was increasing during the fiber pull out, which supports the notion of increasing resistivity during tensile loading. It was also noticed that interfaces between functional additives and concrete matrix affect the electrical contact between them and affect the conductive path and result in a change in conductivity of the composites.

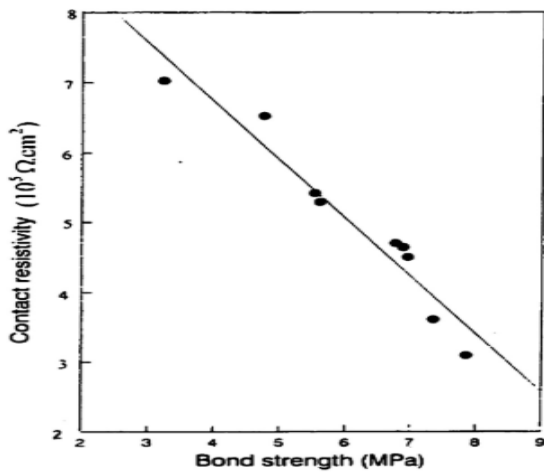


Figure 2.3: Variation of contact electrical resistivity with bond strength at 28 days of curing (Fu and Chung 1995).

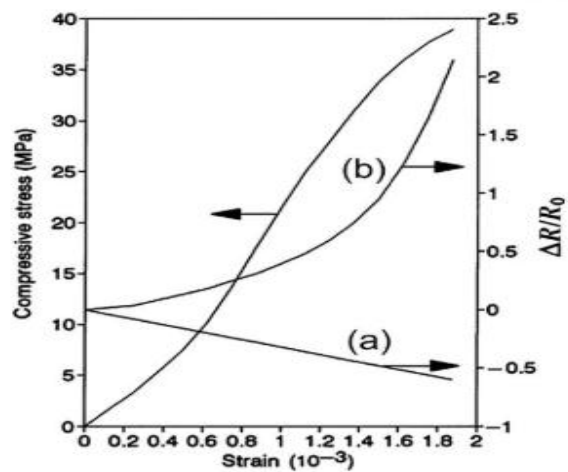


Figure 2.4: Fractional Change in Resistance ($\Delta R/R_0$) vs. compressive strain (a) 28 days of curing (b) 7 days of curing (Fu and Chung 1997)

Fu and Chung (1997) studied the effect of curing age on the piezoresistive behavior of carbon fiber reinforced mortar. The study revealed that during loading at seven days, the

electrical resistivity increased with the increase of compressive load. For loading at 14- and 28-days curing, resistivity decreased (as shown in Figure. 2.4). They attributed this due to the curing effect and the strong bond between the fiber and cement at day seven, and before fiber full-out, weakening of this bond is necessary. In the case of 14- or 28-days curing, the bond is weak, and for this reason, the piezoresistive behavior is quite the opposite.

Fu et al. (1998) enhanced the strain sensing ability by ozone treatment of the fibers and matrix. The electrical resistivity was observed to be repeated in nature and didn't vary with cycling loading (as shown in Figure 2.5).

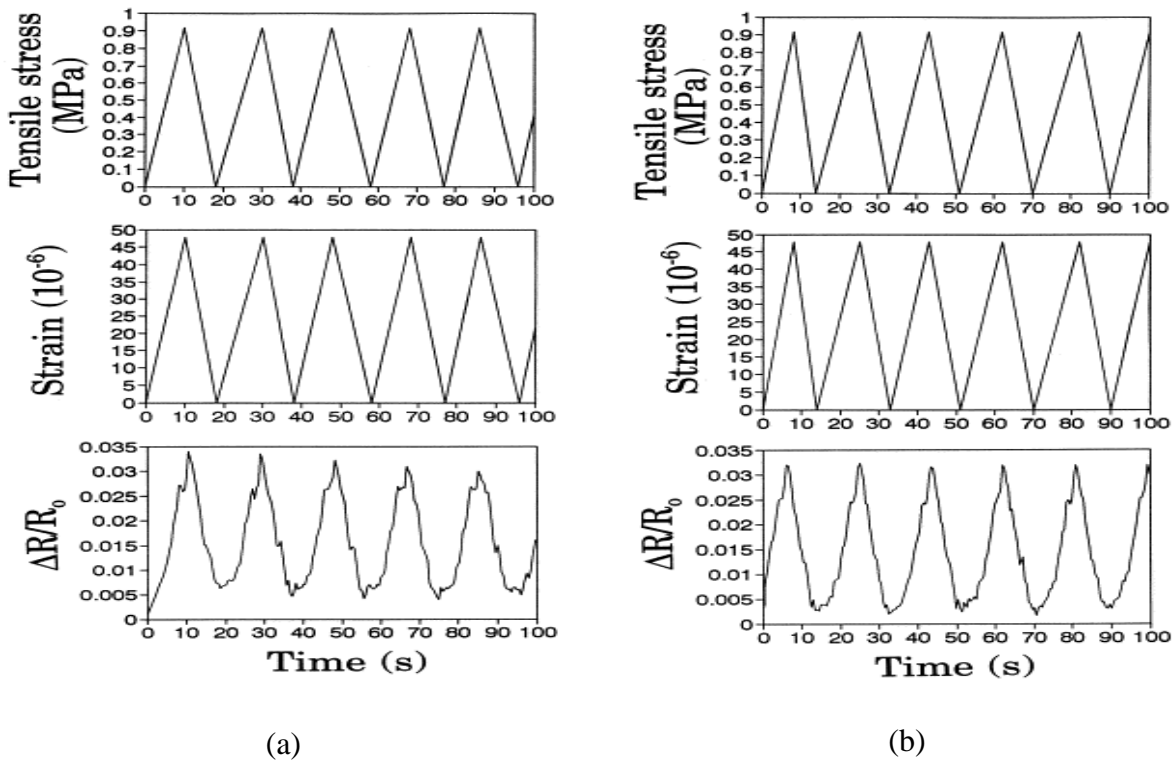


Figure 2.5: Self-sensing comparison of concrete with (a) as received carbon fiber and (b) ozone-treated carbon fiber (Fu et al. 1998).

Low resistivity is desired for piezoresistive analysis, which a higher filler concentration can attain. There is a drawback for higher filler concentration which (Han et al. 2015) stated that

high concentration would increase the cost, and very often, the strength of the composite will decrease. The most suitable way to resolve this discrepancy is to choose a filler concentration near the percolation threshold. For this reason, the percolation threshold is a significant parameter for piezoresistive analysis.

(Wen and Chung 2001a) studied the strain sensing behavior of coated carbon fiber cement on a plain cement specimen. The specimen substrate was 35 mm thick, whereas the coating was 5 mm thick. Rectangular specimens of 160×40×40 mm were tested under 3-point bending, and DC electrical resistivity was measured using the 4-probe method. The result indicated that carbon-fiber-reinforced cement coating could be used for the self-sensing purpose.

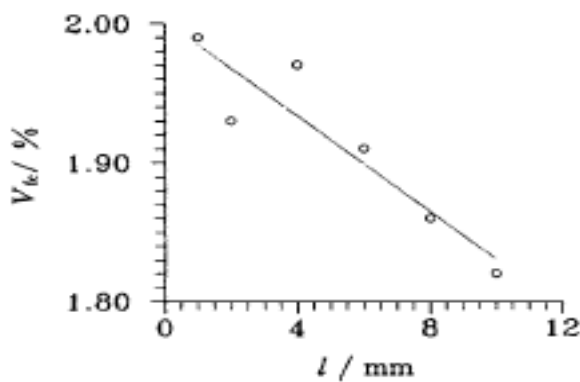


Figure 2.6: Percolation threshold variation with the length of fiber (Wang et al. 2002)

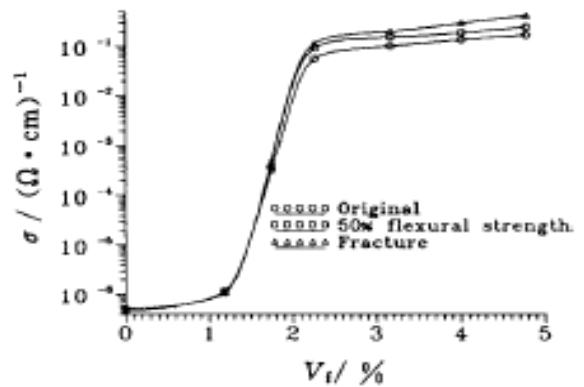


Figure 2.7: Electrical Conductivity vs. Volume fractions of Fiber Content (Wang et al. 2002)

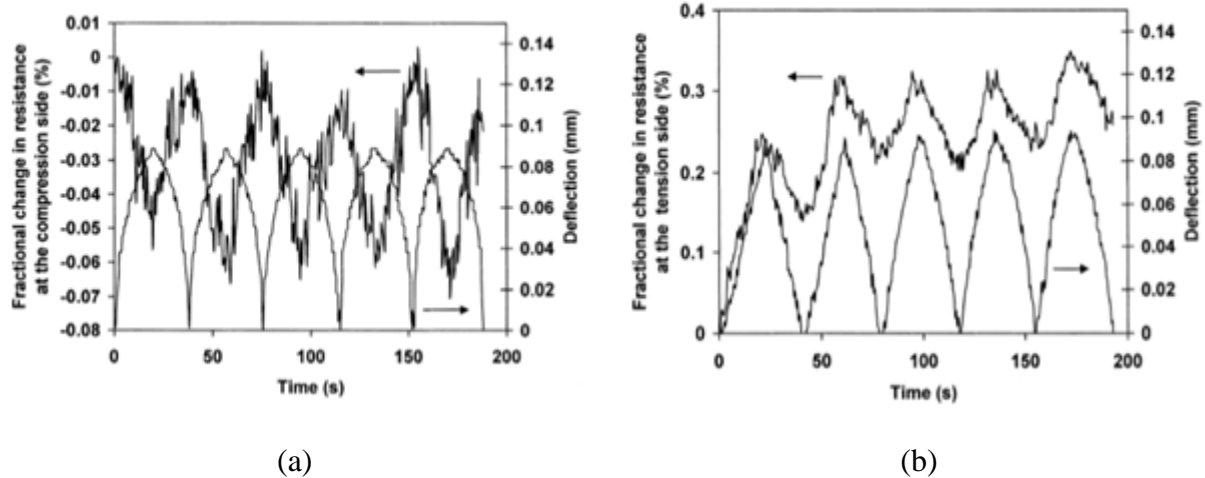


Figure 2.8: Fractional Change in Resistance and Deflection of the specimen under cyclic flexural loading (a) compression side (b) tension side (Wen and Chung 2001a).

2.4 Imparting conductive additives in concrete and its Application

The first notion of self-sensing concrete using piezoresistive analysis was introduced in 1993 by Chen and Chung (Chen and Chung 1993). They added 0.2-0.4% vol. of short carbon fiber to observe the electrical conductivity of concrete. They found that electrical resistivity in concrete decreases when a compressive load is applied, and it varies linearly with the applied load. Later several pieces of research have been focused on studying the sensing properties of concrete. It has been found that with the application of longitudinal compressive stress, the electrical resistivity in that direction is reduced. In the case of tensile load, the resistivity is increased. Additionally, both effects are reversible in the material's elastic range, enabling the strain sensing of the conductive composite. In case of damage sensing that is related to the plastic range of the material, the electrical resistivity is increased on that range and is irreversible (Vilaplana et al. 2013).

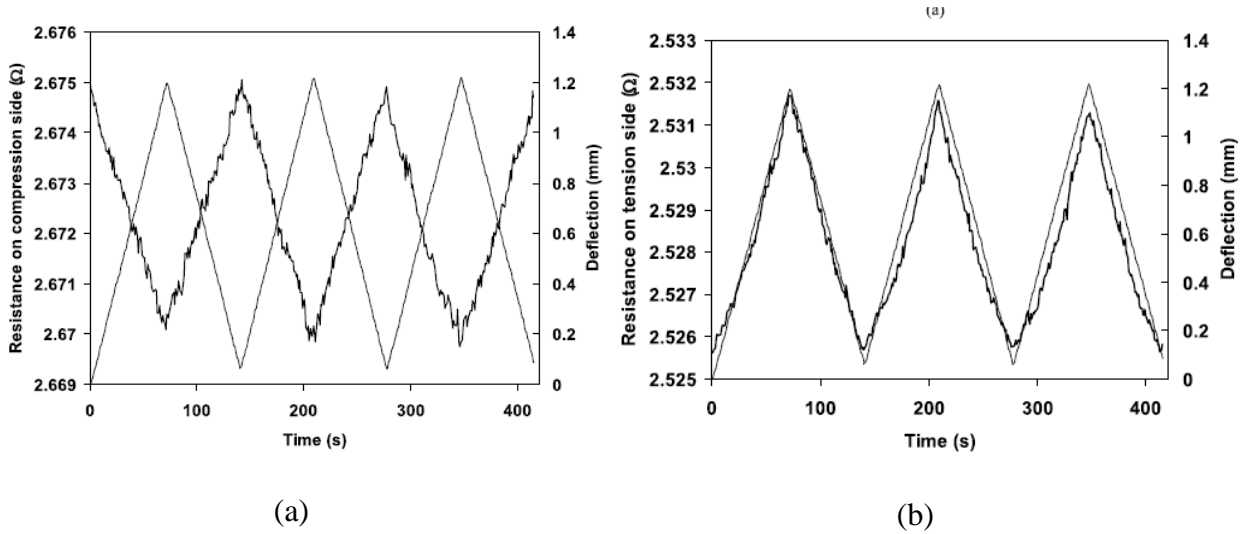


Figure 2.9: Resistance behavior with different deflection levels on concrete specimen (a) Compression surface. (b) Tension surface (Wang and Chung 2006).

Wang et al. (2002) studied the electrical conductivity characterizations using different volume fractions and lengths of carbon fiber content in the cement composite under three different loading levels. SEM images presented in this research showed that carbon fiber content below the percolation threshold doesn't form a continuous path. In contrast, at or above the percolation threshold, a continuous conduction network was formed.

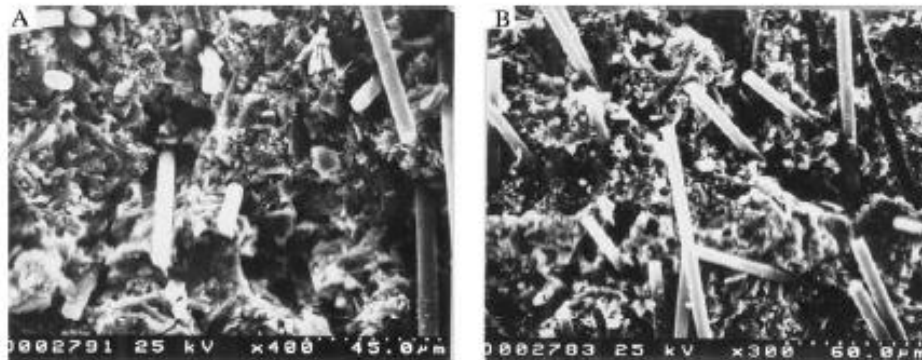


Figure 2.10 SEM photomicrographs illustrating the connection of carbon fibers in cement composites (A) Vf = 1.16%, (B) Vf = 2.21% (Wang et al. 2002)

Li et al. (2006) experimentally investigated the conductivity of concrete with carbon black nanoparticles as conductive fillers in cement composites. A percolation threshold was found in the composite with 12 to 20 wt—% of carbon black in cement composite from the investigation.

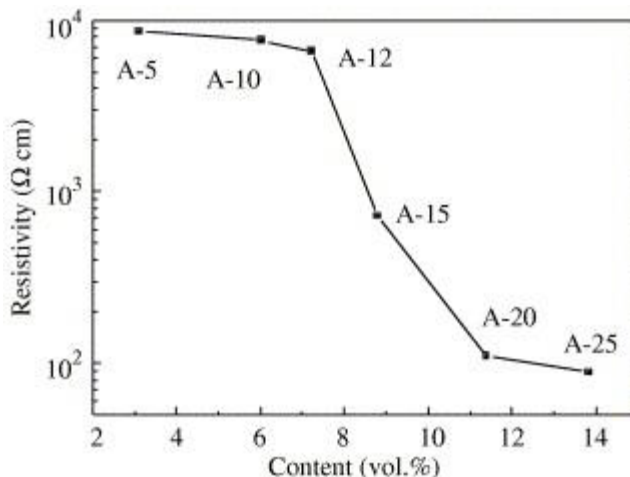


Figure 2.11: Resistivity as a function of the CB volumetric content (Li et al. 2006)

Han et al. (2009a) investigated the use of Nickel powder in the cement-based composite as a piezoresistive sensor. They studied the electrical resistivity using the four probe electrodes method. The results indicated that under uniaxial compression, resistivity decreases to 62.6144% in the elastic region. Another study by Han et al. (2009b) observed that nickel particles form a conductive network in the cement matrix. They concluded that the decrease in resistivity is due to the quantum tunneling effect.

Li et al. (2007) studied the pressure-sensitive properties and microstructure of reinforced cement composite containing carbon nanotube. The carbon nanotube is treated (SPCNT) using H₂SO₄ and HNO₃, and then the electrical resistivity and pressure sensitivity are measured and compared with the untreated carbon nanotube (PCNT) reinforced composite. It has been

observed that in both cases, electrical resistivity is significantly decreased under cyclic compressive loading. The SEM image reveals that treated CNT has more substantial effects on improving the sensitivity. In the case of untreated CNT, a meshwork was formed, which created a forceful effect to reduce the electrical resistivity. It also indicates that the pressure-sensitive is much intensive for treated CNT than untreated CNT composites.

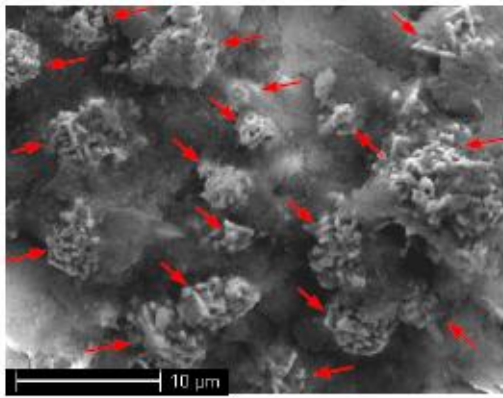


Figure 2.12: SEM photo of Nickel particle in Cement composite (Han et al. 2009a)

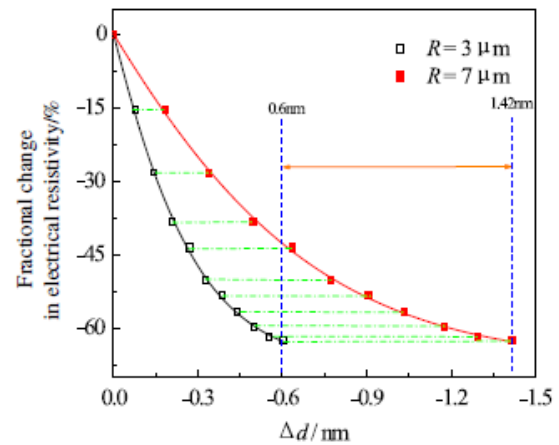


Figure 2.13: Relationship between change in tunneling distance and the fractional change in electrical resistivity of NPCC (Han et al. 2009b)

Fan et al. (2011) investigated the electrical conductivity using carbon fiber (1% wt of cement) and graphite powders (0-50% wt. of cement) simultaneously. In this research, the percolation threshold for the graphite powder was found to be 20% wt. of cement, and the piezoresistive effect was apparent at this content.

Teomete and Kocyigit (2013) investigated the tensile strain sensing using steel fiber in the reinforced cement matrix. The splitting tensile test was performed to investigate the tensile

capability. Total six different specimen containing 0,0.2,0.5,0.8,1.0 and 1.5 vol.% of 6mm steel fiber were used. The electrical resistivity was measured using the four-probe electrode method using embedded copper meshes. The strain sensing demonstrated a good correlation between the electrical resistivity. A large gage factor of 5195 was observed for this composition.

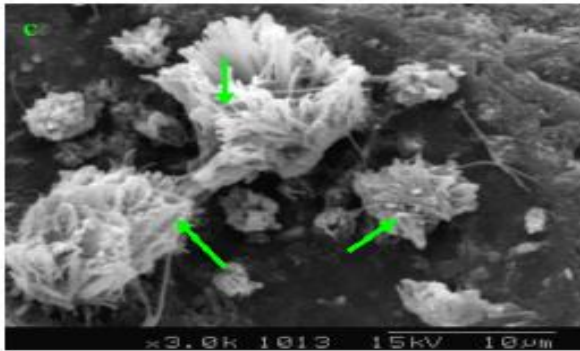


Figure 2.14: The SEM image of treated CNT in composite (Li et al. 2007)

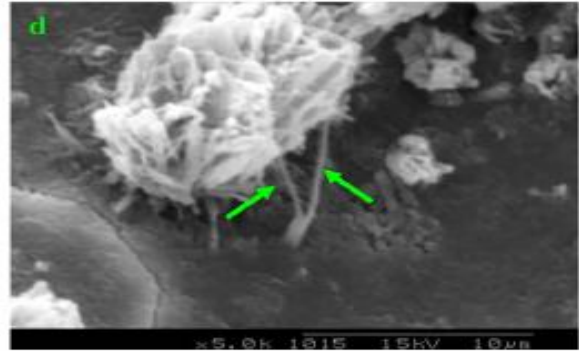


Figure 2.15: The SEM image of untreated CNT in composite (Li et al. 2007)

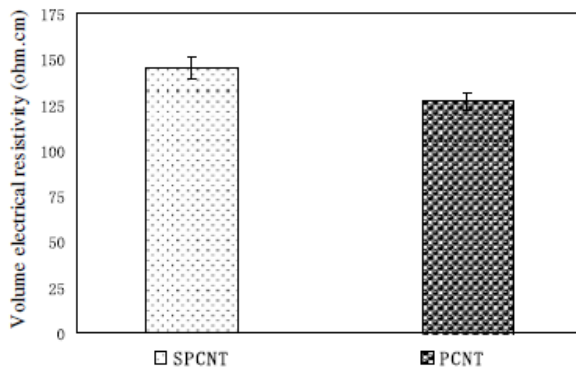


Figure 2.16: Volume resistivity of Carbon nanotube-reinforced composite (Li et al. 2007)

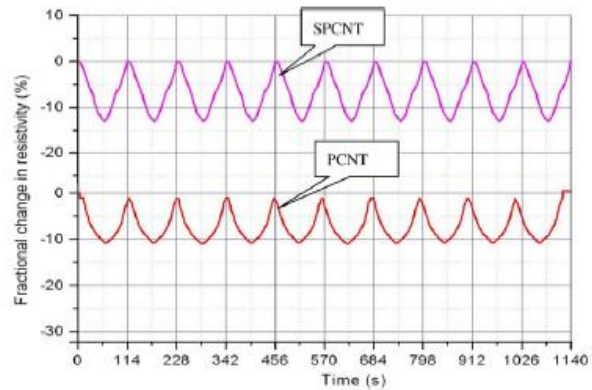


Figure 2.17: The fractional change in resistivity vs. time under cyclic compressive loading (0–15 KN) (Li et al. 2007)

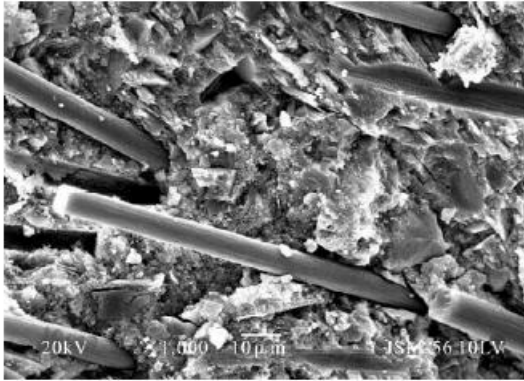


Figure 2.18: SEM image showing the distribution of carbon fibers and graphite particles (Fan et al. 2011)

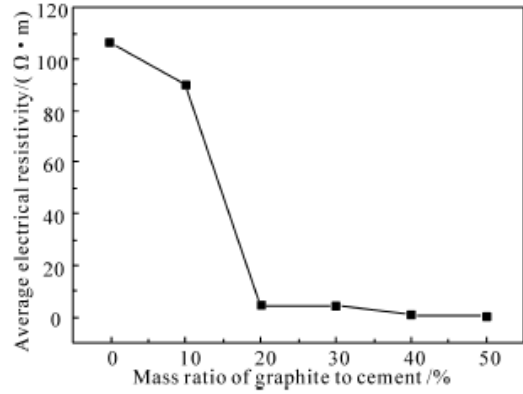


Figure 2.19: Electrical resistivity change with the graphite content (Fan et al. 2011)

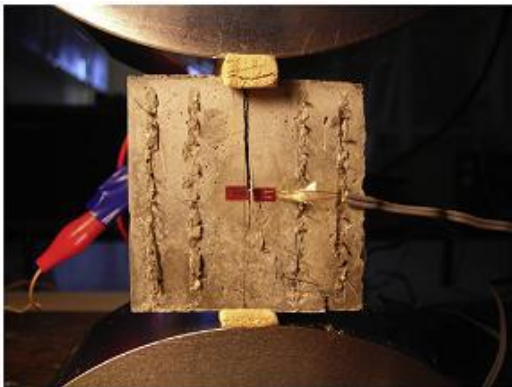


Figure 2.20: The specimen under splitting tensile test (Teomete and Kocyigit 2013)

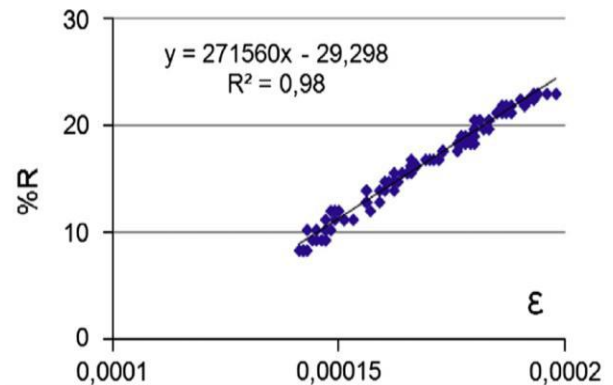


Figure 2.21: Results of resistance vs. deformation from the tensile strain stress for the specimen with 1.5 vol.% (Teomete and Kocyigit 2013)

CHAPTER III

MATERIALS AND EXPERIMENTAL METHODS

3.1 Raw Materials

The cement paste specimens were prepared with Type-1 Portland cement with tap water. The water/cement ratio used in this study was 0.45. The conductive additives used for this study were natural flake type (F-516) graphite powder (<212 μm) produced by Asbury Carbons Inc. The physical properties of graphite powder used in this research are shown in Table-3.1. The conductive additive contents used for the study were 0%, 5%, 10%, 15%, 20%, 25% and 30% by volume of cement paste.

Table 3.1: Physical Properties of Natural Flake type Graphite Powder (Asbury Carbons Inc.).

Asbury ID	Percent Carbon	Typical Size (μm)	Specific Gravity	Surface Area (m^2/g)	Typical Resistivity ($\Omega\text{-cm}$)	Note
F-516	95.45	50-60 (<212)	2.26	5	0.03-0.05	Flake Type

3.2 Specimen Preparation

For mixing the cement paste Hobart Planetary motion mixer is used. A total of 21 specimens in seven different batches were cast. The summary of the Specimen used in the experimental program is shown in Table 3.2. To prepare the samples, cement and graphite are

mixed with a stirring rod for 2 minutes and then placed in the Hobart Mixer (dry mixing). Water was added gradually, and the mixing was continued for 5 minutes. Then cement pastes were placed at the cubic mold (5.08 cm × 5.08 cm × 5.08 cm). After keeping the specimens at mold for 24 hours, all of them are demolded and placed in a water bath for 28 days curing at laboratory room temperature with $20 \pm 2^\circ\text{C}$ and $\text{RH } 95 \pm 5\%$.

3.3 Electrical Property Measurements and Data Processing

Prior to the electrical measurement, each Specimen was removed from the water bath after 28 days of curing, and the surface was dried with paper towels to make SSD conditions so that there remains no chance for surface conduction. In general, the electrical properties are measured using either two-point sensing or four-point sensing methods. Both methods were initially investigated in this research, and the resistivity difference between these two methods was observed as very negligible. Hence, throughout the investigation, the two-point sensing method was used to measure electrical resistivity since it is easier to implement in small concrete blocks. Highly conductive silver paste (Tedpella Inc.) was used on two opposite sides of each cube to maintain full contact between the Specimen and electrodes. Copper tapes were used as the electrode at two opposite surfaces of cube specimens. The properties of conductive silver paste and copper tape are shown in Table 3.3.

For the wet (SSD) condition measurements, the specimens were kept water bath for 24 hours to make it fully saturated. For measurements in dry condition, the specimens were kept in Oven at 110°C for 48 hours. For keeping the Specimen either in SSD or in Dry conditions during the testing, the specimens were wrapped with plastic foil on the whole surface of each sample (keeping copper tape tip out of the wrap) so that moisture doesn't go out from SSD specimens or

enter into Dry specimens. A complete process of the experimental program is shown in Figure 3.1.

Table 3.2: Summary of the Specimen used in the experimental program.

Name	Size/ Dimension (cm * cm * cm)	Cross-sectional Area (Electrode surface area) (cm ²)	Materials/ ingredients	Water / Cement ratio	% of Graphite content, by volume of Mix
GP_0	5.08 × 5.08 × 5.08	5.08 × 5.08	Cement + GF	0.45	0
GP_5	5.08 × 5.08 × 5.08	5.08 × 5.08	Cement + GF	0.45	5
GP_10	5.08 × 5.08 × 5.08	5.08 × 5.08	Cement + GF	0.45	10
GP_15	5.08 × 5.08 × 5.08	5.08 × 5.08	Cement + GF	0.45	15
GP_20	5.08 × 5.08 × 5.08	5.08 × 5.08	Cement + GF	0.45	20
GP_25	5.08 × 5.08 × 5.08	5.08 × 5.08	Cement + GF	0.45	25
GP_30	5.08 × 5.08 × 5.08	5.08 × 5.08	Cement + GF	0.45	30

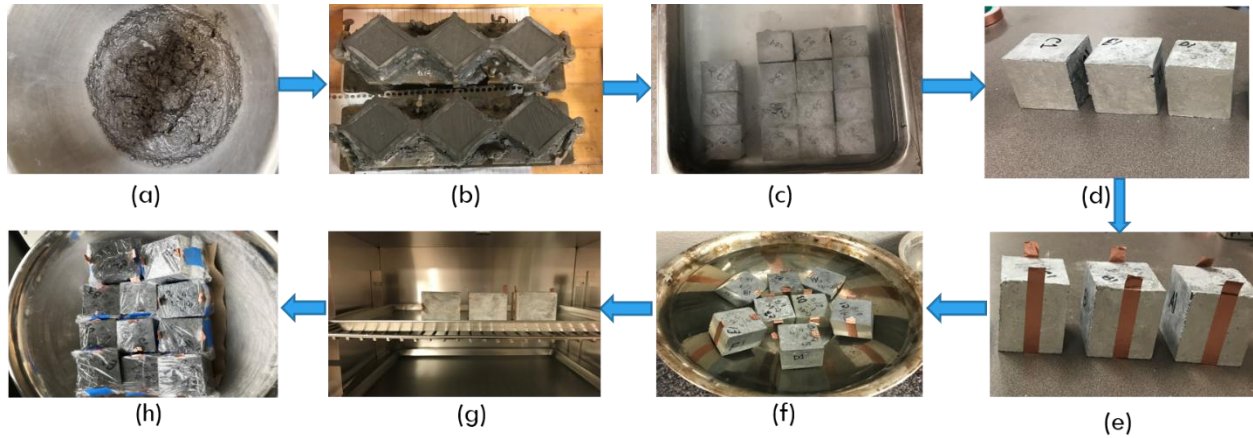


Figure 3.1. Specimen Preparation for Experimental Program: (a) Specimen after applying the conductive silver paste on two opposite sides (b) Attaching copper tape as electrodes (c) Specimen underwater to make it fully saturated (d) Specimen at Oven to make it fully dry (e) Specimen wrapped with plastic foils to control the moisture.

In order to investigate the effect of degree of saturation (DOS) on the electrical properties of conductive cement paste, firstly, the Specimen was made fully saturated. Then the weight of the Specimen was taken as M_w . At that SSD conditions, the resistivity was measured using different devices. The moisture from the Specimen was removed using a progressive drying process, including air dry, oven heating. When the Specimen become fully dry, weight was taken and recorded as M_d . The moisture content in different levels of drying conditions of the Specimen was calculated using the following Equation 1. and the degree of saturation was calculated using Equation 2.

$$[1] \text{ Amount of moisture, } W1 = \frac{M1 - M_d}{M_d} \times 100$$

$$[2] \text{ Degree of saturation (DOS) } = \frac{W1}{W_w}$$

Where W_1 is the moisture content corresponding to the specimen weight M_1 , when it is dried either in the air or in the Oven (not fully dry); M_d is the weight of fully dry Specimen (Specimen was made fully dry keeping it in the Oven for 48 hrs at 110°C). And, W_w is the moisture content of a fully saturated (SSD) specimen.

A Keithley 2400 (C-22) Source Measure Unit (Multimeter-1) was used for the DC resistance measurement using the two-point sensing method. True RMS Digital Multimeter DM-441B (Multimeter-2) is also used to measure DC Resistance. In order to confirm the charging effect of conductive concrete, the static measurements using DC were made by two distinguished methods: 1) continuous monitoring and 2) discontinuous measurement. In the continuous monitoring, the static resistance of the specimens was measured for 5 minutes with continuously connected probes. By connecting the probes continuously, the charging of concrete may occur. In the discontinuous measurement, the probes were connected a couple of seconds to read the resistances and immediately removed after the reading to minimize the charging. The discontinuous measurements were repeated multiple times with 10 minutes time intervals for 2 hours.

Table 3.3: Properties of Electrodes materials

Silver paste	Particle size: 0.4-1.0 μ m	Specific Gravity 2.15 g/cc	Sheet Resistance: 0.04 - 0.066 ohms/sq/mil (25.4 μ m)	Ted Pella, INC.
Copper tapes	W: 6.3mm L: 16.46m T: 2.6 mils (0.066 mm)	8.94 kg/cm ³	Sheet Resistance: 0.005 ohm	Ted Pella, INC.

A Metrohm AUTOLAB PGSTAT302N is used for impedance analysis of cement paste containing graphite. The frequency range used for the measurement was 1 MHz to 1 Hz. In a preliminary test, from high (1 MHz) to low frequency (1 Hz) and from Low (1 Hz) to high frequency (1 MHz) swaps were compared to observe the effect of direction of frequency swapping. Since the results from the increasing frequency swap and the decreasing frequency swap were identical, the study used the decreasing frequency swap from high (1 MHz) to low frequency (1 Hz) for the rest of the measurements. The amplitude of voltage was 500 mV, and 20 data points were recorded per decade of the frequency range. Several researchers have used a similar AC measurement setup to understand cement-based materials' microstructure (Cabeza et al., 2006, Zhu et al., 2017). For data acquisition, a commercial tool, NOVA 2.1 software, is used. The test set up for measuring the resistance/impedance using two different DC equipment and one AC impedance spectroscopy is shown in Figure 3.2.

From the measured resistance (R , Ω), volume resistivity (ρ , $\Omega\text{-cm}$) was calculated using the following Equation 3.

$$[3] \rho = \frac{R \times A}{L}$$

From the measured Impedance (Ω), volume resistivity (Z , $\Omega\text{-cm}$) was calculated using the following Equation 4.

$$[4] Z = \frac{(\text{impedance}) \times A}{L}$$



Figure 3.2: Test Set up for measuring static (DC) resistance through (a) True RMS Digital Multimeter DM-441B (Multimeter-2) (b) Keithley 2400 (C-22) Source Meter (Multimeter-1), and for AC Impedance measurement through (c) Metrohom AUTOLAB PGSTAT302N

Where A is the cross-sectional area of the Specimen (cm^2), L is the Specimen's length (cm). Throughout the test process, the cross-sectional areas are assumed to be constant. The electrical conductivity can be obtained by inverting the volume resistivity.

CHAPTER IV

INVESTIGATION ON ELECTRICAL PROPERTIES MEASUREMENT METHODS

4.1 Introduction

The electrical behavior of conductive concrete is very complex. Therefore, understanding the electrical properties of conductive concrete is necessary. Many researchers have used DC/static electrical measurements to understand electrical properties using different additives (Al-Bayati et al. 2020; Dehghanpour and Yilmaz 2020a; Dong et al. 2021; Dong et al. 2019; Sun et al. 2021). DC measurements, especially when it is measured through continuous measurement, cause polarization in cement-based concrete (Cao and Chung 2004; COPPOLA et al. 2013; Han et al. 2011a; Wen and Chung 2001b). It is challenging to characterize electrical properties using DC/static resistance measurement since electrical polarization causes an increase in the measured resistance. Instead, many researchers used DC methods for various non-structural applications of conductive concrete (Cholker and Tantray 2019; Ding et al. 2019a; Ding et al. 2019b; Dong et al. 2020a; Dong et al. 2020b; Kwon et al. 2019; Nguyen et al. 2019; Sun et al. 2017; Chung 2003a; Cao et al. 2001; Wen and Chung 2000; Yao et al. 2003; Reza et al. 2003; Bontea et al. 2000; Chen et al. 2005; Chung 2002b; Chung 2002a). Therefore, thorough investigations on DC measurements are necessary.

On the contrary, The AC impedance spectroscopy techniques are very useful for characterizing complex electrical systems (Gu et al. 1993b; Wen and Chung 2007). It minimizes polarization by repeatedly varying the input voltage (Wen and Chung 2007) and

characterizes the electrical properties with capacitance, inductance, and resistance. As per the author's literature studies, AC impedance measurements was studied significantly less than DC methods for electrical characterization and various non-structural applications (Ding et al. 2019b; Segura et al. 2019; Papanikolaou et al. 2020; Fulham-Lebrasseur et al. 2020; Zhu et al. 2019; El-Dieb et al. 2018; Sassani et al. 2017; Yoo et al. 2017; Li et al. 2016; Reza et al. 2003; Peled et al. 2001; Fu et al. 1997; Berrocal et al. 2018a; Faneca et al. 2018; Suryanto et al. 2018; Danoglidis et al. 2019; Li and Li 2019; McCarter 1995; MacPhee et al. 1996; Banthia et al. 1992; Hou and Lynch 2009; McCarter et al. 2013). Rather, most of the research using Electrochemical Impedance Spectroscopy (EIS) was conducted to understand the microstructure of conductive concrete, chloride diffusion, and durability analysis while it is subjected to corrosion (Dong et al. 2014a; Mercado-Mendoza et al. 2014a; Zhang and Kong 2014; Kamali and Ghahremaninezhad 2015; Dong et al. 2016b; Dong et al. 2016a; Dong et al. 2018; He et al. 2018a; Chi et al. 2019; Melara et al. 2020; Stefanoni et al. 2020; Cai et al. 2021; McCarter et al. 1988; Gu et al. 1993d; McCarter 1996; Gu et al. 1993c; Cruz et al. 2013; Ravikumar and Neithalath 2013, Tang et al. 2014). In this study, the electrical properties of conductive cement paste will be thoroughly investigated using both static/DC measurements methods and AC impedance spectroscopy.

This section aims to investigate on the electrical properties measurement methods of graphite added conductive cement paste using both static/DC measurements and AC Impedance Spectroscopy. In this research, DC measurements were conducted in two different methods: 1) Continuously connecting probes over time and 2) Connecting and Disconnecting the probes on the specimen. Two different resistance measurement devices (Multimeter-1 and Multimeter-2) were used to compare the consistency of the DC results. Moreover, the effect of different DC voltages on the resistivity of conductive cement paste was also investigated. The moisture level

was appropriately controlled throughout the experimental work, whether the specimen is either in wet (saturated surface dry, SSD) or in dry (48 hours oven dry) conditions.

4.2 Static/DC Resistivity Measurement

The fundamental of DC measurement is that electricity is being provided to the specimens through a one-directional flow of electron/current. Neither electricity nor voltage changes over time; instead remains fixed with respect to time. Due to this characteristic of electric current, it is known as static or Direct Current (DC). Because of the one-directional flow, one side of the Specimen receives exclusively positive electron or negative electron while the other side is in opposite charging mode.

Since most of the previous studies used DC methods to apply conductive concrete in different non-structural applications, thorough investigations on the static/DC measurement method are necessary. In this section, the static/DC measurement results obtained from the continuous monitoring and discontinuous measurement are discussed in detail.

4.2.1 Continuous Monitoring

In this measurement method, electrical probes were connected with the specimens and continuously associated for 5 minutes. The data was gathered at 15-second intervals, and thus the measurement continued for whole periods. The data was collected three times for almost every Specimen. Figure 4.1, Figure 4.2 and Figure 4.3 are showing static resistivity results obtained from continuous monitoring.

In Figure 4.1, Static/DC resistivity of conductive cement paste containing 10% (by volume of cement paste) graphite is shown. The electrical resistivity is increasing over time. At the initial stage, the rate of increase is much higher. With continuously connecting the probe,

electrons are causing a charging effect inside the specimens, and this charging is increasing over time. Specimen either in dry or in wet conditions showing the same phenomena (as shown in Figure 4.1 (a), (b), (c), (d)). Resistivity measured with two distinguished devices (Multimeter-1 and Multimeter-2) gives a similar trend but provides a different rate of resistivity. Whatever measurement machine it is (either Multimeter-1 or Multimeter-2), or whatever the specimens' moisture conditions are (Dry or Wet), the continuous resistivity increases are observed. This characteristic indicates that there is the presence of some capacitance/polarization effect inside the graphite added cement cube. Due to the presence of the capacitance effect, the polarization of opposite electrons is occurring inside the materials, and with time, the polarization is ameliorating, which causes the increase in resistivity.

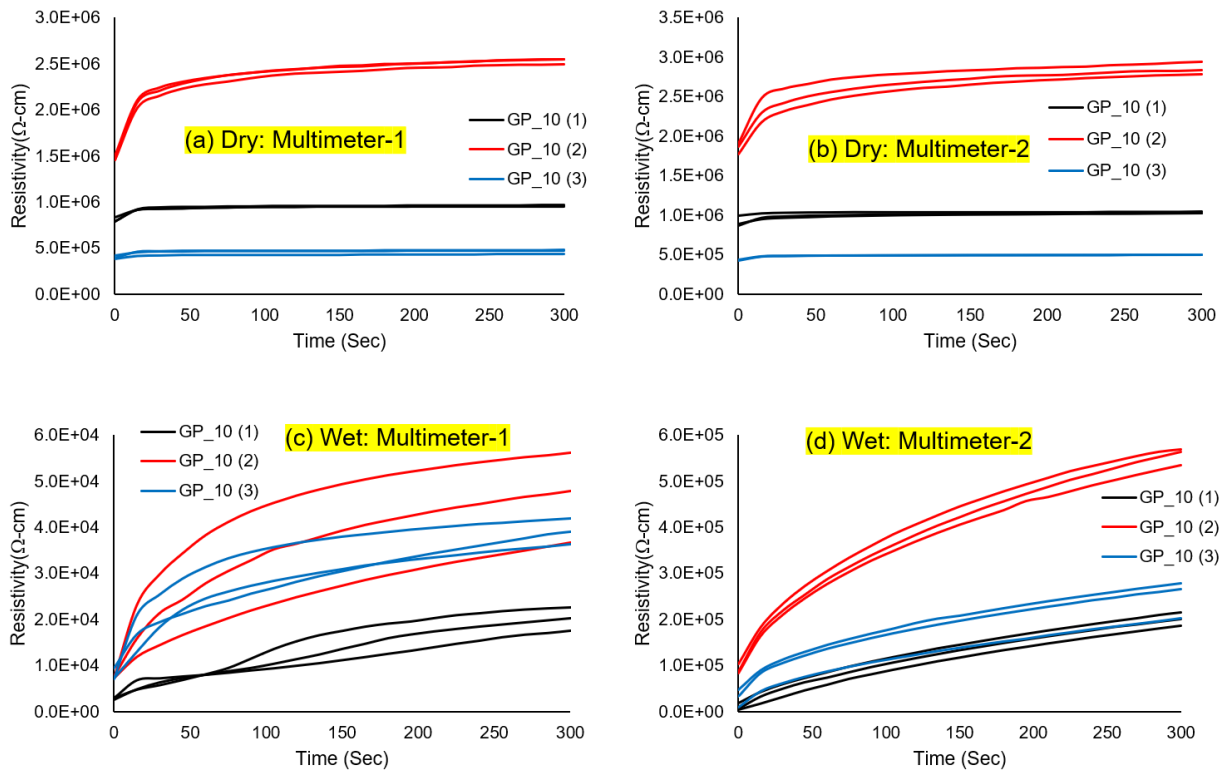


Figure 4.1: Static Resistivity measurement of Specimen GP_10 (10%-graphite) through continuous monitoring for 5 minutes (300 Sec). (a) Using Multimeter-1 at 1V in dry conditions

(b) using Multimeter-2 in dry conditions (c) using Multimeter-1 at 1V in wet conditions (d) using Multimeter-2 in wet conditions.

In Figure 4.2, Static/DC resistivity of conductive cement paste containing 15% (by volume of cement paste) graphite is shown. The Specimen with 15% graphite powder showed a constant Static Resistivity value in dry conditions, as shown in Figure 4.2 (a), (b). Two different DC devices also show similar trends and offer almost the same values while specimens are in dry conditions. There is no charging effect/capacitance is observed. On the other hand, at wet conditions (as shown in Figure 4.2 (c) and (d)), the resistivity is increasing rapidly at the initial stage and continues to increase at a slower rate over time. There is no moisture in dry conditions, while in wet conditions, moisture is present, and specimens show dissimilar phenomena than dry results. Conduction through moisture provides some capacitance effects inside the specimens, which increases the Specimen's static resistivity over time.

In Figure 4.3, Static/DC resistivity of conductive cement paste containing 20% (by volume of cement paste) graphite is shown. The graphite content for these specimens is higher than that of the previous two sets of specimens. However, these specimens also show similar trends observed for specimens with 15% (by volume of cement paste) graphite. There is no charging effect at dry conditions, and at wet conditions, a little charging effect is observed.

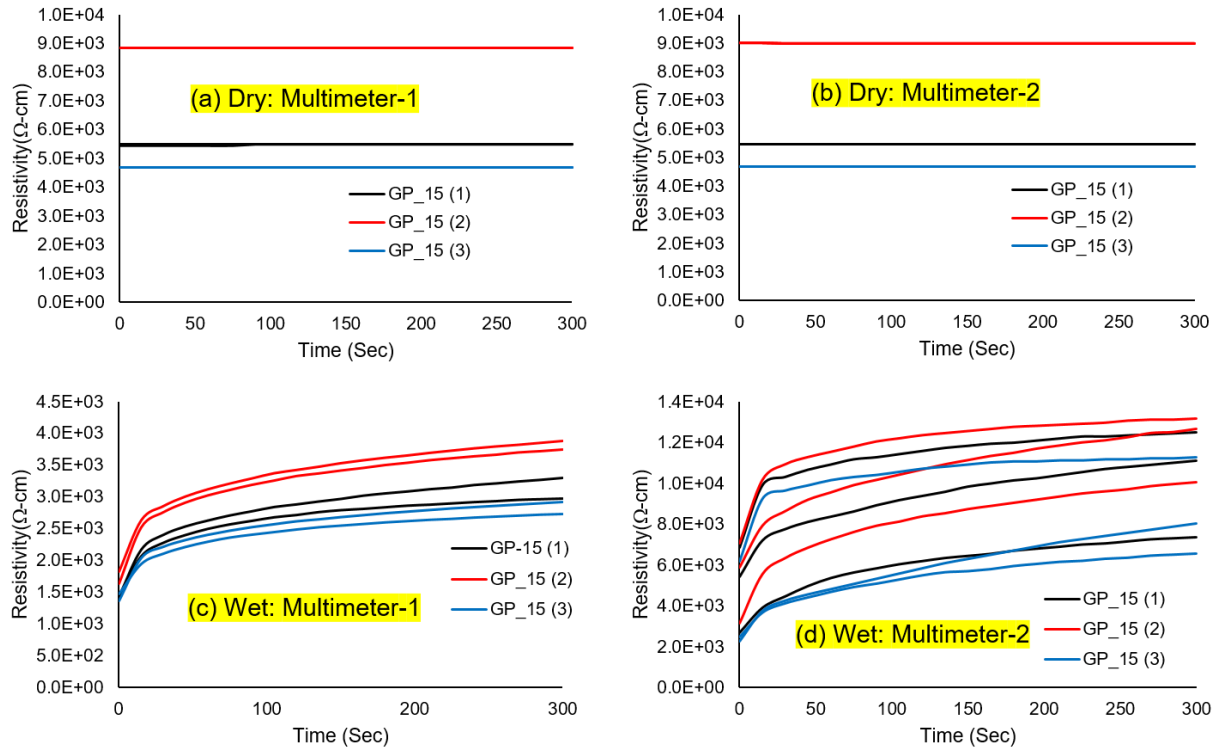


Figure 4.2: Static Resistivity measurement of Specimen GP_15 (15%-graphite) with continuous monitoring for 5 minutes (300 Sec). (a) using Multimeter-1 at 1V in dry conditions (b) using Multimeter-2 in dry conditions (c) using Multimeter-1 at 1V in wet conditions (d) using Multimeter-2 in wet conditions.

Therefore, it can be said that conductive cement paste with a low concentration of fillers has some capacitance/charging effect inside the Specimen, which enables charge storage and cause an increase in static/DC resistivity in case of continuous monitoring. For low concentration graphite in cement paste, the resistivity increase is faster in the initial stage and slowed down as the monitoring continues. Similar phenomena were observed by (Han et al., 2011a) and (COPPOLA et al., 2013) with CNT added cement paste, by (Nguyen et al., 2019) as they added steel fiber, CF and CNT in cement concrete, by (Sun et al., 2017) as they added Graphene Nano-

platelet in cement concrete. Moreover, different resistivity was observed with each distinguished trial. It was challenging to obtain repetitive patterns in the resistivity graphs for the same Specimen with a lower graphite concentration.

Specimens with higher graphite concentration and at dry conditions show constant resistivity and repetitive patterns in the resistivity graph in different trials. However, in wet samples, a slight difference in resistivity was observed in distinguished trials due to some capacitance effect. For some specimens, repetitive patterns in the resistivity graph are observed.

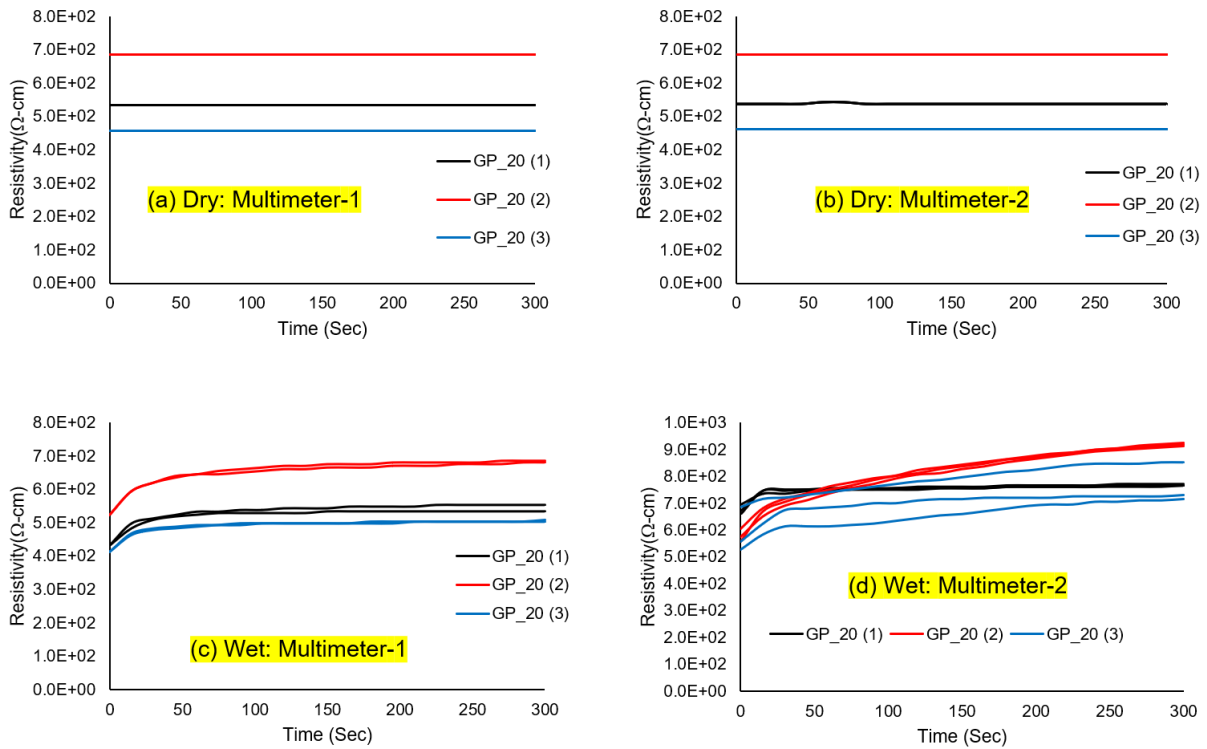


Figure 4.3: Static Resistivity measurement of Specimen GP_20 (20%-graphite) through continuous monitoring for 5 minutes (300 Sec). (a) using Multimeter-1 at 1V in dry conditions (b) using Multimeter-2 in dry conditions (c) using Multimeter-1 at 1V in wet conditions (d) using Multimeter-2 in wet conditions.

4.2.2 Discontinuous Measurements

In this measurement method, electrical probes were connected with the specimens, and it was connected with the Specimen for few seconds to read the resistance value. The data was gathered at 10-minutes intervals, and the measurement continued for a 2-hrs duration.

Figure 4.4 and Figure 4.5 depicts the variation of DC resistivity over time obtained from the discontinuous measurements. The resistivity values obtained using this method were relatively consistent over time for most of the tests except for some cases. Specimens with having different concentrated graphite show consistent results in discontinuous monitoring than continuous DC monitoring. Although wet specimens showed slight fluctuation of resistivity values, it was very consistent in dry specimens. These consistent results are due to the disconnecting of the probes from the specimens that minimizes the charging effects.

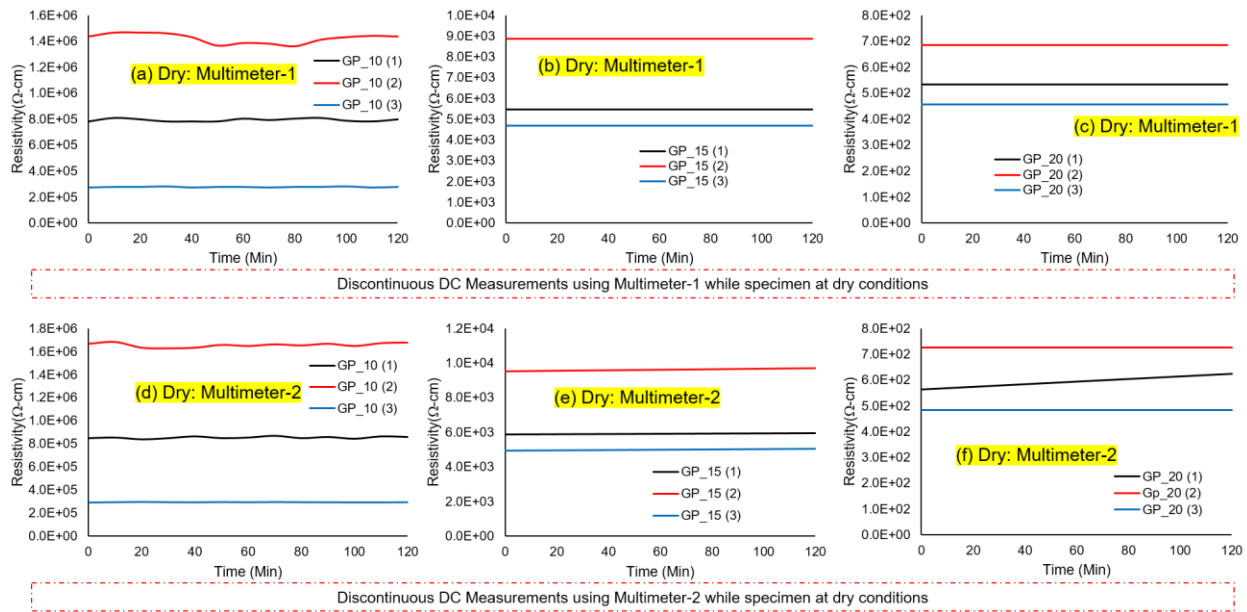


Figure 4.4: Static Resistivity measurement of Dry Specimen GP_10 (10%-graphite) ((a) and (d)), GP_15 (15%-graphite) ((b) and (e)), GP_20 (20%-graphite) ((c) and (f)) with discontinuous monitoring for 2 hrs. at 10 minutes interval. (a), (b), (c) is measured using Multimeter-1 at 1V and (d), (e), (f) is measured using Multimeter-2.

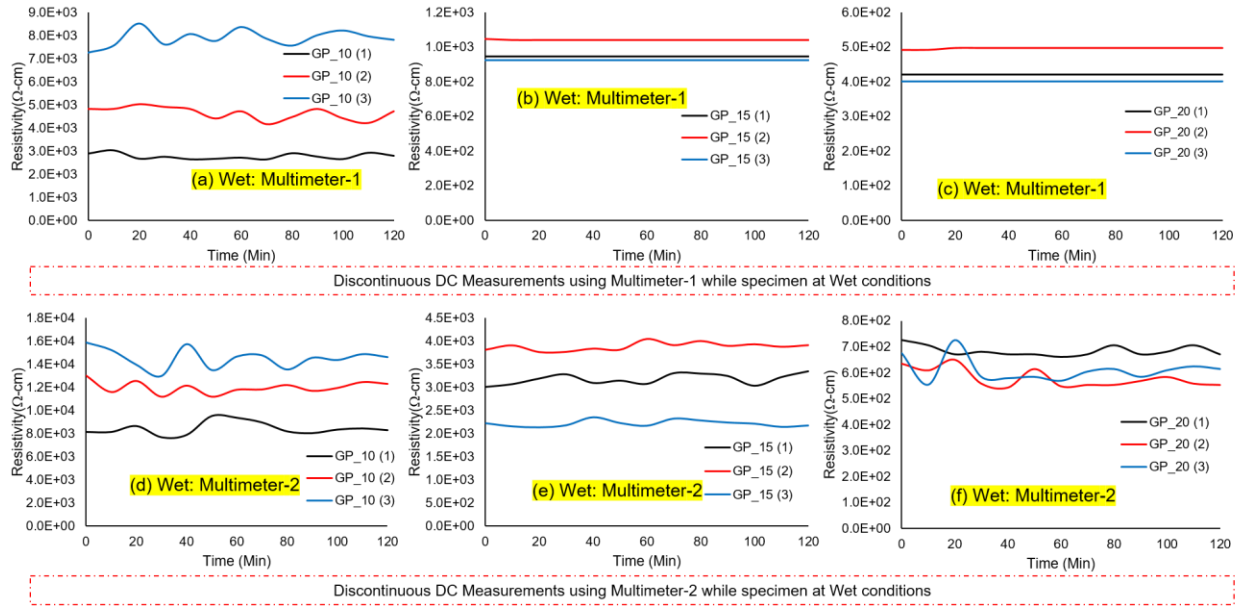
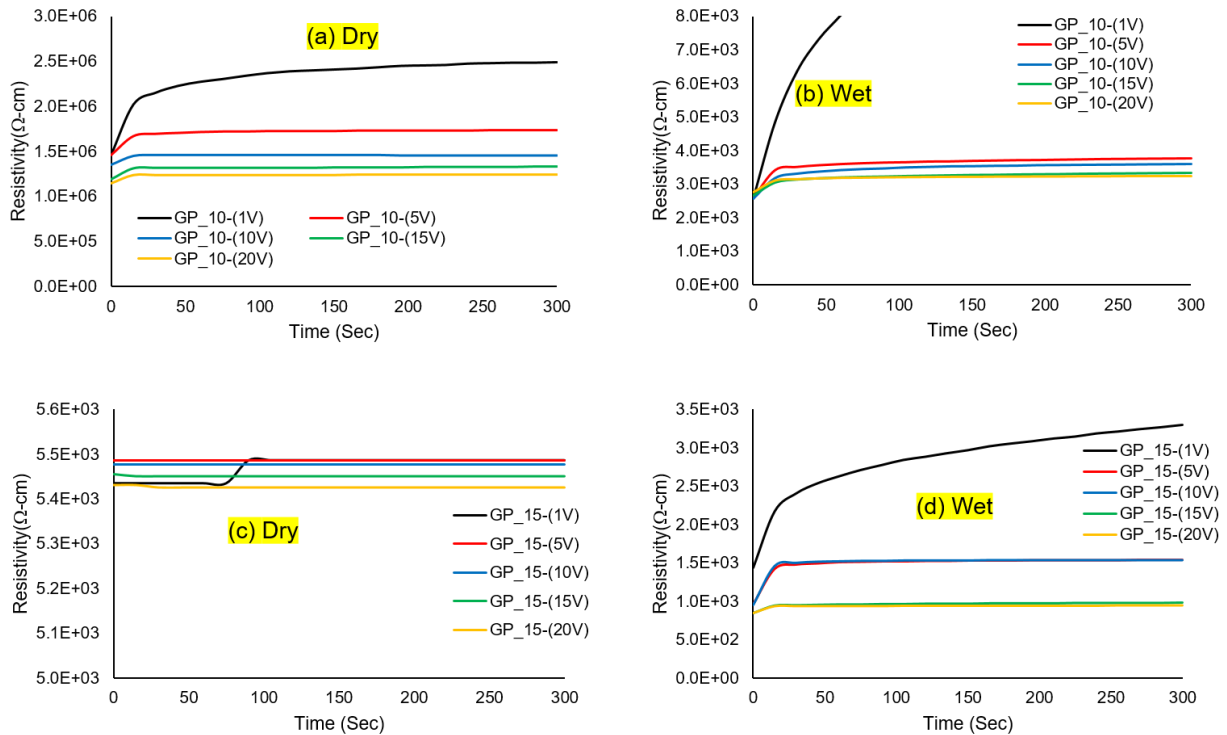


Figure 4.5: Static Resistivity measurement of Wet Specimen GP_10 (10%-graphite) ((a) and (d)), GP_15 (15%-graphite) ((b) and (e)), GP_20 (20%-graphite) ((c) and (f)) with discontinuous monitoring for 2 hrs. at 10 minutes interval. (a), (b), (c) is measured using Multimeter-1 at 1V and (d), (e), (f) is measured using Multimeter-2.

4.2.3 Effect of Voltage on Static/DC Resistivity

In this study, two different devices were used to measure electrical resistivity. Among these two devices, the applied voltage for the measurement can be controlled by Multimeter-1, while another device, "Multimeter-2" does not have manual control of the applied voltage. Figure 4.1, where the graphite concentration is 10% by volume of cement paste shows that two devices in the same moisture conditions give different resistivity values for the same Specimen. The reason can be attributed to the uncontrolled voltage sources of the Multimeter-2. It becomes necessary to explore how the electrical resistivity varies with different voltages. In this section, the effect of DC voltage on electrical resistivity is investigated using both continuous and discontinuous static measurements.

Figure 4.6 and Figure 4.7 show the effect of voltage on static resistivity measurement of conductive cement paste. From the following figures, it can be noticed that at lower concentration of graphite powder (10% by volume of cement paste), either in the continuous monitoring (as shown in Figure 4.6) or the discontinuous measurement (as shown in Figure 4.7), the electrical resistivity of conductive cement paste decreases with voltage increase. This phenomenon is evident whether the Specimen is either in wet or in dry conditions. A similar trend was observed previously by (Dehghanpour and Yilmaz, 2020b) on conductive concrete containing carbon fibers that electrical resistivity decreases with the increase of voltage, and by (Wu et al., 2013), who investigated conductive concrete containing steel and graphite content. The Specimen with 15% and 20% graphite content by volume of cement paste shows little change with the rise in voltage at dry conditions. However, in wet conditions, it is demonstrated that electrical resistivity decreases with the increase of voltage.



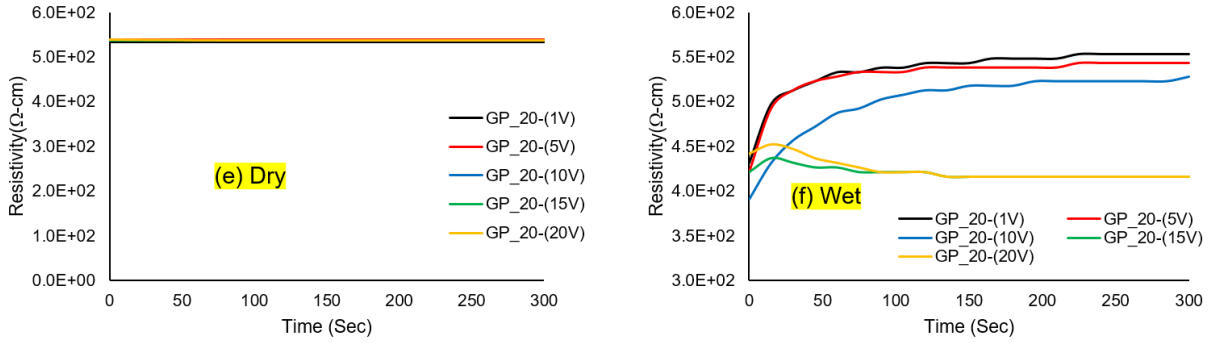


Figure 4.6: Effect of voltage on continuous static resistivity measurement of conductive cement paste specimen GP_10 (10%-graphite) ((a) and (b)), GP_15 (15%-graphite) ((c) and (d)), GP_20 (20%-graphite) ((e) and (f)). (a), (c), (e) is measured when specimens were at Dry Conditions. (b), (d), (f) is measured when specimens were at Wet Conditions

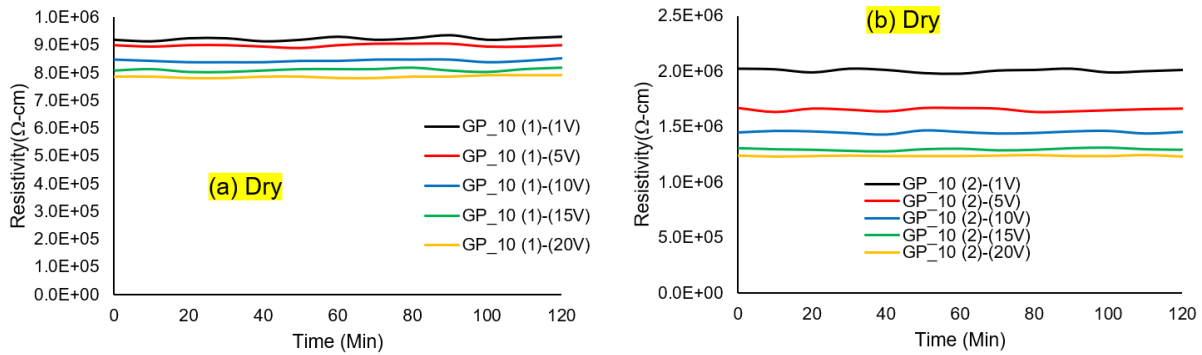


Figure 4.7: Effect of voltage on discontinuous static resistivity measurement of conductive cement paste specimen GP_10 (1) (a) and GP_10 (2) (b) (10%-graphite) at Dry Conditions.

4.2.4 Summary of Static/DC Measurements

Although each measurement in the discontinuous measurement shows relatively consistent resistivity values over time, the magnitudes of static resistivity data vary with the devices and different trials. It is more evident when specimens contain lower concentrations of conductive fillers. It can be presumed that polarization of charges (charging effects) causes the

inconsistent resistivity of conductive concrete. Notably, at continuous resistivity measurements, charging effects play a vital role and cause an increase in resistivity. Also, the voltage of the current source plays a significant role, and resistivity is affected by its variation. Therefore, the static resistivity measurements using DC are not fully capable of characterizing the electrical properties of conductive concrete, especially when the filler concentration is lower than forming a continuous conductive path.

4.3 AC Impedance Measurement

4.3.1 Impedance Spectroscopy Preliminary

In contrast to Direct current, which is the one-directional flow of current/electron in nature, Alternating current changes its current/electron's flow direction. AC is known as two-directional flow, and both electricity and voltage change over time. Because of the two-directional flow, at one time, one side of the Specimen receives a positive electron and later gets a negative electron. Therefore, the chances of polarization of electrons/charges are none. A typical Alternating Current graph is shown in Figure 4.8 (a).

Impedance means frequency-dependent resistance to the current flow of an electrical circuit element (Resistor, capacitor, inductor, etc.). Impedance data is represented either by vector quantity ($|Z(\omega)|$ - impedance and θ - phase angle) or complex quantity ($Z'(\omega)$ and $Z''(\omega)$). impedance of cement paste.

The impedance response, $Z(\omega)$ (in ohms, Ω), in terms of complex quantity for a cement-based specimen, can be written as (McCarter and Brousseau 1990):

$$Z(\omega) = Z'(\omega) + j Z''(\omega) \dots \dots \dots (2)$$

Where, $Z'(\omega)$ is the real or resistive part (known as real Resistance); $Z''(\omega)$ is the imaginary or reactive part (known as Reactance); $j = \sqrt{-1}$; ω is the angular frequency ($= 2\pi f$, where f is the applied frequency (Hz) of AC Current);

The vector quantity is computed as:

$$|Z(\omega)| = \sqrt{Z'^2 + Z''^2}; \text{ Phase angle, } \theta = \tan^{-1} \left(\frac{Z''}{Z'} \right)$$

If $\theta = 0^\circ$ phase, indicate the real impedance/Resistor; $Z = Z'$ (Ohms). If $\theta = -90^\circ$ phase, indicate purely capacitive behavior; $Z = -Z'' = -j/\omega C$ (Farads). If $\theta = 90^\circ$ phase, indicate purely inductance behavior; $Z = Z'' = j\omega L$ (Henrys).

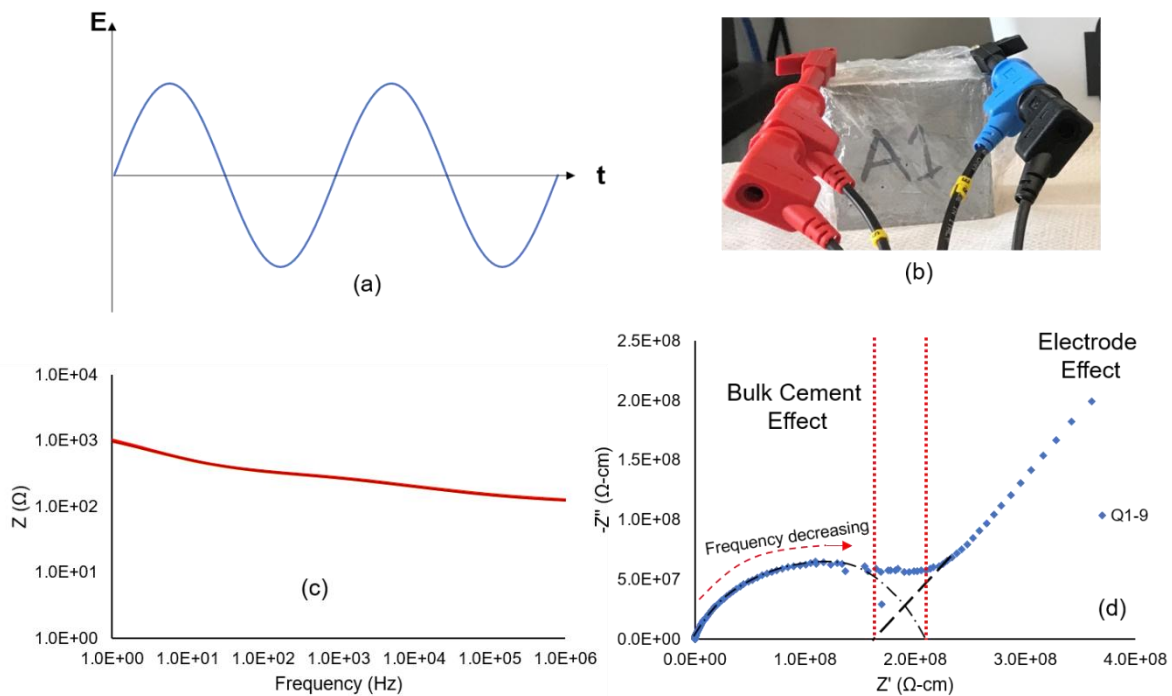


Figure 4.8: (a) Alternating Current (AC) voltage variation with time. (b) A conductive concrete specimen experiencing AC current. (c) A typical Bode plot is showing impedance variation with different AC-frequencies of cement paste. (d) A Typical Nyquist plot shows the variation of real and imaginary impedance.

Two distinguished plots present impedance data. (i) Nyquist Plot (is drawn by imaginary impedance (Z'') vs. the real impedance (Z')); (ii) Bode Plot (is drawn by the $|Z(\omega)|$ vs. the frequency and also Phase angle θ vs. the frequency). A typical impedance response of a concrete specimen placed between two electrodes is shown in Figure 4.8 (c) and (d) while experiencing a wide frequency range of AC.

4.3.2 Impedance Analysis of Conductive Cement Paste

In this section, AC current is applied to conductive cement paste containing graphite. Impedance test on each sample has been done several times with 4 hours intervals. The impedance responses of specimen L having 10% graphite by volume of cement paste are shown in Figure 4.9.

The bode plot of dry Specimen shows that at frequency ranges up to 10,000 Hz, the impedance remains almost constant and ranges beyond 10,000 Hz, showing decreased impedance. The bode plot of wet Specimen shows a continuous decrease in impedance with the increase of AC-frequencies. These results indicate that graphite added cement paste has both capacitance and resistance characteristics. This statement is more acceptable if we see the phase angle variation with frequency of the Specimen from Figure 4.9 (c) and (d). In dry Specimen, the phase angle is close to zero at frequency ranges up to 1000 Hz and started increasing after that. The capacitance behavior is more evident at higher frequency ranges for dry specimens. For the wet Specimen, there is always a presence of phase angle indicating a continuous capacitance behavior in wet conditions.

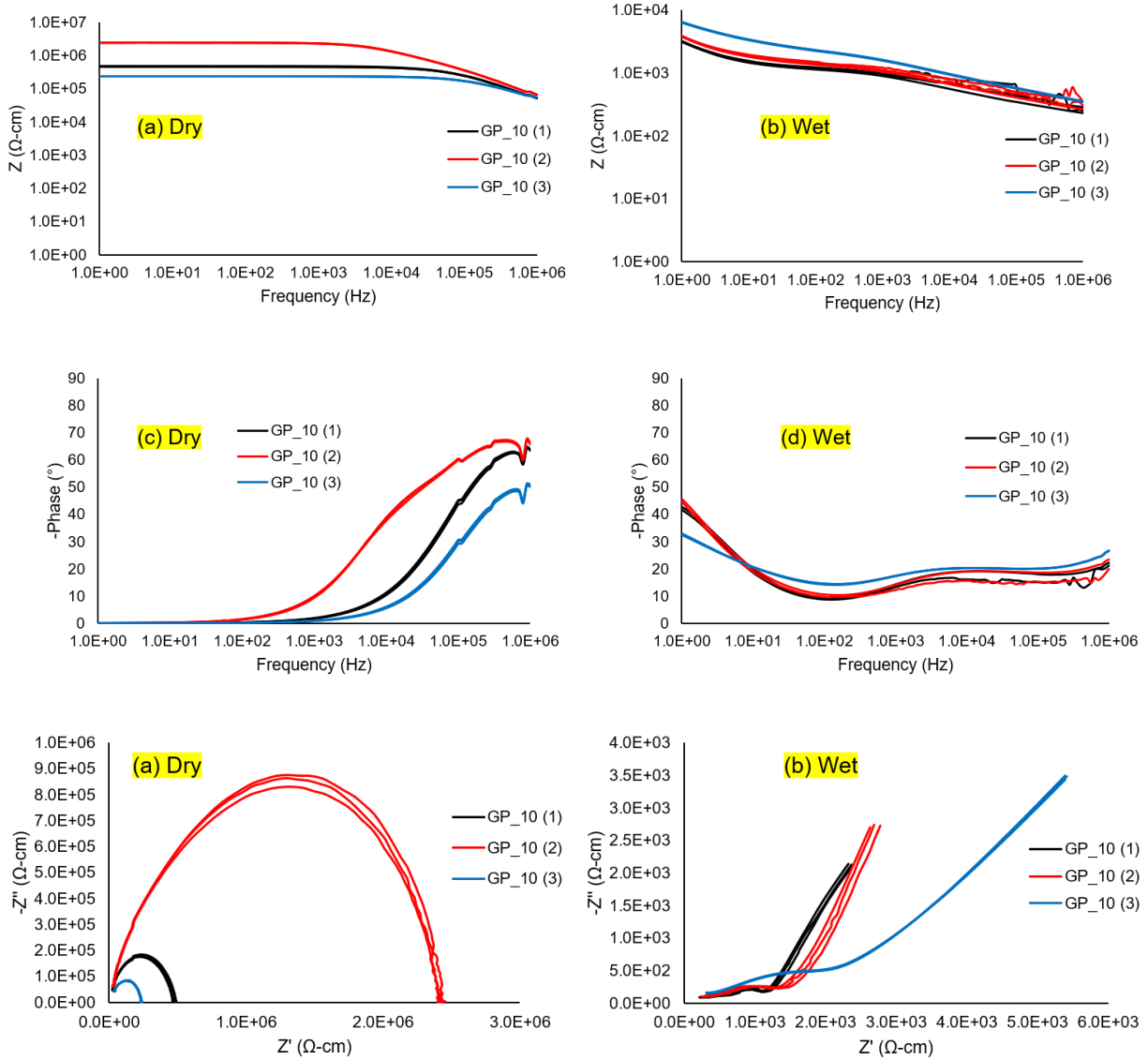


Figure 4.9: Impedance responses of Specimen with having 10% graphite by volume of cement paste. Bode plot of Specimen (a) at Dry Conditions and (b) at Wet Conditions. Phase angle variation with AC frequency of Specimen (c) at Dry Conditions and (d) at Wet Conditions. Nyquist plot of Specimen (e) at Dry Conditions and (f) at Wet Conditions.

On the Nyquist plot for the dry Specimen (shown in Figure 4.9 (e)), the semi-circle represents the bulk conductivity of the specimens. The tail part that describes bulk cement and

electrode interfaces' properties is not visible for the dry Specimen since the lowest AC frequency range was 1Hz. If the frequency range is lowered to 0.1 Hz or 0.01 Hz, then the tail part will be observed for the dry Specimen. On the Nyquist plot for wet specimens (shown in Figure 4.9 (f)), the semi-circle shows the bulk conductivity of the wet specimens, and the tail part represents the properties of the electrode interfaces. In the case of wet specimens, these two effects are distinguishable on Nyquist Plot.

4.3.3 Repeatability in Measurements and Homogeneity of Mixture observation through Impedance Analysis

For each Specimen of a batch in three different distinguish trials, consistent and repeatable results are obtained from the impedance measurements as shown in Figure 4.9. This repeatability is observed whether the Specimen is either in dry conditions or in wet conditions. Although L1, L2 and L3 are prepared from identical mixing batches of cement and graphite powder, there is still a chance that the graphite powder does not mix homogeneously. And hence the different impedance and resistivity values can be observed for other specimens from a single mixing batch. The error range for the same Specimen in three separate trials is shown in the following Tables. The impedance tables (Table 4.1 and Table 4.3) are prepared using impedance values corresponding to 1-Hz AC Frequency. On the other hand, the phase angle tables (Table 4.2 and Table 4.4) are prepared using phase angle values corresponding to 1-MHz AC Frequency. Table 4.1 and Table 4.2 are for dry Specimen, while Table 4.3 and Table 4.4 are for Wet Specimen.

Table 4.1: Error range for Specimen with Different AC Measurements Trials and Observing the Homogeneity of the mixture (Dry-Impedance)

Specimen	Impedance at 1-Hz (in diff trials)	Average of trials	Standard Deviation	% of error in trials	Average of Mix	Standard Deviation	% of error among specimens				
GP_10 (1)	465217.5	475241	10918	-2.11	1039068.2	1190550.5	-54.26				
	473630.2			-0.33							
	486875.6			2.44							
GP_10 (2)	2397259.5	2406792	8339	-0.39			1039068.2	1190550.5	131.62		
	2410378.9			0.14							
	2412739			0.24							
GP_10 (3)	232935.2	235171	3432	-0.95					1039068.2	1190550.5	-77.36
	233454.8			-0.72							
	239123			1.68							

Table 4.2: Error range for Specimen with Different AC Measurements Trials and Observing the Homogeneity of the mixture (Dry-Phase Angle)

Specimen	Phase at 1-MHz (in diff trials)	Average of trials	Standard Deviation	% of error in trials	Average of Mix	Standard Deviation	% of error among specimens				
GP_10 (1)	63.79	63.75	0.16	0.06	60.08	8.36	6.11				
	63.57			-0.28							
	63.89			0.219							
GP_10 (2)	66.03	65.98	0.20	0.08			60.08	8.36	9.81		
	66.15			0.26							
	65.75			-0.34							
GP_10 (3)	51.11	50.51	0.53	1.17					60.08	8.36	-15.92
	50.07			-0.86							
	50.35			-0.31							

From all the Tables, it is evident that each Specimen in different AC measurement trials shows very close values, and the error range among separate trials for most of the Specimen is less than 2%. From Figure 11, it is obvious that GP_10 (1), GP_10 (2), and GP_10 (3) show different impedance values, especially in dry conditions. This is due to the lack of a homogeneous mixture of graphite powder in cement paste. Table 4 and Table 5 (for dry Specimen) shows % of error among Specimen is relatively high, supporting non-homogeneous mixture assumptions. In this article, only the results of specimen with having 10% graphite by volume of cement paste are shown due to the limitations of pages. However, a similar repetitive

pattern is observed for specimens GP_0, GP_5, GP_15, GP_20, GP_25, GP_30 (graphs are shown in Appendix A).

Table 4.3: Error range for Specimen with Different AC Measurements Trials and Observing the Homogeneity of the mixture (Wet-Impedance)

Specimen	Impedance at 1-Hz (in diff trials)	Average of trials	Standard Deviation	% of error in trials	Average of Mix	Standard Deviation	% of error among specimens		
GP_10 (1)	3160.57	3180.37	18.48	-0.62	4476.86	1710.87	-28.95		
	3183.39			0.09					
	3197.16			0.52					
GP_10 (2)	3837.41	3834.2	63.54	0.08			4476.86	1710.87	-14.35
	3896.07			1.61					
	3769.11			-1.69					
GP_10 (3)	6393.78	6416.01	20.1	-0.34	4476.86	1710.87			43.31
	6432.91			0.26					
	6421.34			0.08					

Table 4.4: Error range for Specimen with Different AC Measurements Trials and Observing the Homogeneity of the mixture (Wet-Phase Angle)

Specimen	Phase at 1-MHz (in diff trials)	Average of trials	Standard Deviation	% of error in trials	Average of Mix	Standard Deviation	% of error among specimens				
GP_10 (1)	22.30	21.24	1.07	4.98	23.14	3.05	-8.21				
	20.16			-5.08							
	21.26			0.098							
GP_10 (2)	21.27	21.51	1.79	-1.116			23.14	3.05	-7.02		
	19.85			-7.72							
	23.41			8.84							
GP_10 (3)	26.69	26.66	0.08	0.102					23.14	3.05	15.23
	26.73			0.24							
	26.57			-0.34							

4.3.4 Summary of AC Impedance Measurements

From the above analysis and discussions, it can be concluded that AC impedance analysis provides with better electrical characterization scope for conductive cement paste. Both bode plot and Nyquist plot obtained from impedance spectra depicted the fairly consistent trend in different measurements trials. It can be used as an essential tool for getting repetitive resistivity values and investigating the homogeneity of a mixture of conductive fillers in a concrete mix.

4.4 Conclusion

In this chapter, a thorough investigation on the electrical properties' measurement methods of conductive cement paste containing graphite powder were experimentally investigated, focusing on both static/DC and AC impedance spectroscopy measurement methods.

Due to the charging effect in DC measurement, the measured resistivity values were not consistent in the case of continuous monitoring. The discontinuous static/DC measurement shows relatively consistent resistivity values over time. However, the magnitudes of static resistivity data vary with the devices and different trials. It is more evident when specimens contain lower concentrations of conductive fillers. In case of higher graphite content, both methods provide consistent resistivity values.

It can be presumed that polarization of charges (charging effects) causes the inconsistent static resistivity of conductive concrete. Notably, at continuous resistivity measurements, charging effects play a vital role and cause an increase in resistivity. Also, the voltage of the current source plays a significant role, and resistivity is affected by its variation. The resistivity is observed to be decrease with the increase in DC voltage. Therefore, the static resistivity measurements using DC are not fully capable of characterizing the electrical properties of conductive concrete, especially when the filler concentration is lower than forming a continuous conductive path.

On the other hand, the Bode plots and Nyquist plots obtained by AC impedance spectroscopy showed consistent results when the moisture condition is identical. These results indicate that the electrical properties of the conductive concrete cannot be represented by a single resistivity value and need to be measured by AC impedance spectroscopy.

Moreover, the AC impedance analysis provides with better electrical characterization scope for conductive cement paste. It can be used as an essential tool for getting repetitive resistivity values and investigating the homogeneity of a mixture of conductive fillers in a concrete mix.

CHAPTER V

ELECTRICAL CHARACTERIZATION AND DEGREES OF SATURATION EFFECTS

5.1 Introduction

Researchers have used different conductive fillers to make regular concrete as conductive. These fillers include carbon fibers, steel fibers, Carbon black, graphite powder, graphene Nano-platelets, carbon micro-fiber, Nano Carbon black, Carbon Nanotube, Carbon Nanofibers, etc. (Chen and Chung 1993; Chen and Chung 1995; Wen and Chung 2005; Baeza et al. 2013; Tyson et al. 2011; Kim et al. 2011; Le et al. 2014; Oskouyi et al. 2014). Among these widely used materials, Graphite powder is more economical and provides better conductivity in cement concrete. In this study, flake-type graphite powder (F-516) will be used as conductive additives in the cement-based composite. It is a thumb rule for almost every additive that it will make the composite more conductive when the additives touch each other inside the specimen and form a continuous conduction network. The volume fraction above which there is a continuous conduction path among the fiber content is known as the percolation threshold (Chung 2003c). Most of the previous researches have determined the percolation threshold for different additives at wet conditions (Al-Bayati et al. 2020; Dehghanpour and Yilmaz 2020b; Dong et al. 2021; Dong et al. 2019; Cholker and Tantray 2019; Ding et al. 2019a; Ding et al. 2019b; Dong et al. 2020a; Sun et al. 2021; Sun et al. 2017). Hence, this study will determine the percolation threshold for graphite powder by the cement paste volume for specimen at both dry and wet conditions.

One of the most critical factors that significantly influence the conductivity of concrete is the presence of moisture inside specimens. It is widely known that the moisture in concrete increases the conductivity of concrete (Demircilioğlu et al. 2019). Therefore, controlling moisture conditions is an essential part of understanding the electrical properties of concrete. Most researchers measured the electrical resistivity right after finishing the curing period of concrete or at the surface saturated dry (SSD) conditions (Al-Bayati et al. 2020; Dehghanpour and Yilmaz 2020a; Dong et al. 2021; Dong et al. 2019; Sun et al. 2021; Cholker and Tantray 2019; Ding et al. 2019a; Ding et al. 2019b; Dong et al. 2020a; Dong et al. 2020b; Kwon et al. 2019; Papanikolaou et al. 2020; Zhu et al. 2019; El-Dieb et al. 2018; Sassani et al. 2017; Yoo et al. 2017; Dong et al. 2014a; Dong et al. 2016a; Dong et al. 2018; Demircilioğlu et al. 2019). Some researchers investigated the electrical properties at different dry conditions such as 1, 2, 3, 15, 16, 18, 30, 56 air dry (Segura et al. 2019; Nguyen et al. 2019; Fulham-Lebrasseur et al. 2020; Zhang et al. 2019; Sun et al. 2017), oven-dry for 24 hr. at 70°C or lesser temperature (Nguyen et al. 2019; Zhang et al. 2019; Li et al. 2016).

However, to make the concrete specimen fully dry and observe its electrical properties at that conditions, generally, it needs to be put inside the oven/ or some other places at a higher temperature than the boiling point of water. In this research, specimens were made fully dry by keeping them inside the oven for 48 hrs. at 110°C. Additionally, during the electrical properties' measurement, the moisture was controlled through the plastic wrapping of the whole specimen both in SSD conditions and in dry conditions.

Different moisture levels inside the concrete provide different conduction properties (del Moral et al. 2021; Demircilioğlu et al. 2019; Zhang et al. 2019). Hence, the electrical properties variation with different degrees of saturation level is worthy of investigating.

This section aims to characterize the electrical property of graphite added conductive cement paste using AC Impedance Spectroscopy. In this regard, the study will experimentally investigate the effect of graphite content in cement composite. It will also determine the percolation threshold of graphite powder for both dry and wet specimens. Moreover, the effect of moisture, and the effect of degree of saturation (DOS) on the resistivity of conductive cement paste will be investigated thoroughly using both DC and AC impedance spectroscopy. It should be noted that the moisture level was appropriately controlled throughout the experimental work, whether the specimen is either in wet (saturated surface dry, SSD) or in dry (48 hours oven dry) conditions.

5.2 Investigating the Effect of Graphite Content

In this study, graphite powder is used as conductive additives with varying volume content in cement paste. The volume fraction varied from 0% (control specimen), 5%, 10%, 15%, 20%, 25% and 30%. The graphite powder's volume was measured with respect to the volume of cement paste. Since the initial investigation on this research depicted that moisture plays a significant role in the electrical resistivity of conductive cement paste, the effect of graphite was investigated for the Specimen both at dry and wet conditions. For each graphite content and also for the control mixture (0% GP), three specimens were prepared, and each Specimen was tested at three different trials. Among these nine representatives and repetitive data, only one data for each mixture is shown in the following Figures to understand the graphite effects better.

5.2.1 Graphite effects on dry Specimens

In Figure 5.1, 5.2 and 5.3, the effect of graphite content on dry cement-paste specimens is shown. It is evident from Figure 5.1 that the control specimen (0% graphite) is showing higher impedance/resistivity values throughout the AC frequency ranges compare to all other specimens. The value is much higher (more than 10^{11} Ω -cm) at lower AC frequency ranges. Figure 5.1 also shows that adding graphite powder in cement paste significantly affects the electrical properties. The increase in graphite content reduces the electrical resistivity when the Specimen is in dry conditions.

Both control specimen and 5% graphite specimen shows a decrease in impedance value with the increase in AC frequency. The fundamental of AC Impedance Spectroscopy implies that both capacitance and inductance have a relationship with AC frequency. In general, capacitance has an inverse relationship with AC frequency, and it reduces when the Frequency increases. In contrast, inductance has a proportional relationship with AC frequency, and it increases when the Frequency also increases. Since these specimens' impedance reduces with AC frequency, they certainly have a capacitance effect inside them at dry conditions.

Specimen with 10% graphite content shows a constant impedance value up to 100000 Hz AC frequency, and beyond that, it decreases. Specimen with 15% or more graphite content, the impedance is almost constant throughout the Frequency ranges, indicating negligible or no capacitance effect. Thus, by increasing the graphite content, the capacitance effect can be eliminated especially, when the Specimen is in dry conditions. This statement is validated by Figure 5.2, which depicts the phase angle variation with different Frequency ranges for distinguished conductive specimens at dry conditions.

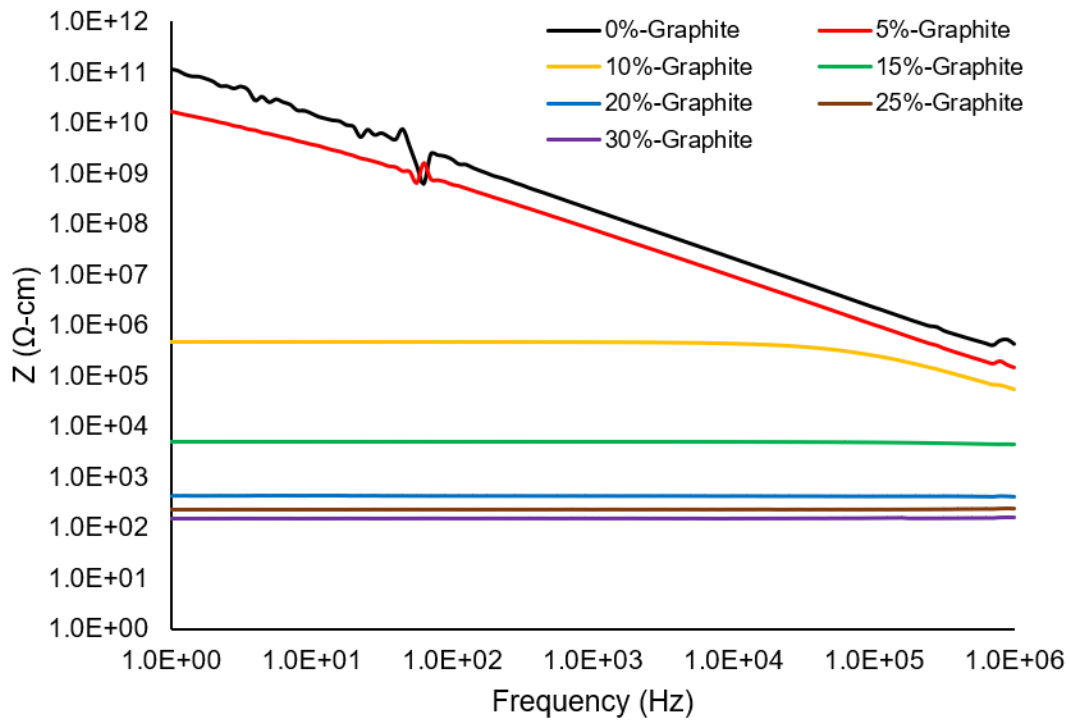


Figure 5.1: Impedance variation with AC frequencies of All Specimens at Dry Conditions

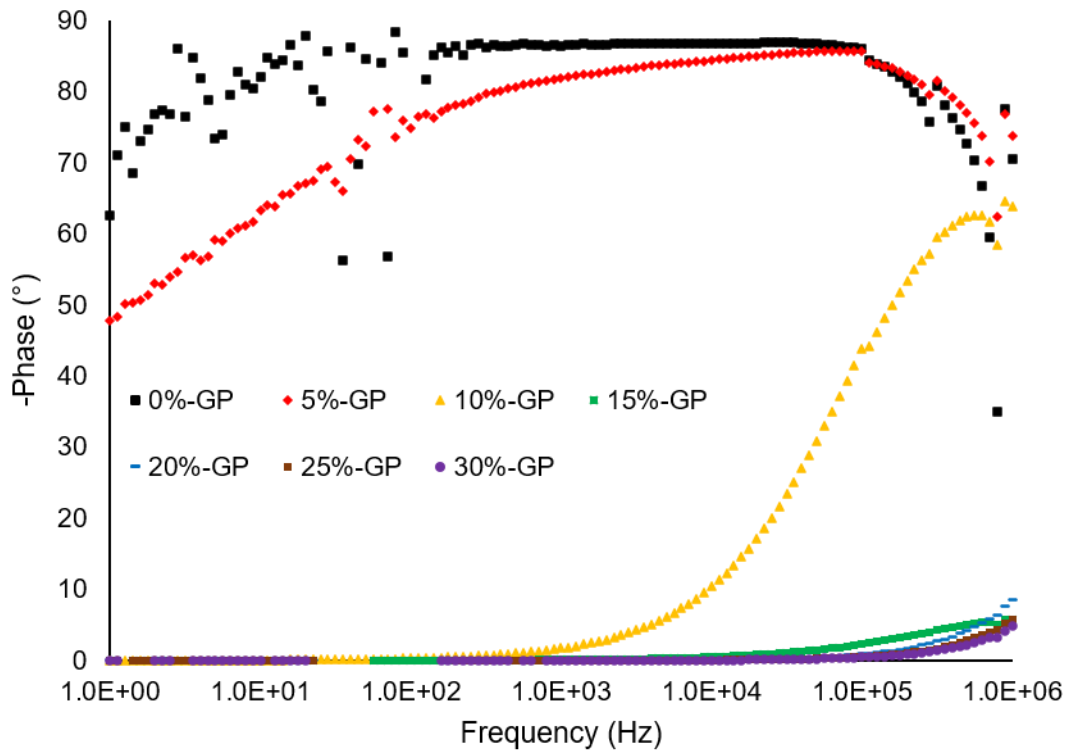


Figure 5.2: Phase angle variation with AC frequencies of All Specimens at Dry Conditions

In the control specimen and 5% graphite specimen, the phase angle is much higher, and it ranges from 70° to 85° (as shown in Figure 5.2). Moreover, it remains at this range (70° to 85°) throughout the frequency swaps, indicating higher capacitance characteristics of the Specimen. However, the Specimen with 10% graphite or more shows relatively lower phase angle values. With the increase in graphite content in cement paste, the phase angle is significantly reduced. For some specimens, at Frequency ranges up to 100000 Hz, the phase angle value has reached almost zero.

The Nyquist plot shown in Figure 5.3 depicts the variation of real and imaginary impedance for Specimens (having different graphite content) at dry conditions. For the control specimen, both real and imaginary impedance values are observed as much higher than all other specimen types. Moreover, on the Nyquist plot, only half of the semi-circle is visible, representing the bulk resistivity of cement paste. Almost a similar Nyquist plot is observed for Specimen with 5% graphite content. For these two specimen sets, if the AC frequency ranges are reduced to 0.1 Hz or 0.01 Hz, the whole semi-circle might be observed, and the electrode-interface portion would be noticeable.

In the case of Specimen with 10% graphite content, an apparent semi-circle is observed, indicating a proper combination of capacitance and resistance characteristics inside the Specimen. Both real and imaginary impedance value is observed as much lower compared to the control specimen. Specimen with 15% or more graphite content has the lowest real and imaginary impedance values, indicating that both of these values are reduced significantly with a higher amount of graphite. Additionally, Nyquist plots for these specimens are consist of a part of the semi-circle, not the whole. It is evident from the plot that if the AC frequency ranges are increases to 10 MHz or more, then the full semi-circle will be observed.

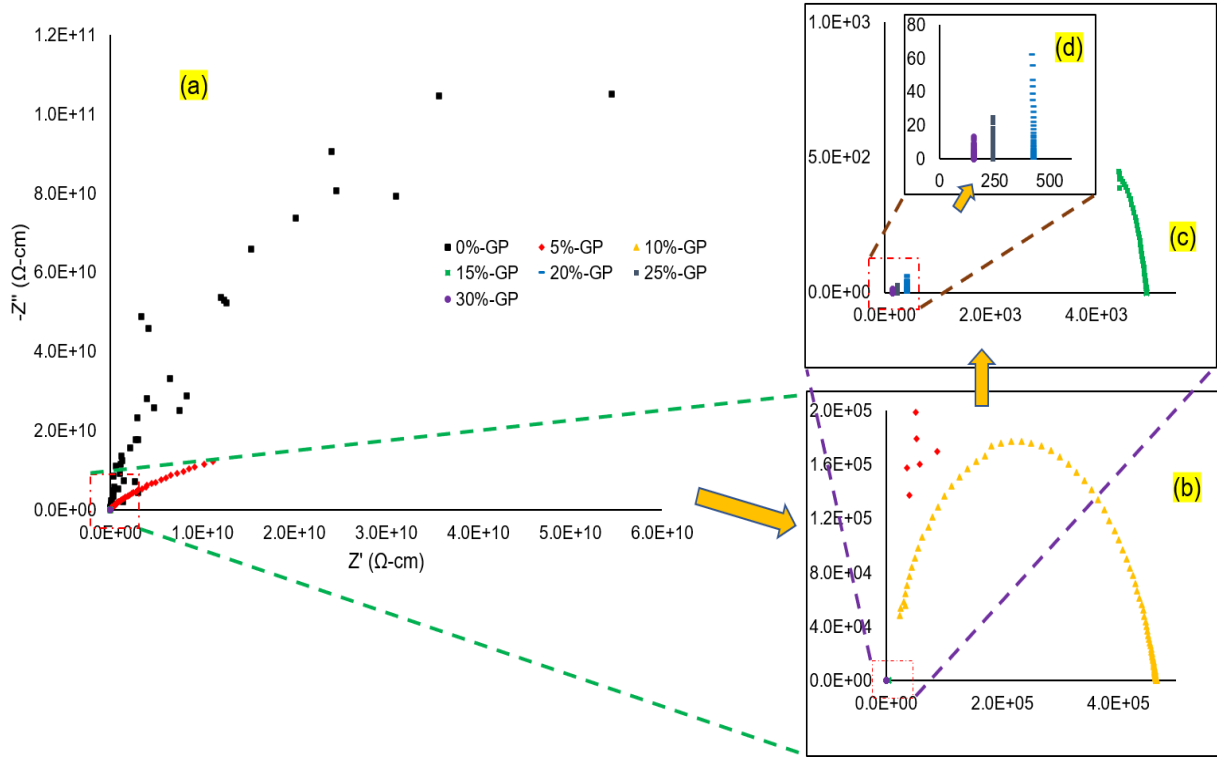


Figure 5.3: Nyquist plot showing Real and Imaginary impedance variation of All Specimens at Dry Conditions.

Moreover, the Specimen with 20% or more graphite content shows almost a fixed resistance value, and only the capacitance is changing with Frequency at a significantly slower rate. The observed maximum capacitance value is very lower and can be neglected. This characteristic indicates that Specimen with higher graphite content has an almost negligible capacitance effect inside it.

5.2.2 Graphite effects on wet Specimens

In Figures 5.4, 5.5 and 5.6, the effect of graphite content on wet cement-paste specimens is shown. It is evident from these figures is that adding graphite powder has a significant impact on wet cement paste's electrical properties. Adding more graphite powder in cement paste reduces the impedance (as shown in Figure 5.4) of the wet Specimen. The main contrast of wet specimens with dry specimens is that the impedance value decreases with the AC frequency increases for every mixture type. This characteristic indicates the wet Specimen always contains some capacitance inside it, whatever the graphite content is. Our study with dry Specimens shows that having higher concentrated graphite powder in cement paste eliminates the capacitance effect.

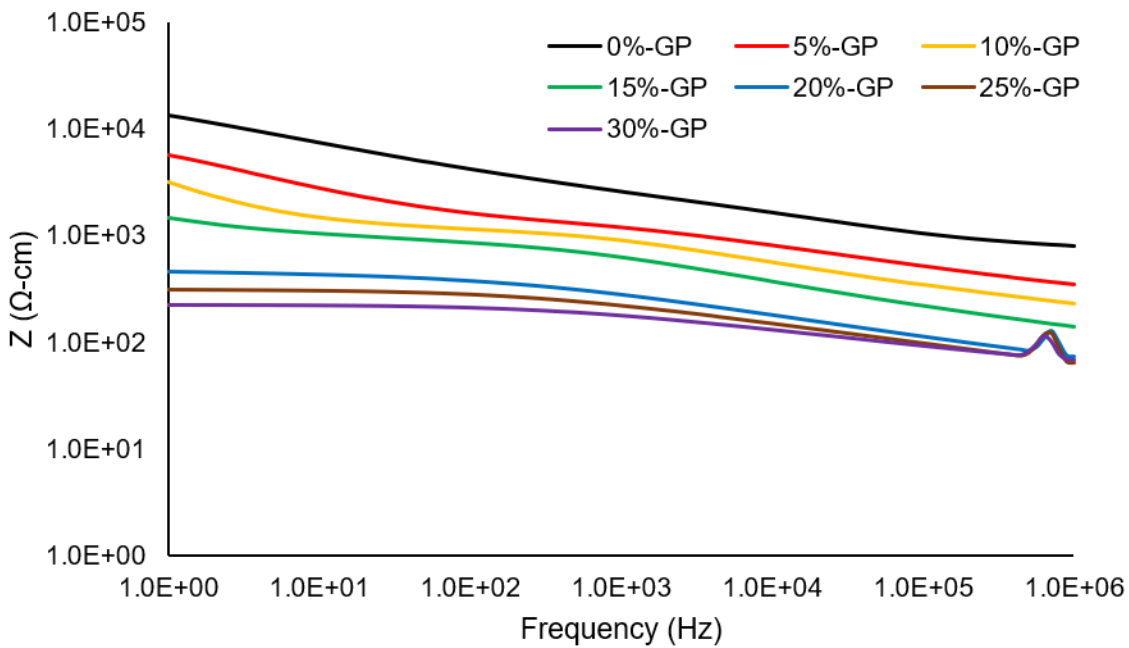


Figure 5.4: Impedance variation with AC frequencies of All Specimens at Dry Conditions

The phenomenon observed for the wet Specimen is due to the presence of moisture inside it that causing a constant capacitance effect. It is more apparent from the phase angle variation

with graphite content graph (Figure 5.5) for the wet Specimen. When the AC frequency is above 10 Hz, there is a phase angle for every specimen type and varies from 5° to 30°. For some specimen types (control specimen, 5%, and 10% graphite contents specimens), the phase angle is higher at low AC frequency. It reduces with Frequency increases up to a specific limit and then increases again. For Specimen with having 15% or more graphite content, the phase angle increases with AC frequency.

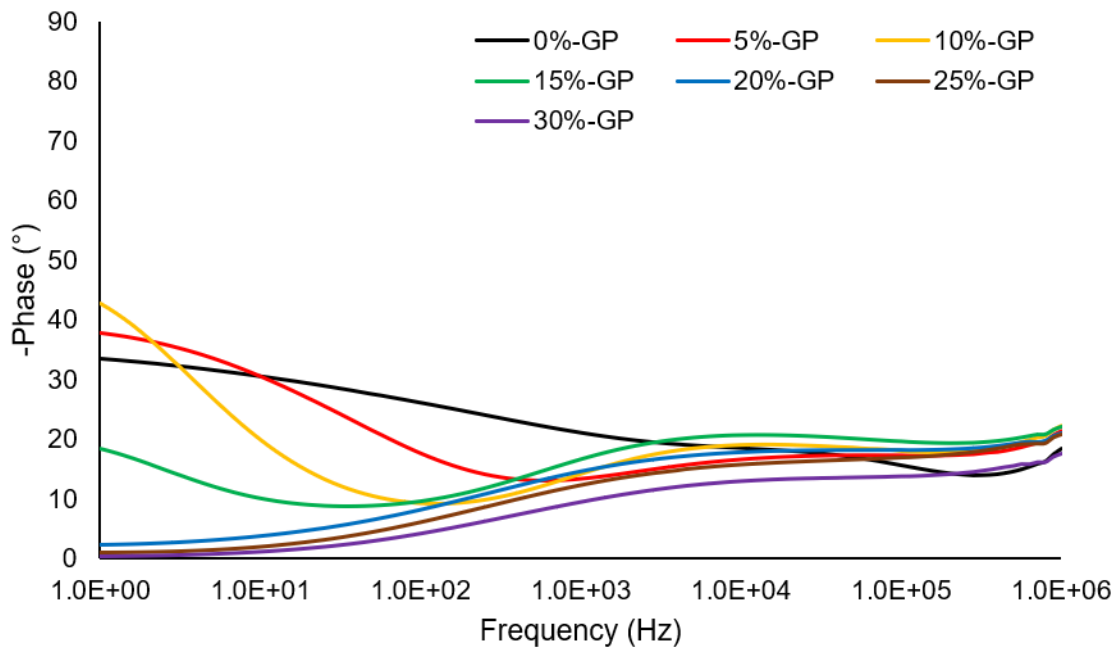


Figure 5.5: Phase angle variation with AC frequencies of All Specimens at Dry Conditions.

Nyquist plots shown in Figure 5.6 depict that at wet conditions, the number of semi-circles representing the variation of real and imaginary impedance is more compared to specimens at dry conditions. For every Specimen, the semi-circle is visible, indicating a mixture of capacitance and resistance at wet conditions, even though it has a higher amount of graphite. Both control specimen and Specimen with less than 15% graphite content show the electrode-interface behavior at the measured AC frequency ranges from 1 Hz to 1 MHz. On the contrary,

in the higher graphite content specimens, the electrode-interface behavior is not visible from the Nyquist Plot. For wet specimens, the higher number of semi-circles suggests that the conduction mechanism of wet Specimen is different from dry specimens. It contains more complex circuit elements inside it than the dry specimens have.

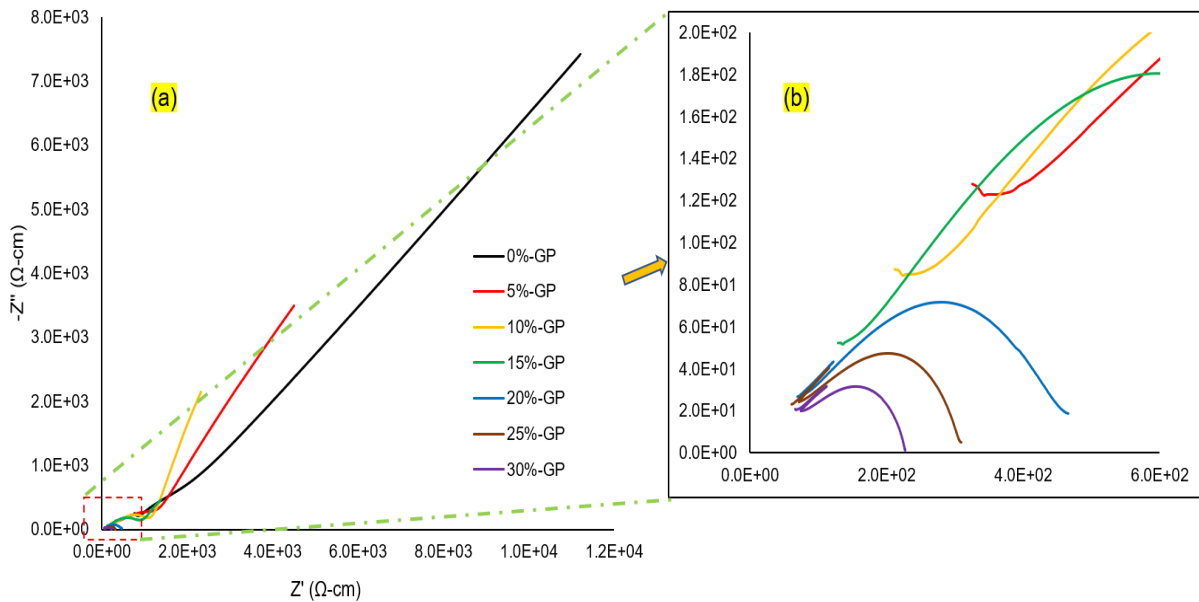


Figure 5.6: Nyquist plot showing Real and Imaginary impedance variation of All Specimens at Dry Conditions.

5.2.3 Summary of the Effect of Graphite content

This section investigates the effect of graphite content for wet and dry specimens with different amounts of graphite powder in cement paste. It has been found that the effect of graphite powder is noticeable for specimens in both conditions. In dry specimens, both the impedance and the capacitance effect inside the cement paste are reducing with the addition of graphite powder. The Nyquist plot tends to show a fixed resistance value for higher concentrated graphite content while changing a slight capacitance value. In the case of the wet specimens, the

impedance observed was significantly lower than the dry specimens, and it decreases with the increase of graphite content in cement paste. However, the impedance reduction rate for dry specimens is much higher than for wet specimens. Moreover, there is always present the capacitance behavior inside the conductive cement paste in wet conditions even for higher concentrated graphite additives. The reason could be attributed to the presence of moisture inside it that playing a vital role in these characteristics.

5.3 Determining the Percolation Threshold of Graphite Powder

The minimum amount of conductive additives/fillers requires to form a continuous conductive network inside the Specimen is known as the percolation threshold. Beyond this threshold, the resistivity remains almost constant with an increase of filler content. Most of the previous researchers tried to determine the percolation threshold of conductive cement composite just after removing it from curing, which means when the Specimen is in SSD (wet) conditions. This study will experimentally investigate the percolation threshold of graphite powder for both dry and wet specimens. In this regard, a total of 7 mixture types specimens were prepared with varying graphite content of 0%, 5%, 10%, 15%, 20%, 25% and 30% by volume of cement paste, and then impedance was measured for both dry and wet specimens.

The impedance value observed for dry and wet Specimens at 1-Hz AC frequency is selected and plotted against graphite content. For each graphite content, a total of 9 data points is obtained from the impedance analysis (For each mixture type, three specimens were prepared, and three different AC impedance analyses had been performed). Then the average of these 9 data points is determined, representing the approximate resistivity of that mixture type. After

that, the average impedance was plotted with their corresponding graphite content in Figure 5.7 for dry Specimens and in Figure 5.8 for wet Specimens.

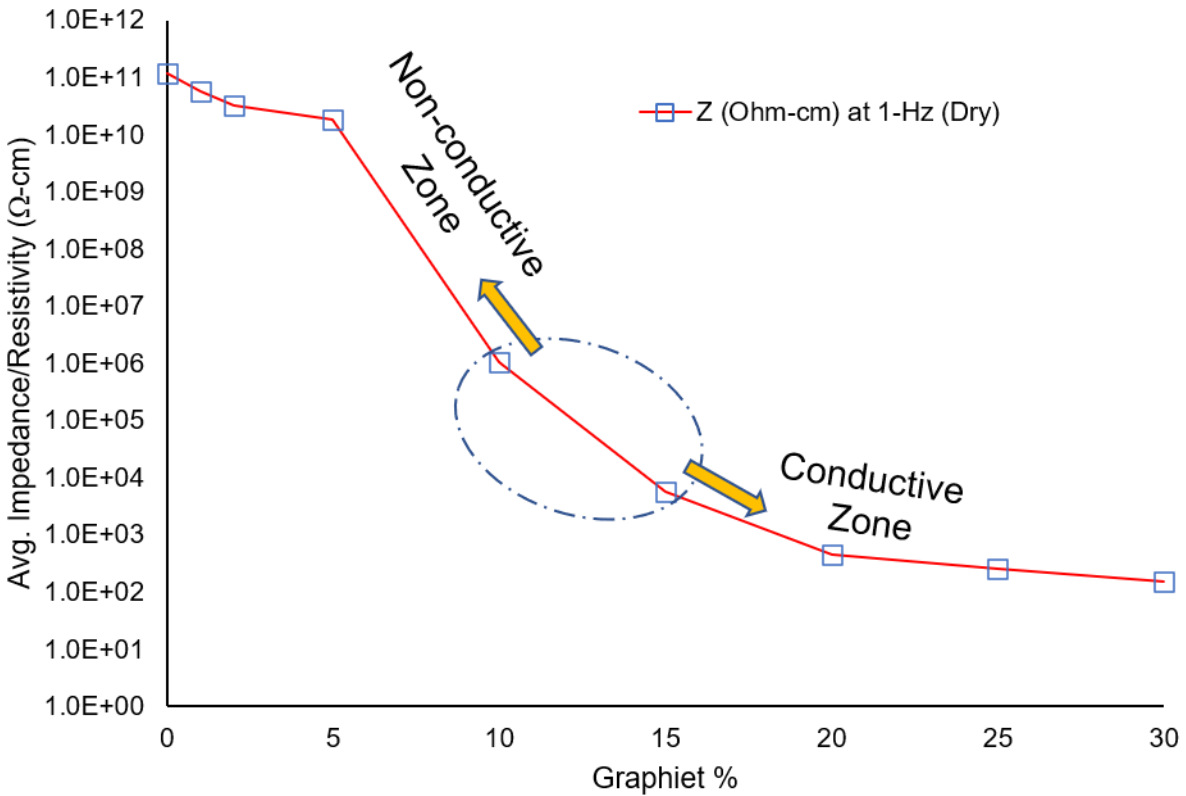


Figure 5.7: Impedance (Resistivity) variation with graphite content at Dry conditions.

The percolation threshold is observed between 15%-20% by cement paste volume in dry and wet conditioned specimens. In addition, it has been observed from Figure 5.7, and Figure 5.8 is that the rate of decrease in impedance is much higher for dry specimens compared to the wet specimens. For graphite content varying from 0%-30%, impedance for dry specimens varies from 10^{11} (Ω -cm) to 10^2 (Ω -cm), and for wet specimens the impedance varies from 10^4 (Ω -cm) to 10^2 (Ω -cm).

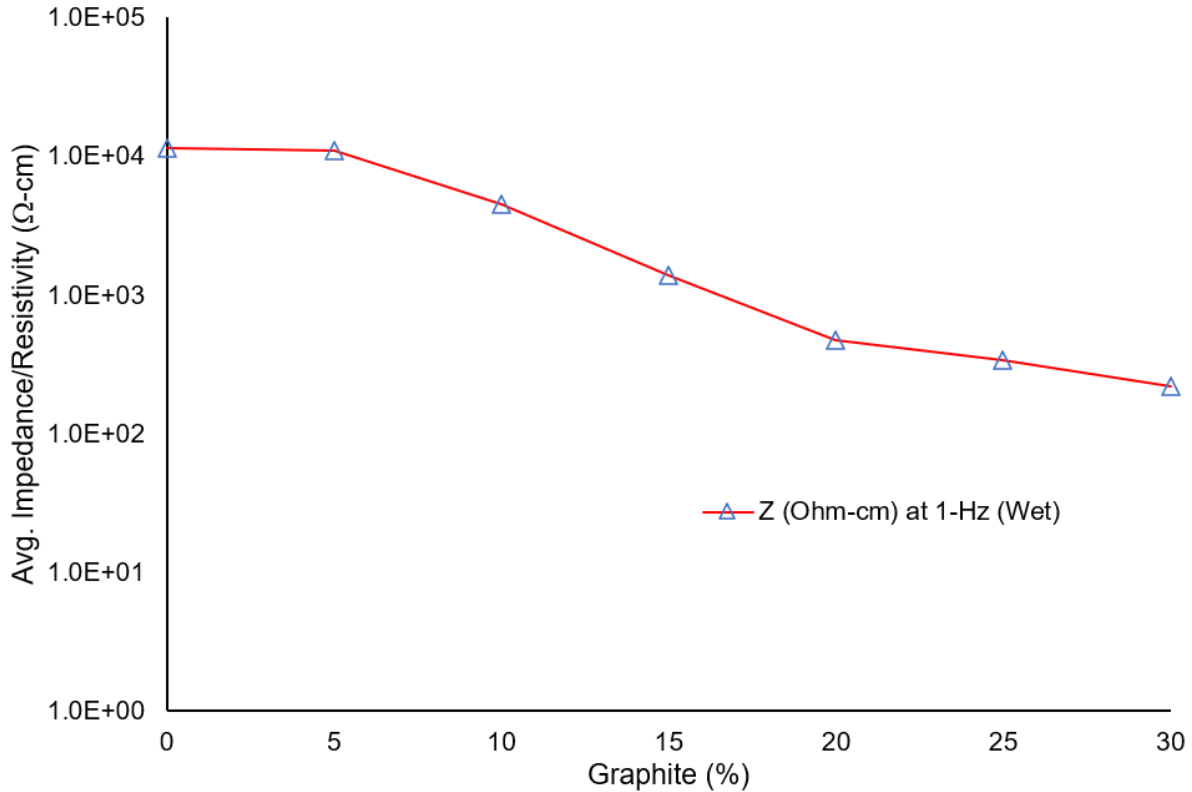


Figure 5.8: Impedance (Resistivity) variation with graphite content at Wet conditions.

5.4 Investigating the Effect of Moisture and Degree of Saturation

5.4.1 Effect of Moisture

As expected, cement paste's moisture condition substantially influences both static resistivity and AC impedance of Specimen L (10% graphite by cement paste volume). The wet (SSD) resistivity/impedance is approximately four orders lower than the dry ones. In the case of impedance measurements, the dry Specimen's average impedance is 1.04×10^7 (Ω -cm), while the wet Specimen's average impedance is 4.5×10^3 (Ω -cm) at low (1-Hz) frequency. At high frequency, the dry Specimen's impedance is 5.4×10^4 (Ω -cm), while the wet Specimen's impedance is 3.5×10^2 (Ω -cm) (dry values obtained from Figure 5.1 and wet values obtained

from Figure 5.4). The ions in cement paste can move when the pores and capillaries are filled with water, and such ionic movements provide another conduction mechanism in cement paste.

The phase angle for the dry Specimen is increased with frequency, and a wide variation is observed, ranging from 0° to 65° . The phase angle decreases with frequency increases for the wet Specimen, and the variation was not linear, ranging from 45° to 21° . The average phase angle for the dry Specimen at 1-MHz AC frequency is observed as 60° , while at the lower frequency, it is almost zero. On the other hand, the average phase angle for the wet Specimen at 1-MHz frequency is observed as 23° , while at the lower frequency, it is close to 45° (dry values obtained from Figure 5.2 and wet values obtained from Figure 5.5).

5.4.2 Investigating the Effect of Degree of Saturation

Static resistivity and AC impedance for wet specimens represent that moisture plays a significant role in the electrical properties of conductive cement paste. Hence, it is worth investigating how these properties vary with different levels of moisture or commonly known as degrees of saturation (DOS). For this investigation, the Specimen was made fully saturated, and then moisture was removed from the Specimen in different ways such as air dry, oven heating. The summary of the moisture content, degree of saturation of specimens are shown in Table 5.1. Both static resistivity and AC impedance variation was observed at different moisture levels/conditions.

Table 5.1: Moisture level and corresponding DOS of Specimens

Trials	1	2	3	4	5	6	7	8	9	10
GP_0 (1) (0% graphite)										
Moisture	55.71	51.99	45.20	37.40	32.57	26.44	20.07	15.11	4.89	0.00
Moisture (%) with compare to dry weight of specimen	30.80	28.74	24.99	20.68	18.01	14.62	11.10	8.35	2.70	0.00
Degree of Saturation (%)	100.00	93.32	81.13	67.13	58.46	47.46	36.03	27.12	8.78	0.00
GP_15 (1) (15% graphite)										
Moisture	50.49	46.00	40.23	33.73	28.40	21.27	15.89	11.23	3.94	0.00
Moisture (%) with compare to dry weight of specimen	26.25	23.92	20.92	17.54	14.77	11.06	8.26	5.84	2.05	0.00
Degree of Saturation (%)	100.00	91.11	79.68	66.81	56.25	42.13	31.47	22.24	7.80	0.00
GP_20 (3) (20% graphite)										
Moisture	53.93	41.34	34.84	27.73	22.55	17.08	12.93	10.15	5.87	0.00
Moisture (%) with compare to dry weight of specimen	28.42	21.78	18.36	14.61	11.88	9.00	6.81	5.35	3.09	0.00
Degree of Saturation (%)	100.00	76.65	64.60	51.42	41.81	31.67	23.98	18.82	10.88	0.00

5.4.2.1 Investigating DOS effect through AC Impedance Measurement. The

Specimen with no graphite (0% by volume of cement paste) has shown higher impedance values when there is no moisture/ the Specimen is at dry conditions. With the increase of moisture, the impedance is decreasing.

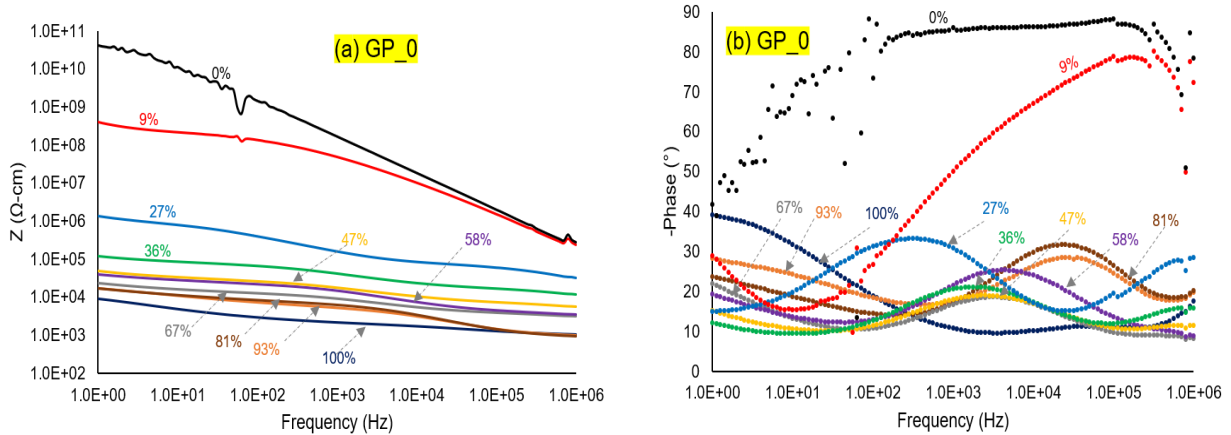


Figure 5.9: Bode Plot showing (a) Impedance and (b) Phase Angle variation with different degrees of saturation of Specimen GP_0 (1) (0% graphite).

At dry conditions, the rate of impedance change is much higher with the increase of frequency (as shown in Figure 5.9 (a)), indicating a higher capacitance effect at these conditions. This rate decreases with the addition of moisture levels. At dry conditions, the phase angle is also showing higher values. At almost 90% dry conditions, the phase angle is closed to dry phase angles at higher frequencies. Specimen containing 10% or more moisture shows almost a similar variation in phase angle and their ranges are practically the same (as shown in Figure 5.9 (b)).

The effect of moisture variation is understandable from the imaginary vs. real impedance variation graph (as shown in Figure 5.10). The bulk-cement effect, moisture effect, and electrode-interface effects are clearly distinguishable from the graphs at higher moisture levels. Nyquist plots consist of multiple semi-circles at higher moisture levels. With the decrease of

moisture level, the semi-circle radius of the Nyquist plot tends to increase, indicating the increase in both real and imaginary impedance. However, the number of semi-circles is decreasing with the decrease in moisture level. The tailing effect is starting to disappear at the measurable frequency ranges (1 Hz to 1 MHz) with the reduction of moisture levels. However, if the measurement frequency ranges can increase to 0.1 Hz or 0.01 Hz, tailing behavior can be observed. Almost the same phenomenon is observed for GP_0 (2) and GP_0 (3) specimens prepared from the same mix containing 0% graphite powder in the cement paste.

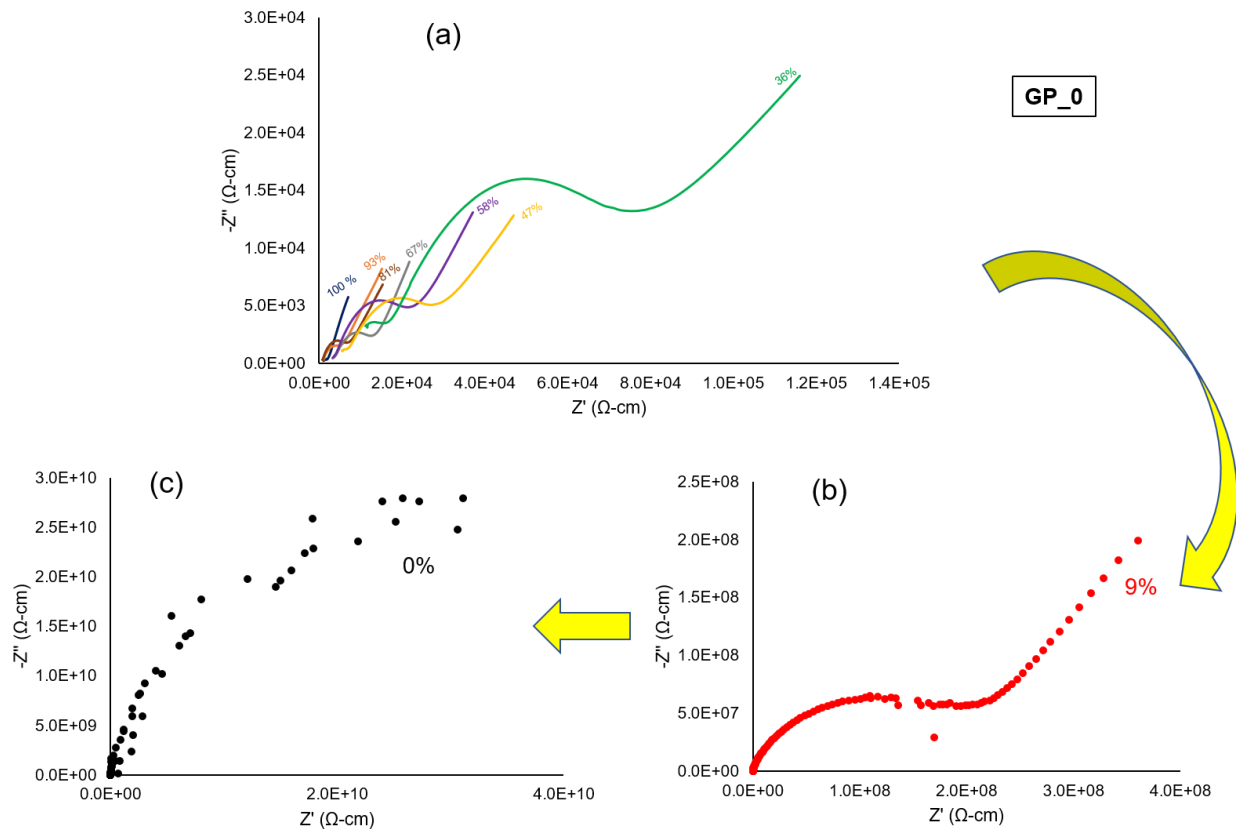
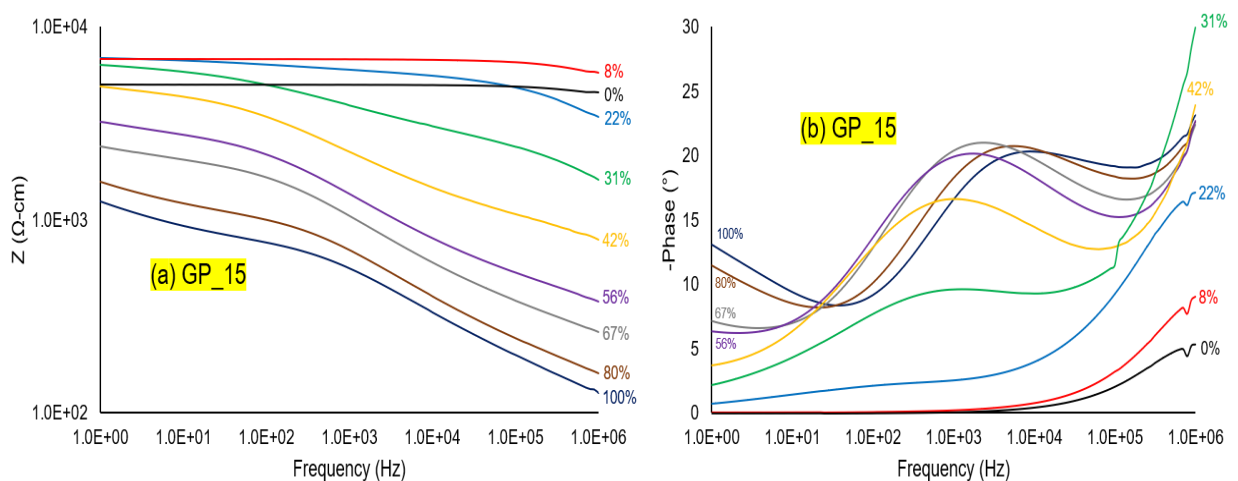


Figure 5.10: Nyquist Plot showing Imaginary and Real Impedance variation with different degrees of saturation of Specimen GP_0 (0% graphite)

The Specimen with 15% graphite shows that at a higher degree of saturation, the impedance is lower, and with the decrease of DOS, the impedance increases up to a certain level.

When the DOS decreases to 10%, the impedance reaches the maximum level. DOS lower than 10% or when the Specimen is closing without moisture ranges, the impedance decreases (as shown in Figure 5.11 (a)). This phenomenon is repetitively observed for other specimens (GP_15 (2) and GP_15 (3)) of the same mixture (15% graphite by cement paste volume). The reason can be attributed to the reduction of capacitance effect. Figure 5.11 (b) shows that DOS lower than 10%, the phase angle is significantly smaller, and up to 10000 Hz of AC frequency. It is almost negligible, which implies that there is almost no capacitance effect at dry conditions.

The Nyquist plot is shown in Figure 5.11 (c), depicting that the number of semi-circles disappears sequentially with the decrease of moisture content. Moreover, both imaginary and real impedance increases with the reduction of moisture content. However, at moisture content less than 20%, the Nyquist plot tends to be just a part of a semi-circle instead of representing the whole. The imaginary and real impedance are also started decreasing at lower moisture levels. It can be seen from Figure 5.11 (c) that at no moisture level, both real and imaginary impedance is lower than that of moisture level 22%. Almost the same phenomenon is observed for the rest of the specimens (GP_15 (2) and GP_15 (3)) prepared from the same mix containing 15% graphite powder in the cement paste.



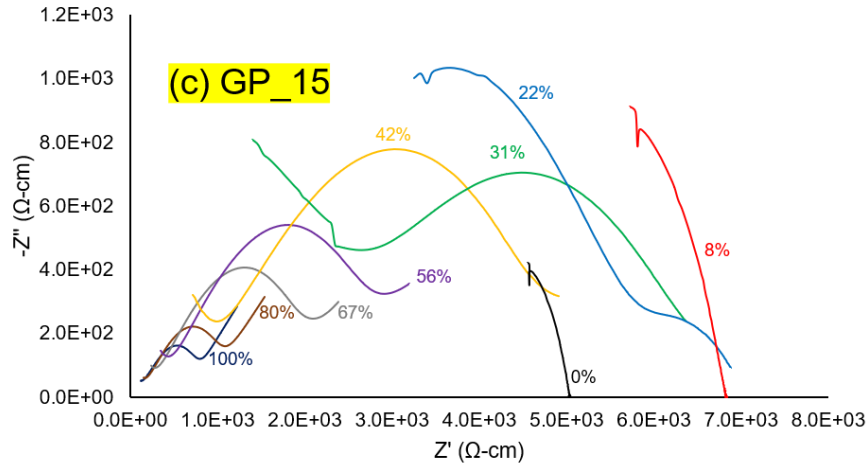


Figure 5.11: (a) Impedance (Bode Plot), (b) Phase Angle, and (c) Imaginary vs. Real Impedance (Nyquist Plot) variation with different degrees of saturation of Specimen GP_15 (15% graphite)

Specimen with 20% graphite powder shows almost a similar impedance behavior observed for Specimen with 15% graphite. The Bode plot (as shown in Figure 5.12 (a)) depicts that there is minimal effect of moisture at lower frequency ranges. The impedance value observed at this range is almost close enough, and a very slight difference is observed. When the moisture level is less than 30%, the impedance remains nearly constant with the increase of frequency. Beyond that moisture levels, impedance started to decrease with AC-frequency. The effect of the degree of saturation is more tangible in the case of phase angle variations. With the increase of DOS, phase angle increases, and at no moisture level, the phase angle is almost in a negligible range, especially up to 100000 Hz AC-frequency.

Nyquist plot (as shown in Figure 5.12 (c)) depicts almost the similar phenomena observed for Specimen with 15% graphite content. The number of semi-circles disappears with the decrease of moisture content. At moisture levels between 11-24%, both the real and imaginary impedance increases more rapidly, and lower than 11%, impedance started to

decrease. Moreover, the impedance value observed for this Specimen at any moisture level is much lower than compared to other specimens.

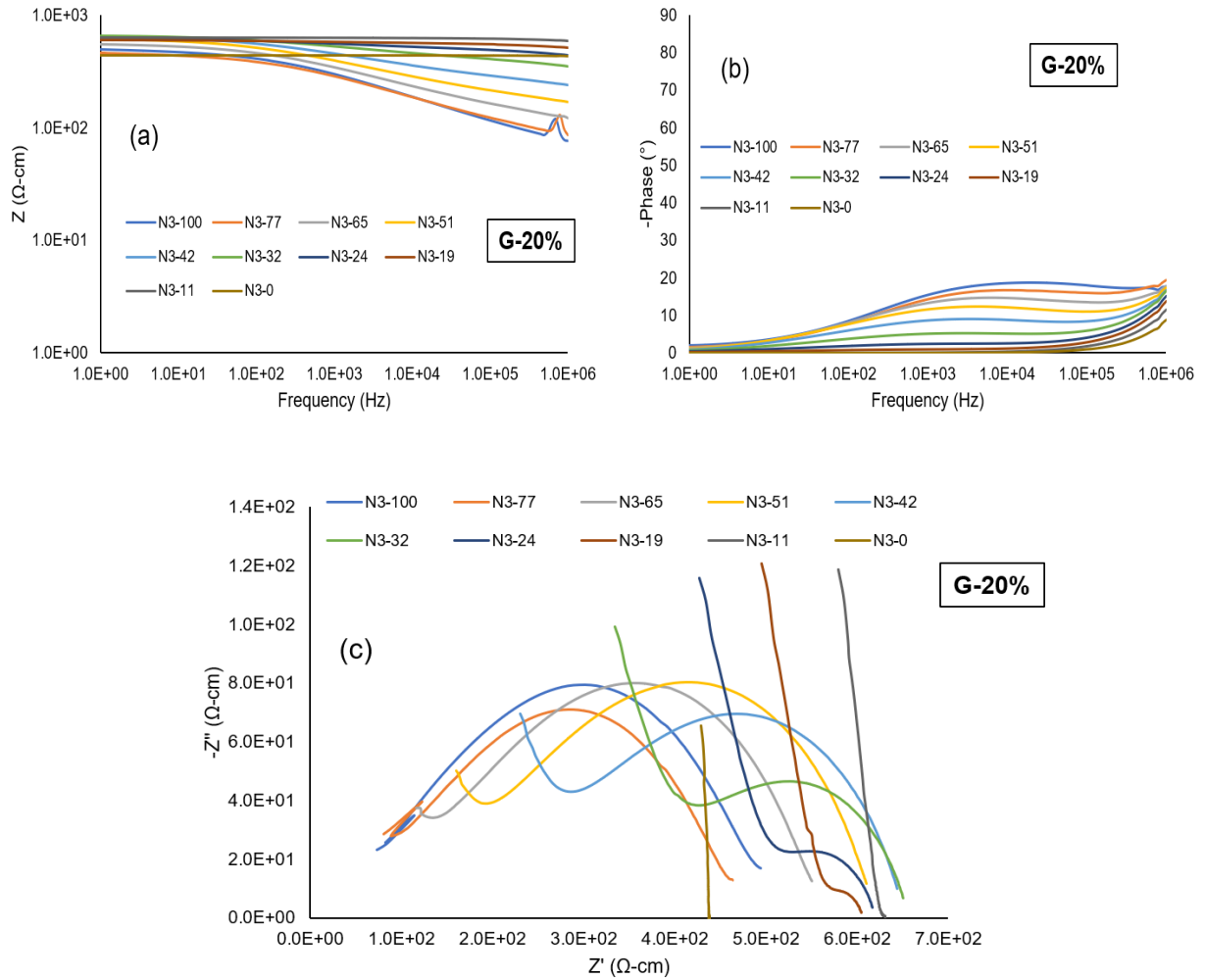


Figure 5.12: (a) Impedance (Bode Plot), (b) Phase Angle, and (c) Imaginary vs. Real Impedance (Nyquist Plot) variation with different degrees of saturation of Specimen GP_20 (20% graphite).

5.4.2.2 Investigating DOS effects through DC measurements. This section investigates the effect of the degree of saturation on the electrical properties of conductive concrete using discontinuous static resistivity measurements.

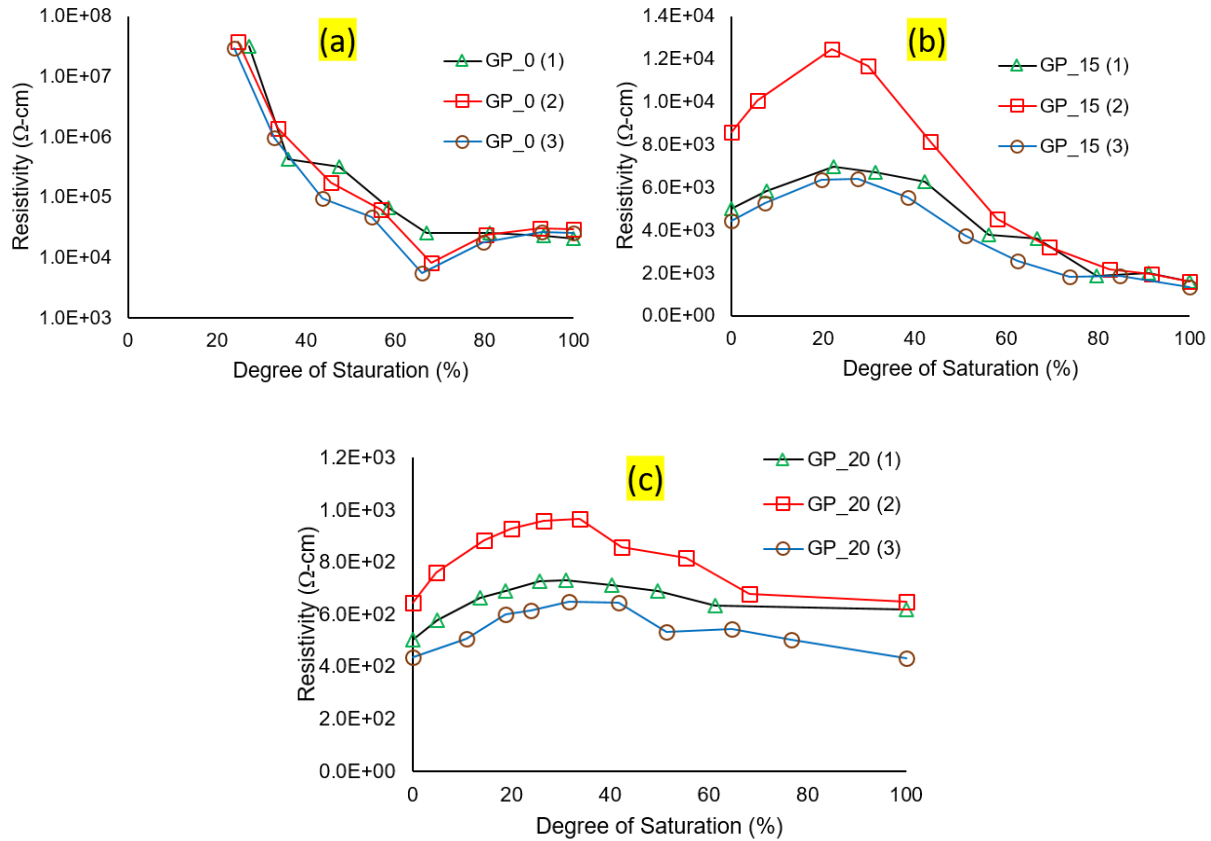


Figure 5.13: Static/DC Resistivity variation with different degree of saturation of (a) Specimen GP_0 (0% graphite) (b) Specimen GP_15 (15% graphite) (c) Specimen GP_20 (20% graphite).

Figure 5.13 (a), the Specimen with 0% graphite, shows that the static resistivity increases with the decrease of degree of saturation. All three Specimens (GP_0 (1), (2), (3)) from this mixture exhibit a similar phenomenon. However, it was not possible to measure the resistivity values when DOS was lower than 20%. The resistivity values of the control specimen beyond that DOS limit are too high to the further side of measurement ranges of the device.

Specimen with 15% graphite (as shown in Figure 5.13 (b)) shows that with the decrease of DOS, static resistivity increases, and when it's starts becoming lower than 30%, the resistivity started to decrease. This trend was evident for the rest of the specimens and even Specimen with

20% graphite (as shown in Figure 5.13 (c)). However, in the specimen set N, the dry resistivity (at 0% DOS) and wet resistivity (at 100% DOS) are almost the same. In dry conditions, the conduction is due to the graphite particle. Whereas in the wet condition, the conduction is due to both moisture and graphite. Generally, wet resistivity is supposed to be lower than dry. Still, in this case, it is mainly affected by multiple factors such as capacitance and purity of water, which disable reducing resistivity.

5.4.3 Summary of the effect of moisture on Electrical properties of conductive concrete

Moisture plays a very significant role in the electrical properties of conductive concrete. It is evident from both DC and AC measurements that electrical resistivity increases with the decrease in DOS up to a certain level. For some specimens, this level is observed as 20% or lower than that. Below this DOS, electrical resistivity started to decrease, and this can be attributed to the reduction in capacitance effect provided by moisture.

5.5 Conclusion

In this chapter, the electrical characterization of conductive cement composite containing graphite powder has been performed through AC impedance spectroscopy. The study investigated the effect of graphite content for wet and dry specimens with different amounts of graphite powder in cement paste. It has been found that the effect of graphite powder is noticeable for specimens in both conditions.

In dry specimens, both the impedance and the capacitance effect inside the cement paste are reducing with the addition of graphite powder. The Nyquist plot tends to show a fixed resistance value for higher concentrated graphite content (20% or more) while changing a slight capacitance value.

In the case of the wet specimens, the impedance observed was significantly lower than the dry specimens, and it decreases with the increase of graphite content in cement paste. However, the impedance reduction rate for dry specimens is much higher than for wet specimens. Moreover, there is always present the capacitance behavior inside the conductive cement paste in wet conditions even for higher concentrated graphite additives. The reason could be attributed to the presence of moisture inside it that playing a vital role in these characteristics.

The results show that the percolation threshold for graphite added cement paste is between 15%-20% by cement paste volume for both wet and dry specimens.

The results also show that moisture plays a significant role in electrical resistivity measurement. For every test, Dry specimens show higher resistivity than wet specimens, as expected. It is evident from both DC and AC measurements that electrical resistivity increases with the decrease in DOS up to a certain level. For some specimens, this DOS level is observed as 20% or lower than that. Below this DOS, electrical resistivity started to decrease, and this can be attributed to the reduction in capacitance effect provided by moisture.

CHAPTER VI

ELECTRICAL EQUIVALENT CIRCUIT OF CONDUCTIVE CONCRETE

6.1 Introduction

AC impedance spectroscopy can be used for qualitative evaluation of the microstructure and electrical properties of the cement-based composite. However, the electrical mechanism in cement composite becomes very complicated when it is subjected to electrical voltage. These complex electrochemical systems can be a combination of parallel or series connections of resistor, capacitor, and inductor.

The conductive cement composite comprises different additives, solids, liquid interfaces, minerals, and chemical components that can depict distinct electrical properties. These electrical properties can be represented by the mixture of different circuit elements inside it. Researchers have proposed several circuit models to represent the microstructural properties of cement-based materials. As per the authors' investigation, very few researchers have proposed equivalent circuit models for conductive cement composite.

This study aims to offer electrical circuit models for cement composite with conductive graphite powder additives. Moreover, previous studies on electrical equivalent circuits for cement-based materials failed/were disregarded to represent the model for wet specimens and dry specimens separately. In this study, authors have tried several distinguished models to find a discrete representative equivalent circuit's model for wet and dry specimens. The proposed models have been simulated using two widely recognized distinguish simulation software such

as EC Lab 10.2 and NOVA 2.1. The simulated results obtained for these two distinguished models showed similar outcomes, and therefore, simulation results obtained from EC lab software are presented in this article.

6.2 Fundamental/Theoretical Background on Electrical Equivalent Circuit

The main component of the Electrical equivalent circuit is Resistor, capacitor, and inductance. Apart from these three other components, such as Warburg resistance of charge diffusion, the constant phase element is also used to represent the electrical behavior of materials. In cement-based materials, a combination of Resistor and capacitor/constant phase elements are generally used to form electrical equivalent circuits. In Figure 6.1, the resistor, capacitor, and inductance components are shown.

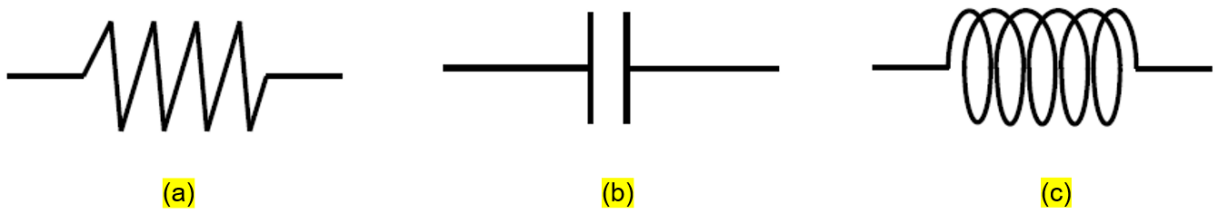


Figure 6.1: Three main components of Electrical Equivalent Circuit (a) Resistor (b) Capacitor (c) Inductor.

6.2.1 Resistor

The simplest component is Resistors which obey Ohm's law. That means the voltage difference at two terminals of a resistor is proportional to the applied current.

$$\Delta V = (R)(\Delta I) \dots\dots\dots (5)$$

Where, ΔV is the voltage difference, ΔI is current, and R is the resistance. In Resistor, it doesn't have any reactive part indicating no phase shift and is independent of Frequency.

$$Z_R = R \dots\dots\dots (6)$$

The Nyquist plot of a resistor is just a single point on the x-axis at any frequency. The typical impedance response of a pure resistor is shown in Figure 6.2.

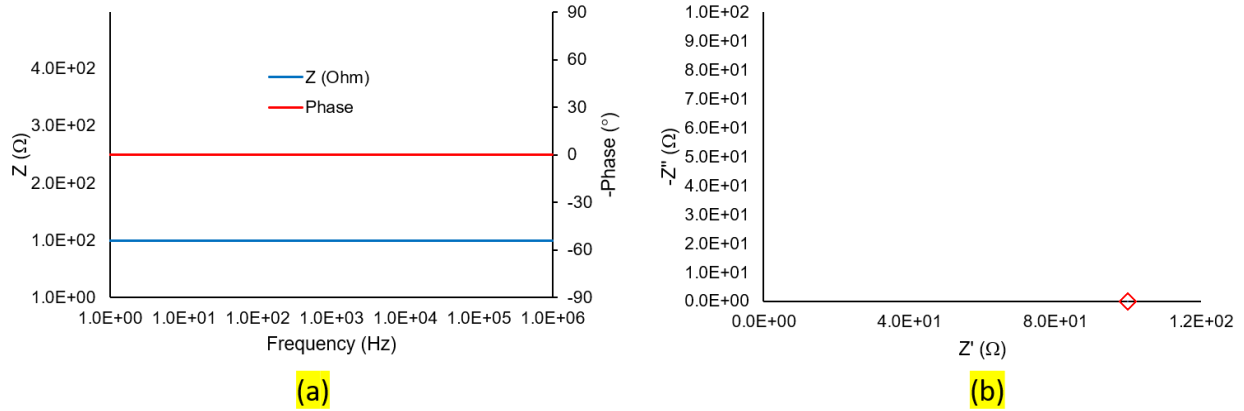


Figure 6.2: Impedance response of Resistor (100-Ω Resistance) (a) Bode Plot (b) Nyquist Plot.

6.2.2 Capacitor

In the case of a capacitor, the voltage difference at two terminal points of an ideal capacitor is proportional to its charge.

$$Q(t) = C \times \Delta V \dots\dots\dots (7)$$

Where, $Q(t)$ is the total amount of charge in the capacitor, and C is the capacitance. The capacitor has purely reactive Impedance, and for an ideal capacitor, the resistance is equal to zero. In a capacitor, the Impedance has an inverse relationship with the Frequency that means Impedance decreases with the AC frequency increases. If w a DC voltage is applied to the capacitor, it will start charging, and after a particular time, it will be fully charged, and there will be no more current flow. In that instances, the Impedance will be infinity.

$$Z_C = (1/j\omega C) \dots\dots\dots (8)$$

The Nyquist plot for an ideal capacitor will be a vertical line parallel to (-Z''-axis). Since the real impedance/resistance for an ideal capacitor is zero and the phase angle will be equal to (-90°). The typical impedance response of a pure resistor is shown in Figure 6.3.

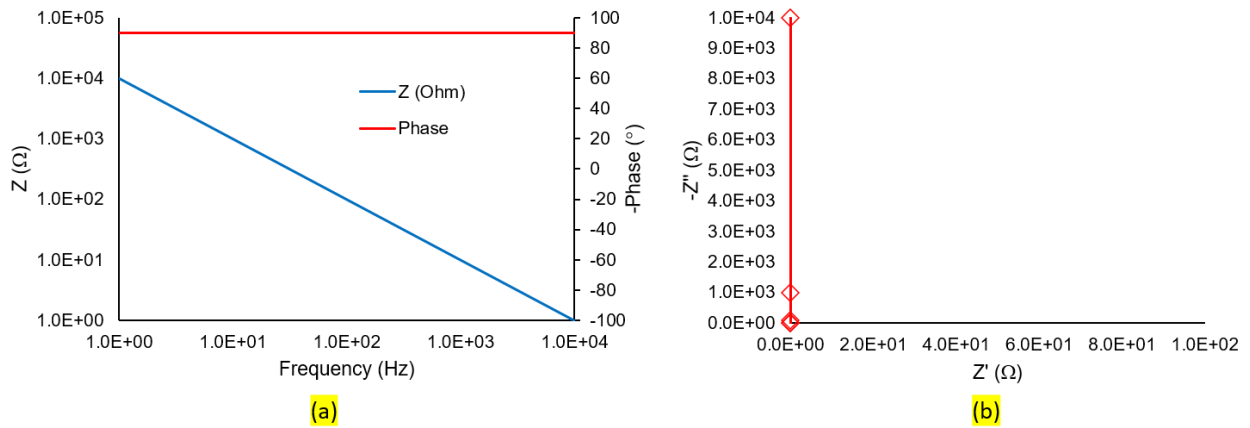


Figure 6.3: Impedance response of an Ideal Capacitor (a) Bode Plot (b) Nyquist Plot.

6.2.3 Simple R-C Circuits

When these R and C circuits are *in series*, the total Impedance can be found by adding two impedance values obtained from the resistor and capacitor two components.

$$Z_{total} = Z_R + Z_C = R + (1/j\omega C) \dots\dots\dots (9)$$

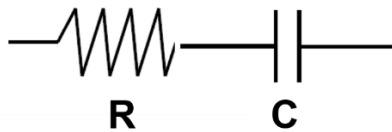


Figure 6.4: Series R-C Circuit

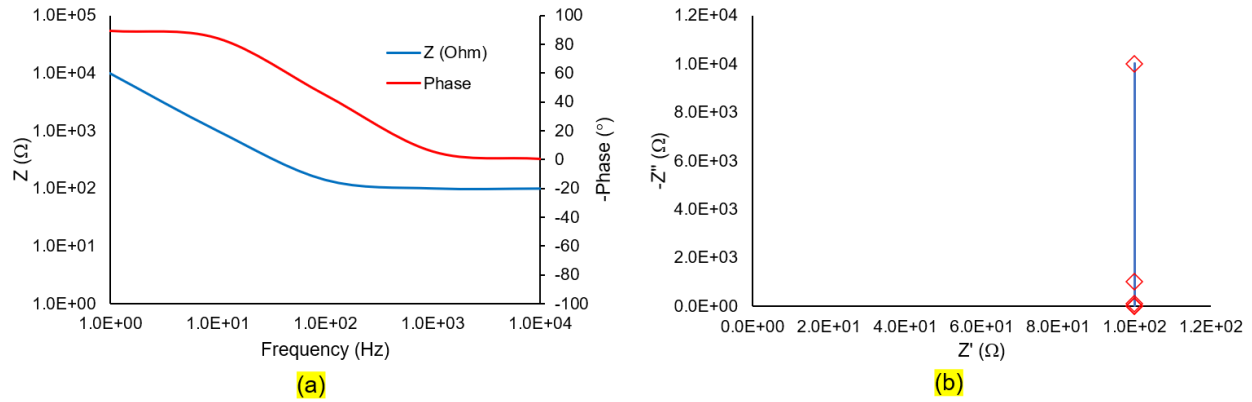


Figure 6.5: Impedance response of a series R-C Circuit (a) Bode Plot (b) Nyquist Plot.

In the case R-C *in parallel* connections, the reciprocal of total Impedance is equal to the additive of reciprocal of Resistor and Capacitor's Impedance.

$$\frac{1}{Z_{total}} = \frac{1}{Z_R} + \frac{1}{Z_C} = \frac{1}{R} + j\omega C = \frac{1 + j\omega RC}{R}$$

$$\Rightarrow Z_{total} = \frac{R}{1 + j\omega RC} \dots\dots\dots (10)$$

From Eq. 10, it can be seen that if $\omega \rightarrow \infty$, that means at higher Frequency the Impedance reaches to almost zero and ideal circuits behaves like the capacitor (since at infinite Frequency the ideal capacitor's Impedance is zero). On the other hand, if $\omega \rightarrow 0$, that means at lower Frequency the Impedance becomes equal to the resistance of the Resistor. An ideal capacitor in parallel with a resistor forms a semi-circle in the Nyquist plot (as shown in Figure 6.7 (b))

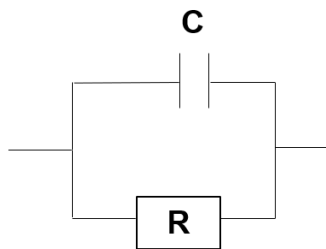


Figure 6.6: Parallel R-C Circuit

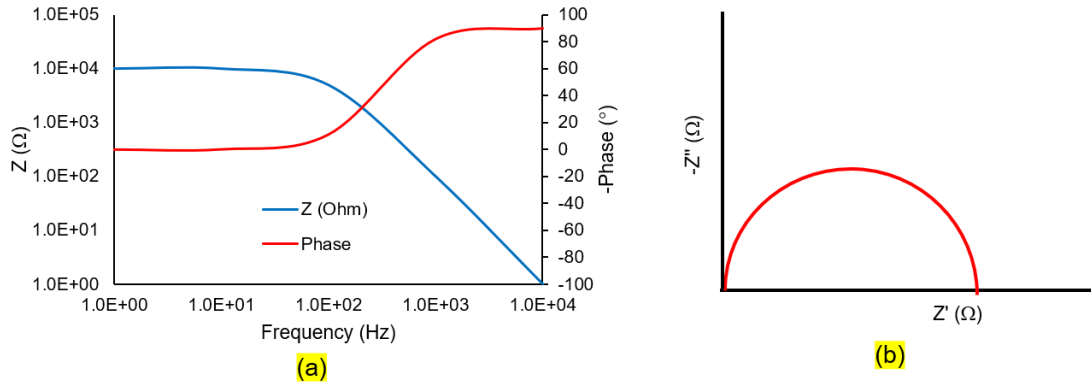


Figure 6.7: Impedance response of a Parallel R-C Circuit (a) Bode Plot (b) Nyquist Plot.

6.2.4 Simplified Randle Circuit

One of the most common electrical equivalent circuit models is Randle Cell. The components of this circuit include R_s (a solution resistance), C_d (double layer capacitance), and R_C (charge transfer/polarization resistance). This model is the starting point for the more complex electrical equivalent circuit model of different materials. A typical Nyquist plot of a Randle cell is shown in Figure 6.9.

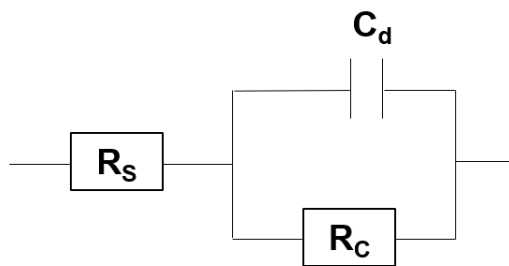


Figure 6.8: A simple Equivalent Circuit/Randle Cell

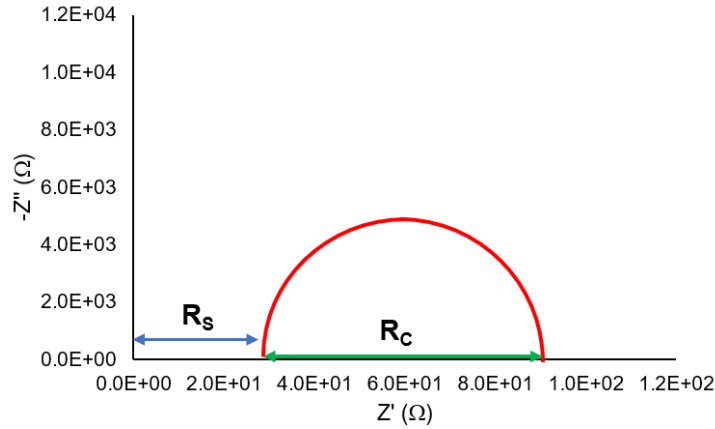


Figure 6.9: Typical Nyquist plot of a Randle cell

6.2.5 Constant Phase Element

In most of the materials, the capacitors do not behave as an ideal capacitor does. Especially for cementitious materials, the Nyquist plot doesn't form a perfect semi-circle; instead, it takes the form of a circular arc whose center is slightly depressed to the real impedance axis ((Cabeza et al., 2002, McCarter and Brousseau, 1990, Ball et al., 2011) (shown in Figure 6.10). This is due to the dielectric dispersion in the system causing a decrease in the capacitance with AC frequency increases. This effect can be addressed in modeling the electrical equivalent circuit by replacing the capacitor with the constant phase element (CPE). The constant phase element is a complex circuit component, and it is frequency dependent. The impedance of a CPE can be expressed as:

$$Z_{CPE} = \frac{1}{Q_o (j\omega)^a} \dots\dots\dots (11)$$

Where \$Q_o\$ is a pseudo-capacitive coefficient, \$\omega = 2\pi f\$ angular frequency, \$f\$ is the AC frequency. "a" is an arbitrary constant with having no physical meaning. It can take values from \$0 \le a \le 1\$. When \$a = 1\$, the constant phase element will behave like an ideal capacitor (\$C = Q_o\$),

for $a = 0$ indicates a perfect resistor. When $a < 1$, the double layer capacitor on a real cell behaves like a CPE and doesn't behave as an ideal capacitor. Moreover, the semi-circle will be distorted, and the unit represents CPE is Fs^{a-1} .

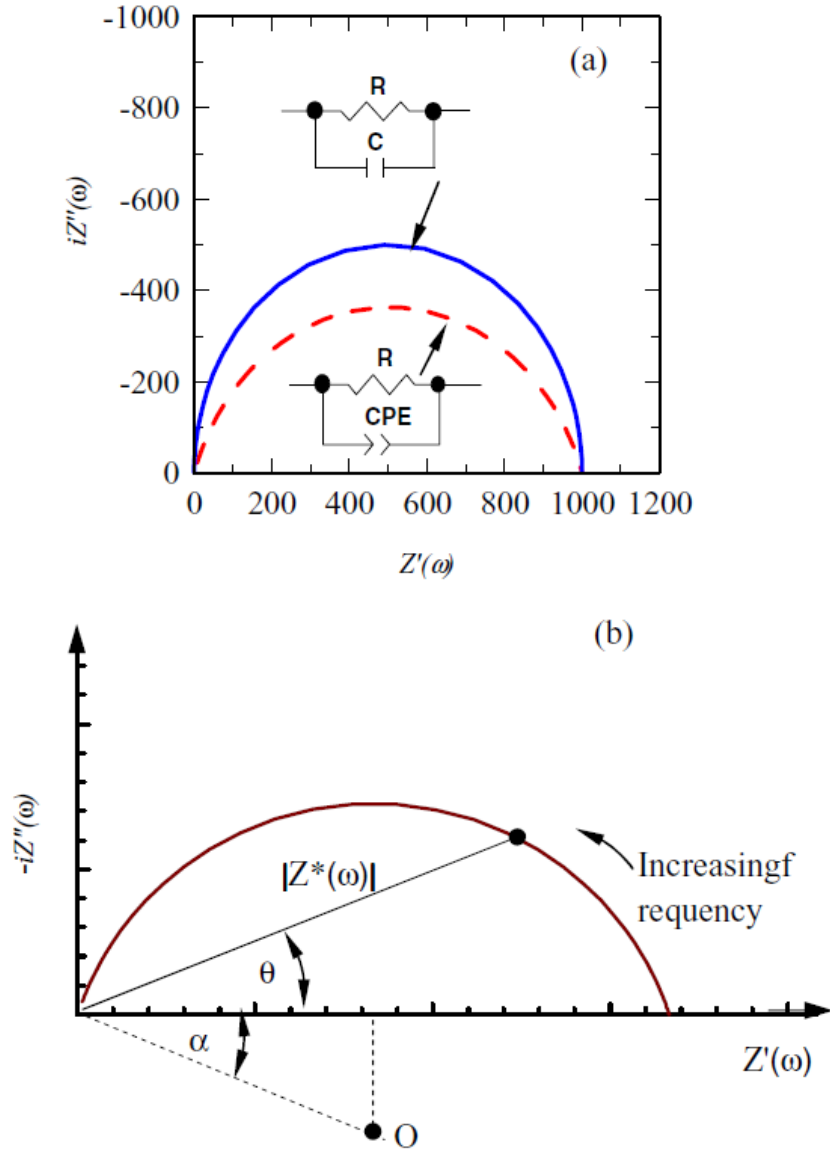


Figure 6.10: Influence of CPE in Nyquist Plot ((McCarter et al. 2015))

Replacing the capacitor with CPE the simplified equivalent circuit or Randle cell is used for determining the electrical equivalent circuit of cement-based materials.

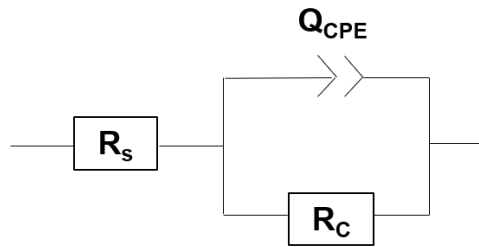


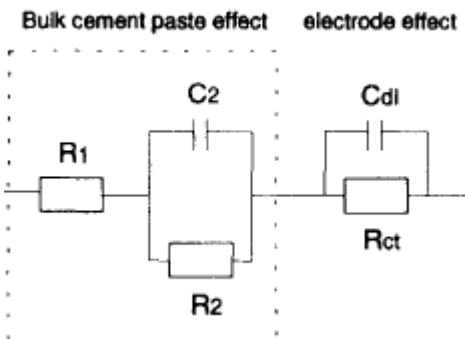
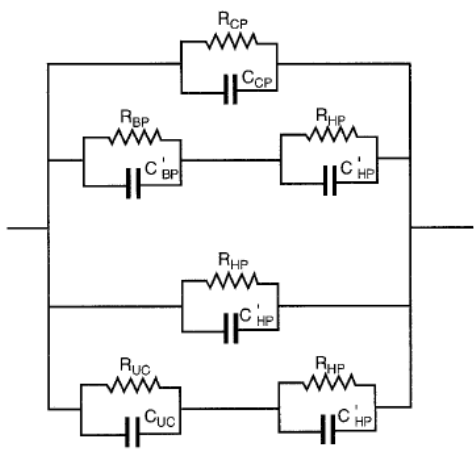
Figure 6.11: A typical Randle Cell element used to find equivalent circuit for cementitious materials.

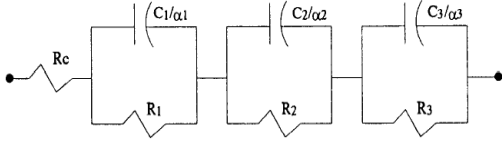
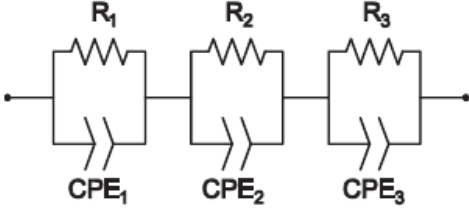
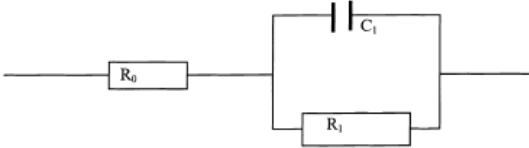
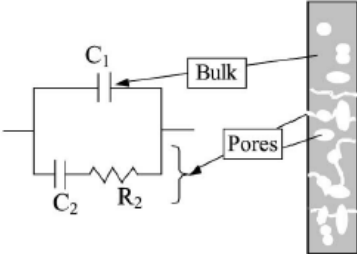
6.2.6 Electrical Equivalent Circuit Models proposed by other Researchers

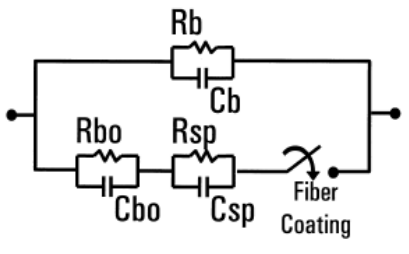
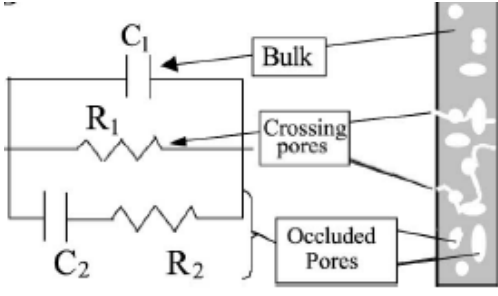
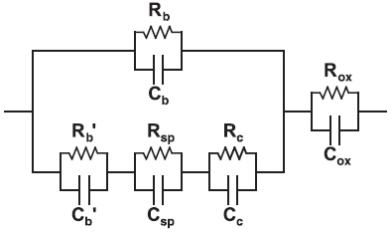
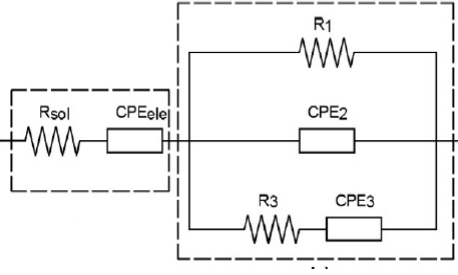
In this section, different electrical equivalent circuit model proposed and used by other researchers to model the responses of cementitious materials. These models are presented in

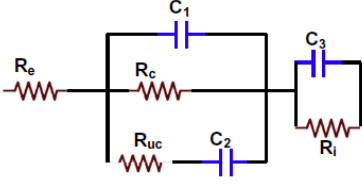
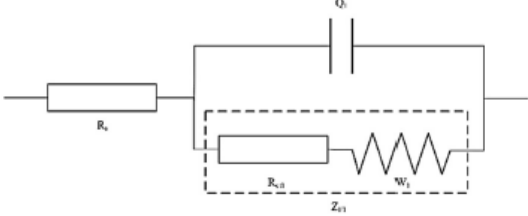
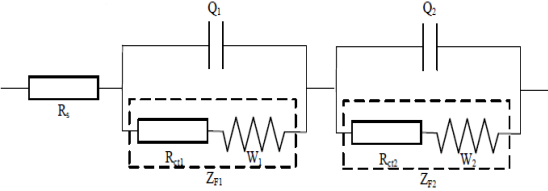
Table 6.1

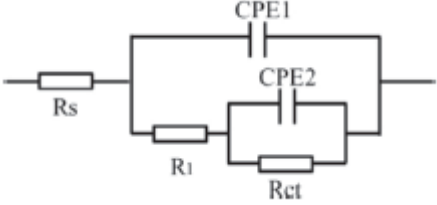
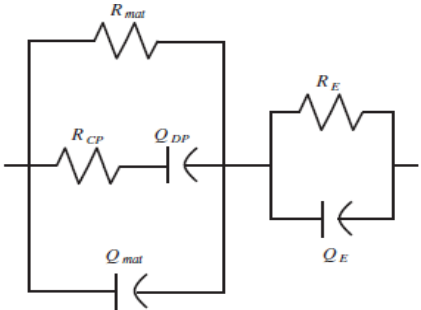
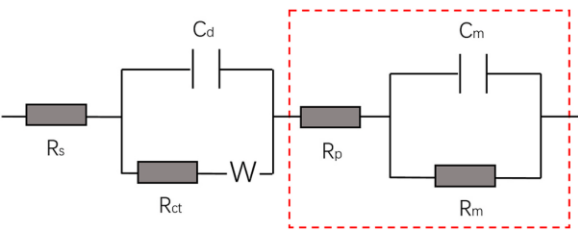
Table 6.1: Different Electrical Equivalent Circuit used in other cement-based materials research

Equivalent Circuit	Purpose	Authors
<p>(a)</p>  <p>Bulk cement paste effect electrode effect</p>	<ul style="list-style-type: none"> • Micro-cracking behavior in Fiber reinforced cement composite • to investigate the carbonation process of cement mortar • Corrosion Monitoring/chloride ion transportation • Understanding the microstructure of cement-composite 	<p>(Gu et al. 1993a; McCarter and Brousseau 1990; Dong et al. 2016b; Liu et al. 2017; He et al. 2018b)</p>
<p>(b)</p> 	<ul style="list-style-type: none"> • Understanding the microstructure of cement-paste 	<p>(MacPhee et al. 1996)</p>

<p>(c)</p> 	<ul style="list-style-type: none"> Understanding the microstructure of cement-paste 	<p>(Keddam et al. 1997)</p>
<p>(d)</p> 	<ul style="list-style-type: none"> Understanding the microstructure of cement-paste 	<p>(McCarter et al. 2015; Ball et al. 2011; Berrocal et al. 2018b)</p>
<p>(e)</p> 	<ul style="list-style-type: none"> Understanding the microstructure of cement-paste Electrical Characterization of Conductive (CNT) cement composite Corrosion Monitoring/chloride ion transportation 	<p>(Song 2000; Han et al. 2012; Liu et al. 2017)</p>
<p>(f)</p> 	<ul style="list-style-type: none"> Understanding the microstructure of cement-paste 	<p>(Cabeza et al. 2002; Cabeza et al. 2006)</p>

<p>(g)</p> 	<ul style="list-style-type: none"> Understanding the microstructure of fiber-reinforced cement-composite 	<p>(Torrents et al. 2000; Torrents et al. 2001; Mason et al. 2002)</p>
<p>(h)</p> 	<ul style="list-style-type: none"> Understanding the microstructure of cement-composite Microstructural Characterization of Conductive cement composite 	<p>(Cabeza et al. 2002; Li and Li 2019)</p>
<p>(i)</p> 	<ul style="list-style-type: none"> Understanding the microstructure of fiber-reinforced cement-composite 	<p>(Hixson et al. 2003)</p>
<p>(j)</p> 	<ul style="list-style-type: none"> Understanding the microstructure of cement-composite 	<p>(Cruz et al. 2013)</p>

<p>(k)</p> 	<ul style="list-style-type: none"> • Chloride ion migration models in cement-composite 	<p>(Ravikumar and Neithalath 2013; Vance et al. 2014)</p>
<p>(l)</p> 	<ul style="list-style-type: none"> • To investigate the carbonation process of cement mortar. • Understanding the microstructure of cement-composite • Corrosion Monitoring 	<p>(Dong et al. 2014b; Dong et al. 2015; Dong et al. 2016a; Dong et al. 2016b; Li et al. 2016; He et al. 2018b; Kim et al. 2020)</p>
<p>(m)</p> 	<ul style="list-style-type: none"> • To investigate the carbonation process of cement mortar. • Chloride ion transportation 	<p>(Dong et al. 2014b; Dong et al. 2015; Dong et al. 2016a; Dong et al. 2016b; Li et al. 2016; Dong et al. 2018)</p>

<p>(n)</p> 	<ul style="list-style-type: none"> Corrosion Monitoring/chloride ion transportation 	<p>(Liu et al. 2017)</p>
<p>(o)</p> 	<ul style="list-style-type: none"> To investigate chloride ion diffusion 	<p>(Mercado-Mendoza et al. 2014b)</p>
<p>(p)</p> 	<ul style="list-style-type: none"> detecting the breakage rate of microcapsules for self-healing cementitious materials 	<p>(Ren et al. 2020)</p>

6.3 Electrical Equivalent Circuit for Dry Specimens

In this section, an equivalent circuit model for dry cement composite has been proposed, and then evaluated its efficacy comparing with the experimental data. In Figure 6.12, the proposed equivalent circuit model for dry conductive cement composites is shown. In dry conditions, the AC impedance spectrum is consisting of the impedance of bulk cement composite (cement with graphite) and the impedance of interface between bulk and electrode. In the equivalent circuit, the bulk effect is represented by $(R_1(Q_2/R_2))$, and the electrode interface effect

is represented by (Q3/R3). The proposed equivalent circuit model is used to obtain fitted data for the control specimen and Specimen with 10%, 15%, and 20% graphite content compared with the dry experimental data. The comparison of dry experimental data and fitted model's data (including Bode plot, Phase angle, and Nyquist Plots) are shown in the following figures (Figure 6.13, 6.14, 6.15, 6.16)

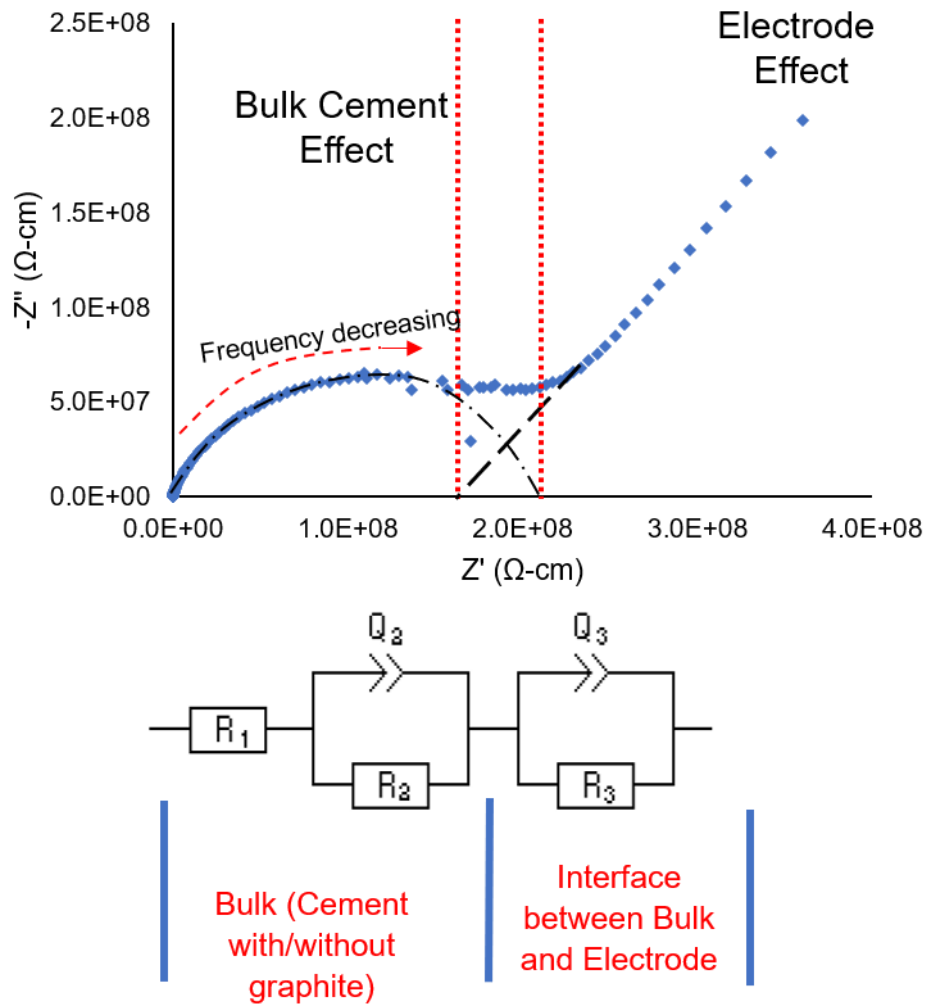


Figure 6.12: Proposed Electrical Equivalent Circuit model for conductive cement composite specimens containing graphite powder at dry conditions.

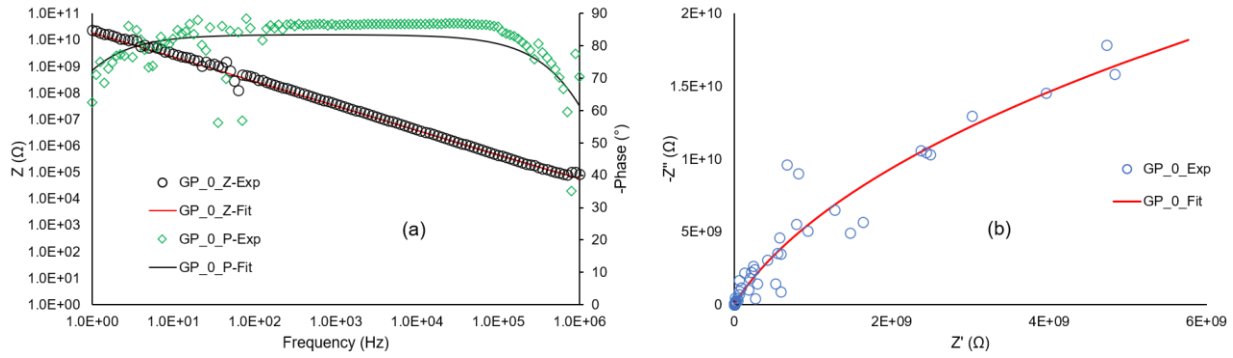


Figure 6.13: Comparison between experimental and equivalent circuit fit of Specimen with 0% graphite at Dry Conditions (a) Bode Plot and Phase Angle (b) Nyquist Plot. (solid lines represent the fitting data and symbols represent the experimental data)

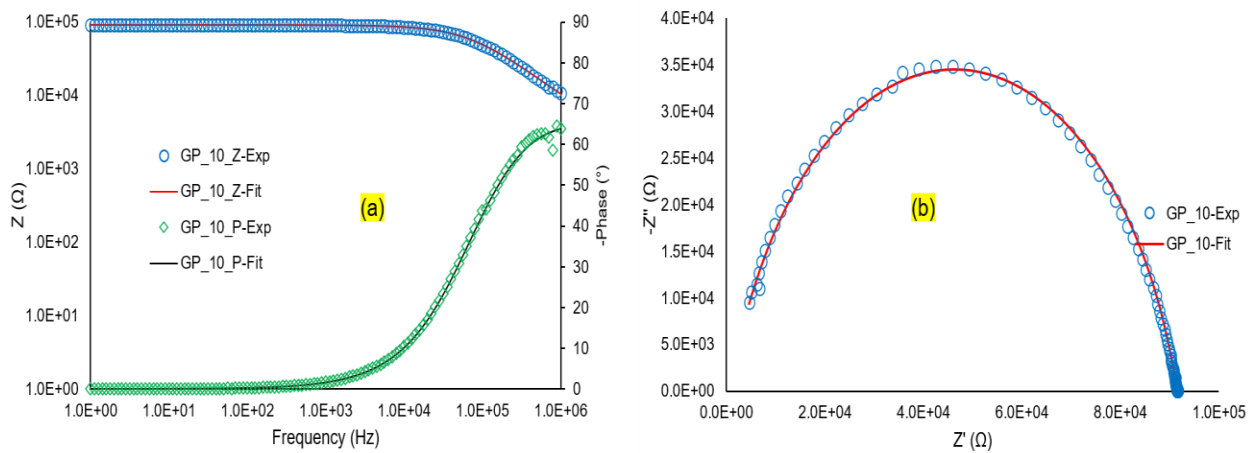


Figure 6.14: Comparison between experimental and equivalent circuit fit of Specimen with 10% graphite at Dry Conditions (a) Bode Plot and Phase Angle (b) Nyquist Plot. (solid lines represent the fitting data and symbols represent the experimental data)

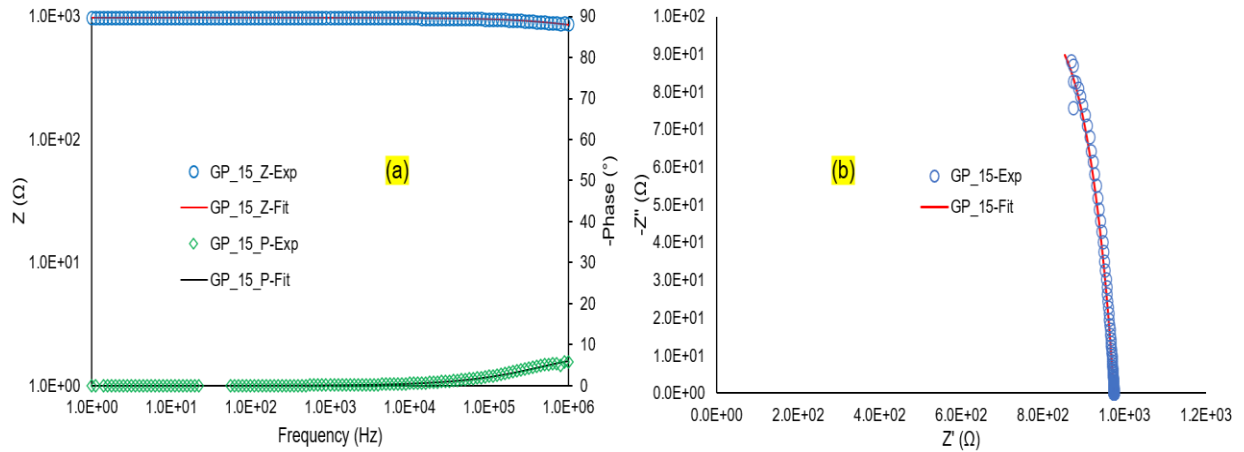


Figure 6.15: Comparison between experimental and equivalent circuit fit of Specimen with 15% graphite at Dry Conditions (a) Bode Plot and Phase Angle (b) Nyquist Plot. (Solid lines represent the fitting data and symbols represent the experimental data)

It is evident from Figures 6.13, 6.14, 6.15, 6.16 that the fitting results obtained from the proposed model for dry specimens are matched thoroughly with the experimental data of corresponding specimen types obtained through AC impedance spectroscopy. The fitting is noticeable for different AC impedance graphs such as Nyquist plot, Bode Plot and Phase angle variation with AC frequency. Moreover, the models' results are well fitted for all specimens with lower or higher concentrated graphite contents. Therefore, the equivalent circuit proposed for dry conductive cement composite is very effective and reliable for studying the electrochemical system. The simulated parameters of the proposed equivalent circuits for different graphite contents are presented in Table 6.2.

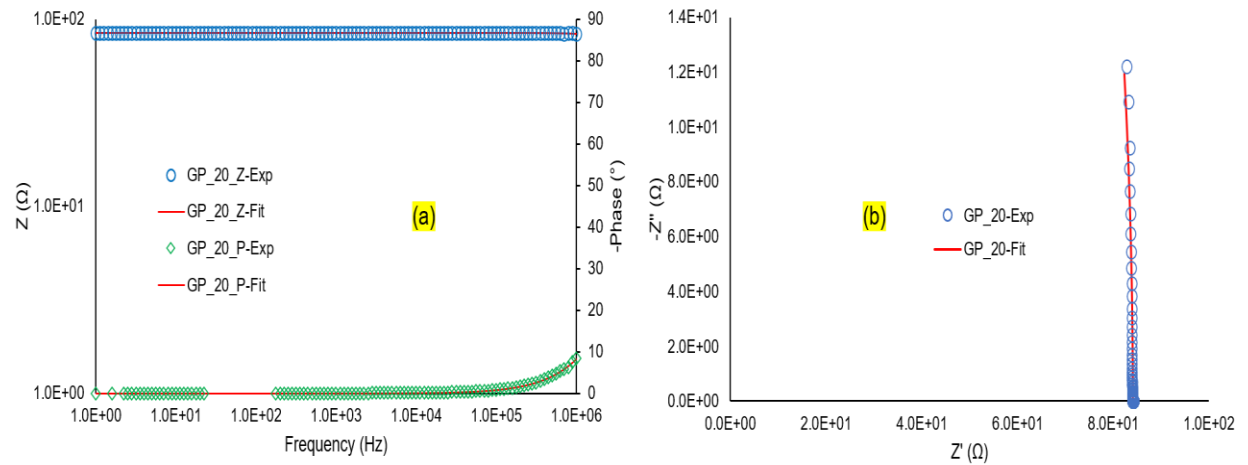


Figure 6.16: Comparison between experimental and equivalent circuit fit of Specimen with 20% graphite at Dry Conditions (a) Bode Plot and Phase Angle (b) Nyquist Plot. (Solid lines represent the fitting data and symbols represent the experimental data)

Table 6.2: Summary of Equivalent Circuit fitting results for Specimens at Dry Conditions

Component (Units)	Specimen with Graphite Content			
	GP_0	GP_10	GP_15	GP_20
R_1 (Ω)	0.224×10^{-111}	0.5656×10^{-18}	15.4	0.3817×10^{-12}
R_2 (Ω)	98.17×10^9	1222	324.6	0.189×10^{-249}
Q_2 (F. $s^{(a-1)}$)	9.147×10^{-12}	42.07×10^{-12}	59.9×10^{-9}	-95.24
a_2	0.9278	1	0.6682	0
R_3 (Ω)	23049	90209	635.1	84.14
Q_3 (F. $s^{(a-1)}$)	26.52×10^{-12}	0.2251×10^{-9}	1.484×10^{-9}	0.2736×10^{-9}
a_3	0.4654	0.8309	0.4106	1

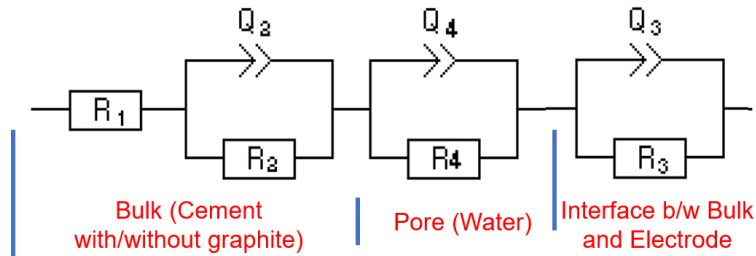
From Table 6.2, it is evident that the R_2 (which represents the resistance of bulk cement composite) value decreases with the increase of graphite content, indicating the effectiveness of adding conductive additives in cement composite. Moreover, the value of a_2 is also reduced with graphite content, which indicates that adding graphite powder reduces the constant phase elements values, thus eventually reducing the capacitance effect.

6.4 Electrical Equivalent Circuit for Wet Specimens

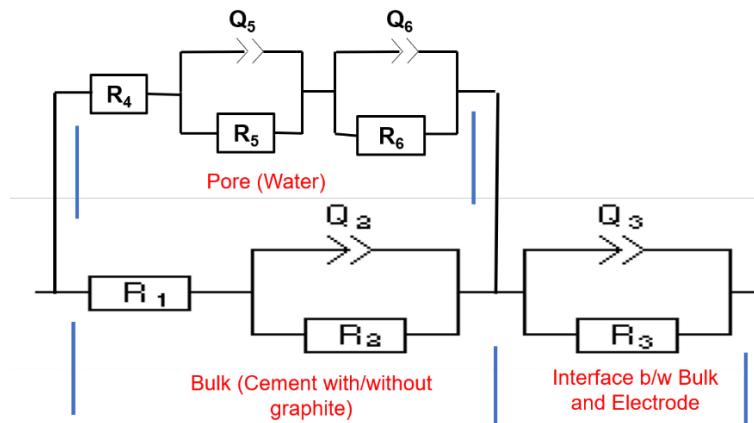
In this section, two different equivalent circuit models for wet cement composite have been studied, and then evaluated their efficacy comparing with the experimental data. The first model (as shown in Figure 6.17 (a)) had been proposed by McCarter et al. (2015) and Keddam et al. (1997) for cement composite. Their study measured the impedance just after 28 days of curing of specimens, which means the specimens were in wet conditions. The main drawback of their proposed equivalent circuit model is that they considered the water conduction elements (capacitance and resistance) in series to the bulk cement composite conduction elements. However, it is practical to assume that water creates a new conductive path inside the Specimen. The applied electrical charges are divided between these paths creating a parallel network to the bulk cement conduction path.

Furthermore, there is a high possibility that the bulk conductive path is susceptible to be influenced and changed due to the presence of moisture. Moreover, the moisture can be composed of several circuit elements due to having chemicals, different dissolved solids, or biological components. Besides, the Nyquist plot of wet specimens comprises multiple semi-circles indicating multiple circuit elements at wet conditions. This research has proposed a more

meaningful equivalent circuit for wet conductive cement composite considering all these issues. At first, an element for pore water is selected, and then the simulated results are compared with the experimental data (both the model and comparison are shown in the Appendix). The comparison showed that another element is necessary for the pore water portion to represent the water conduction path more accurately. Hence, two elements for the pore water portion are selected. The proposed equivalent circuit (as shown in Figure 6.17 (b)) becomes more representative of the microstructure of wet conductive cement composite.



(a)



(b)

Figure 6.17: Electrical Equivalent Circuit model for conductive cement composite specimens containing graphite powder at wet conditions (a) Model-1 (Keddani et al., 1997, McCarter et al., 2015, Ball et al., 2011, Berrocal et al., 2018a) (b) Model-2 proposed in this study.

Initially, it is assumed that the dry bulk conduction path is not influenced/affected by the moisture inside the specimen. Hence, the value of components R_1 , R_2 , Q_2 , R_3 , Q_3 obtained from the dry specimen (as presented in Table 6.2) fitting results can be used in the wet specimens' model. That is fixing components R_1 , R_2 , Q_2 , R_3 , Q_3 values for simulation to obtain the other components' values.

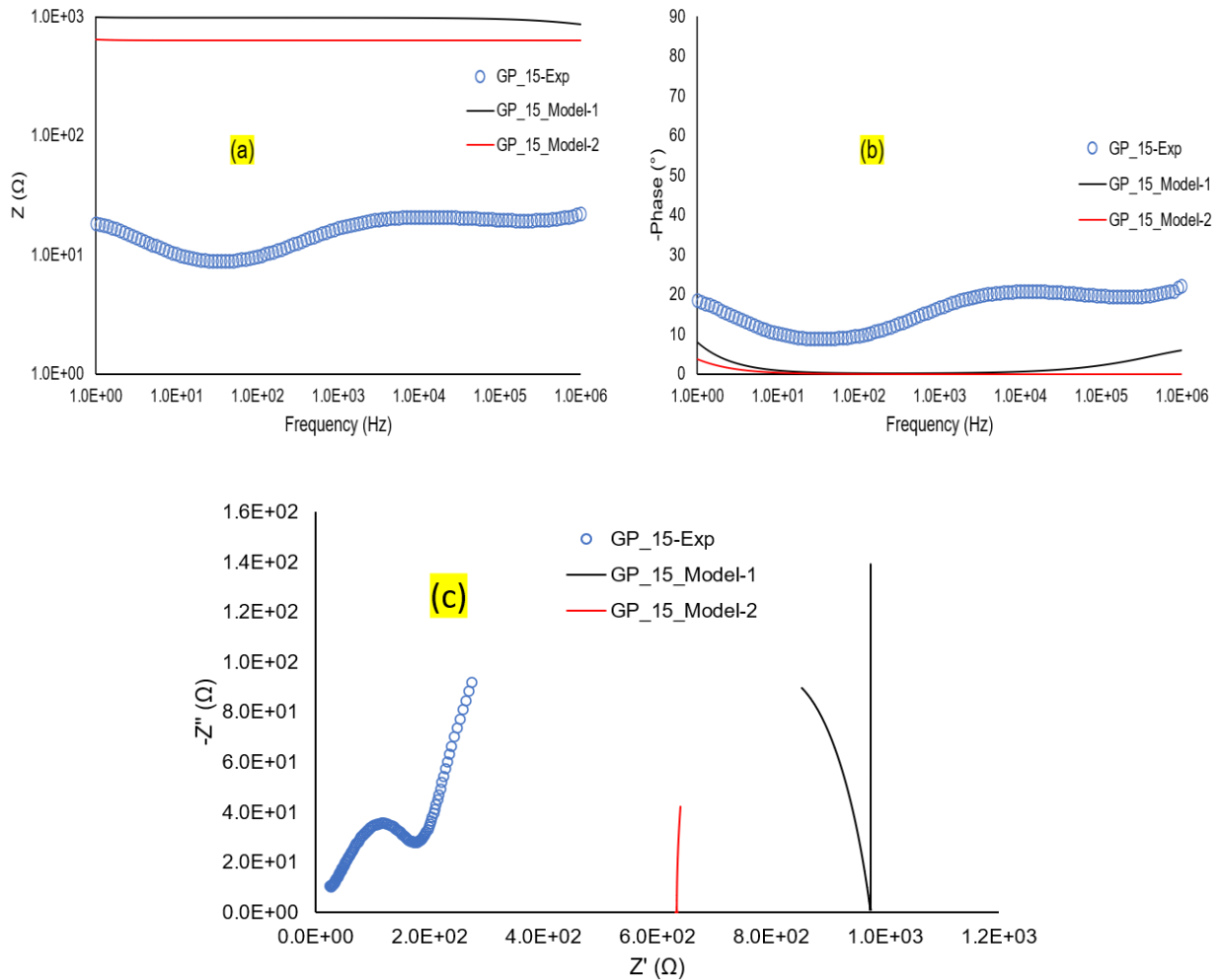


Figure 6.18: Comparison between experimental and equivalent circuit fit of Specimen with 15% graphite at Wet Conditions (fixing dry R_1 , R_2 , Q_2 , R_3 , Q_3 values in the model) (a) Bode Plot (b) Phase Angle (c) Nyquist Plot. (Solid lines represent the fitting data and symbols represent the experimental data).

Additionally, without fixing the values of the component from dry specimens have also been performed to substantiate the initial assumption. The comparison of experimental and fitting results for these two analyses of the wet specimen with having 15% graphite content is shown in Figures 6.18, 6.19, and the model outcomes are presented in Table 6.2.

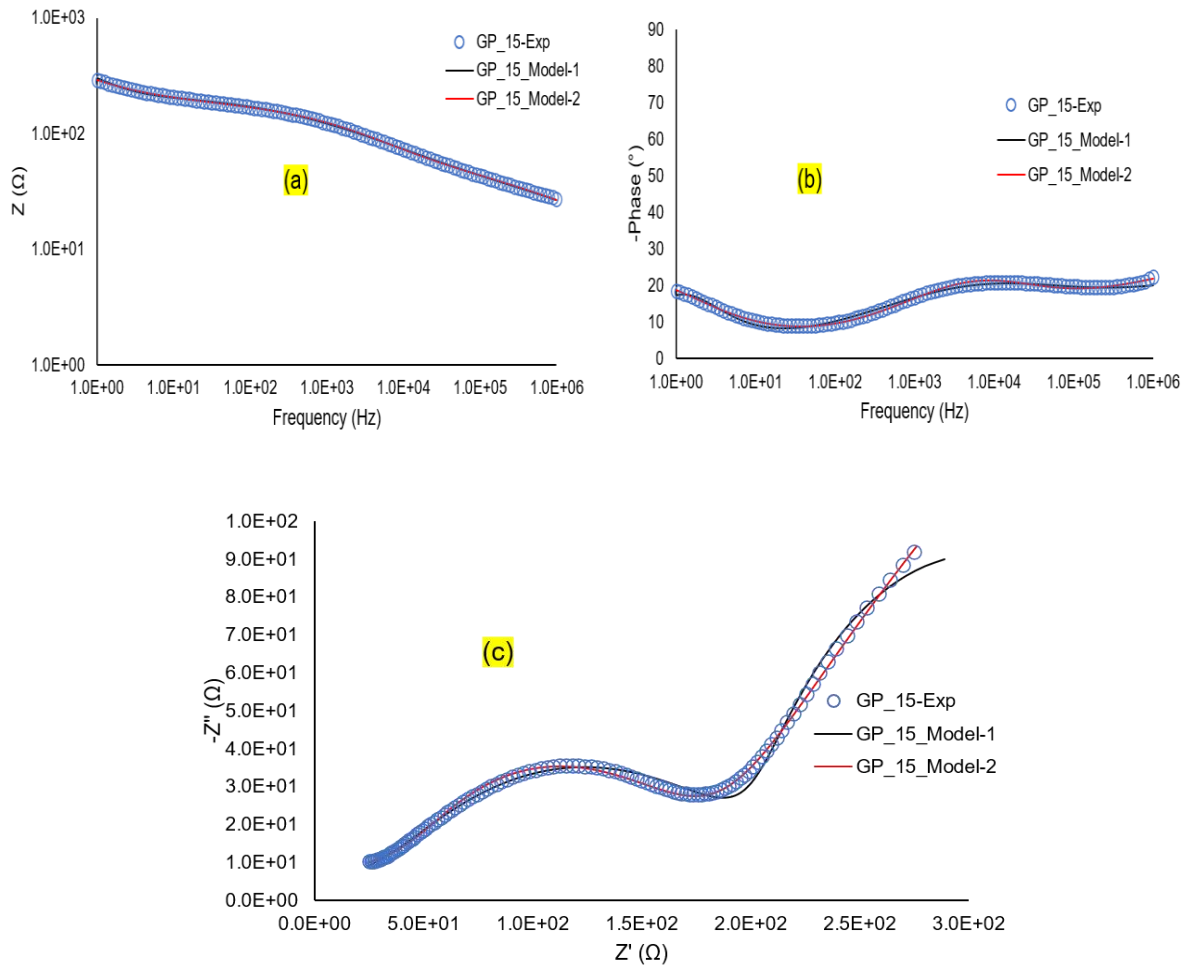


Figure 6.19: Comparison between experimental and equivalent circuit fit of Specimen with 15% graphite at Wet Conditions (without fixing dry R_1 , R_2 , Q_2 , R_3 , Q_3 values in the model) (a) Bode Plot (b) Phase Angle (c) Nyquist Plot. (Solid lines represent the fitting data and symbols represent the experimental data).

It is evident from Figure 6.18 that fixing components value from dry specimens doesn't fit very well with the wet specimens' experimental results. In contrast, non-fixing fitting results matched perfectly with the experimental results (as shown in Figure 6.19). Moreover, Table 6.3 represents the data of R_1 , R_2 , Q_2 , R_3 , Q_3 obtained from the non-fixing models' outcomes indicating that these values are noticeably different from the dry specimen's values. This characteristic suggests that the initial assumption is not valid, and the bulk conduction path is also influenced by the presence of moisture inside the specimen.

Therefore, for the rest of the analysis, non-fixing values methods have been used to find the simulated results for specimens with other graphite contents. The comparison among the experimental, model-1 and model-2 fitting results is shown in Figures 6.20, 6.21 and 6.22, and models' outcomes are presented in Table 6.4 and Table 6.5

Table 6.3: Summary of Equivalent Circuit Model-1 and Model-2 fitting results for Specimens at Wet Conditions (fixing components values)

Component (Units)	Specimen with Graphite Content and Circuit types		
	GP_15 (fixing values for Model-1 and Model-2)	GP_15 (Wet-Model-1 outcome) (without fixing values)	GP_15 (Wet-Model-2 outcome) (without fixing values)
$R_1 (\Omega)$	15.4	4.394	0.9156
$R_2 (\Omega)$	324.6	189	397.8
$Q_2 (F. s^{(a-1)})$	59.9×10^{-9}	0.1231×10^{-3}	94.9×10^{-6}
a_2	0.6682	0.4435	0.357
$R_3 (\Omega)$	635.1	24.91	775.5
$Q_3 (F. s^{(a-1)})$	1.484×10^{-9}	29.8×10^{-6}	2.425×10^{-3}
a_3	0.4106	0.4406	0.5905

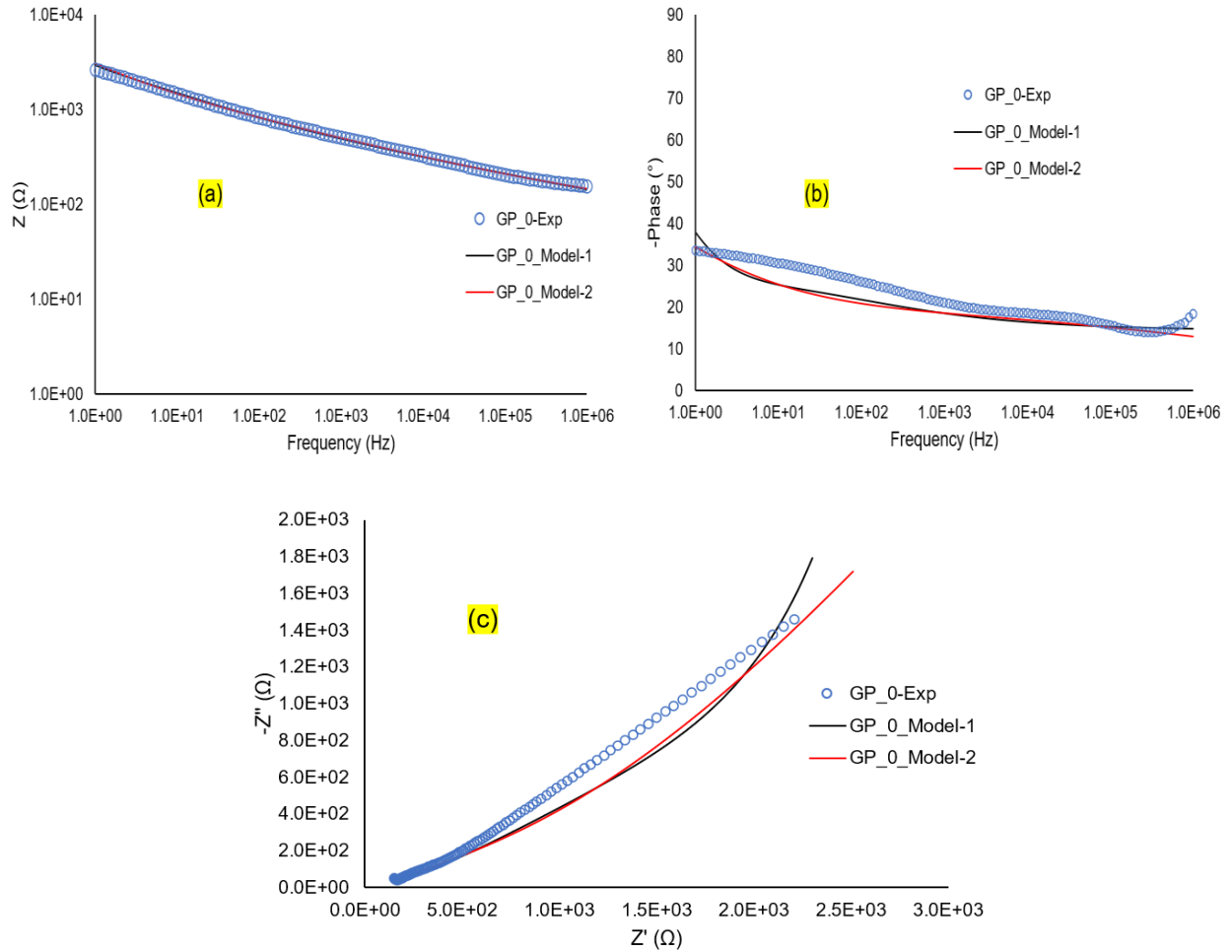


Figure 6.20: Comparison between experimental and equivalent circuit fit of Specimen with 0% graphite/control specimen at Wet Conditions (without fixing dry R_1 , R_2 , Q_2 , R_3 , Q_3 values in the model) (a) Bode Plot (b) Phase Angle (c) Nyquist Plot. (Solid lines represent the fitting data and symbols represent the experimental data).

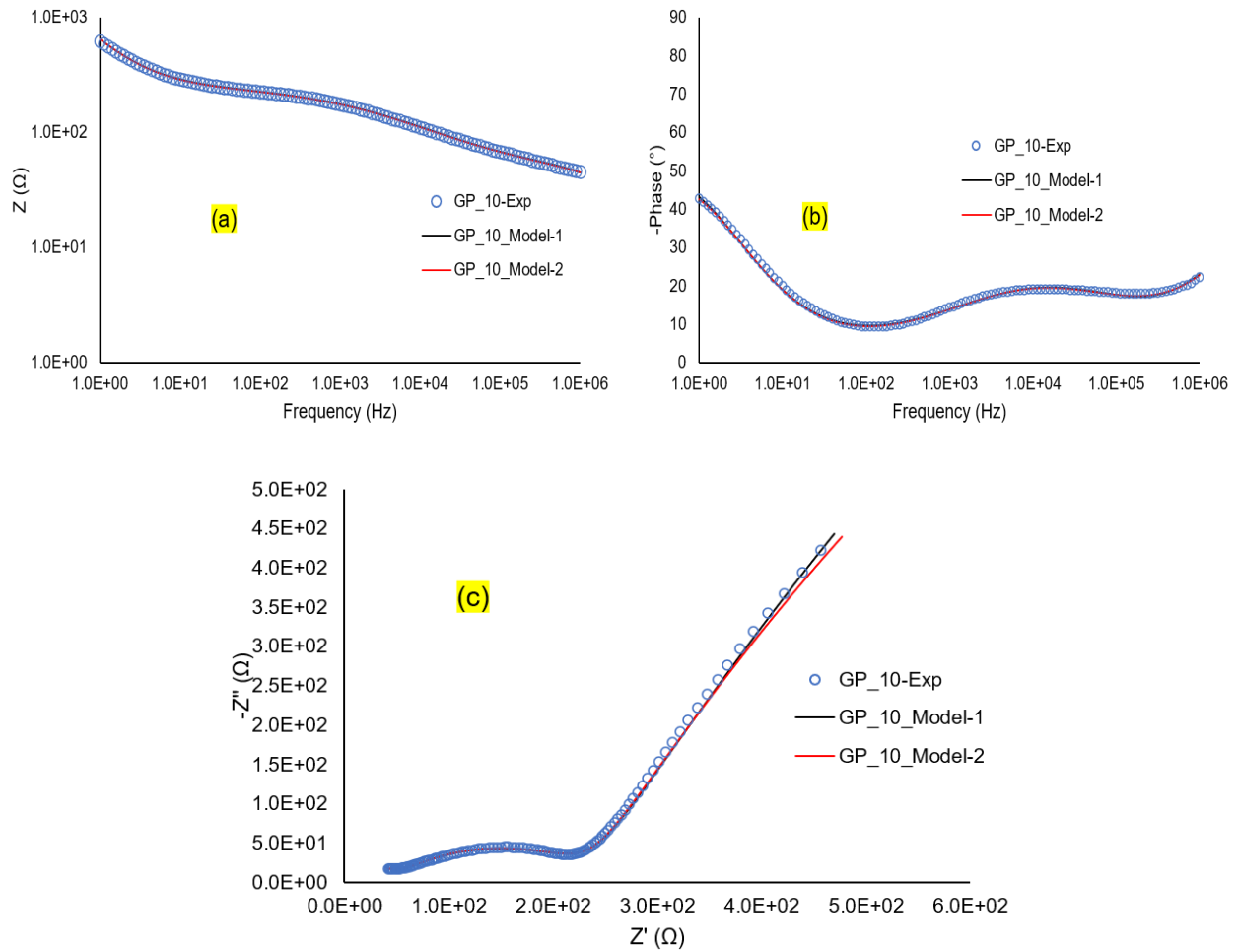


Figure 6.21: Comparison between experimental and equivalent circuit fit of Specimen with 10% graphite/control specimen at Wet Conditions (without fixing dry R_1 , R_2 , Q_2 , R_3 , Q_3 values in the model) (a) Bode Plot (b) Phase Angle (c) Nyquist Plot. (Solid lines represent the fitting data and symbols represent the experimental data).

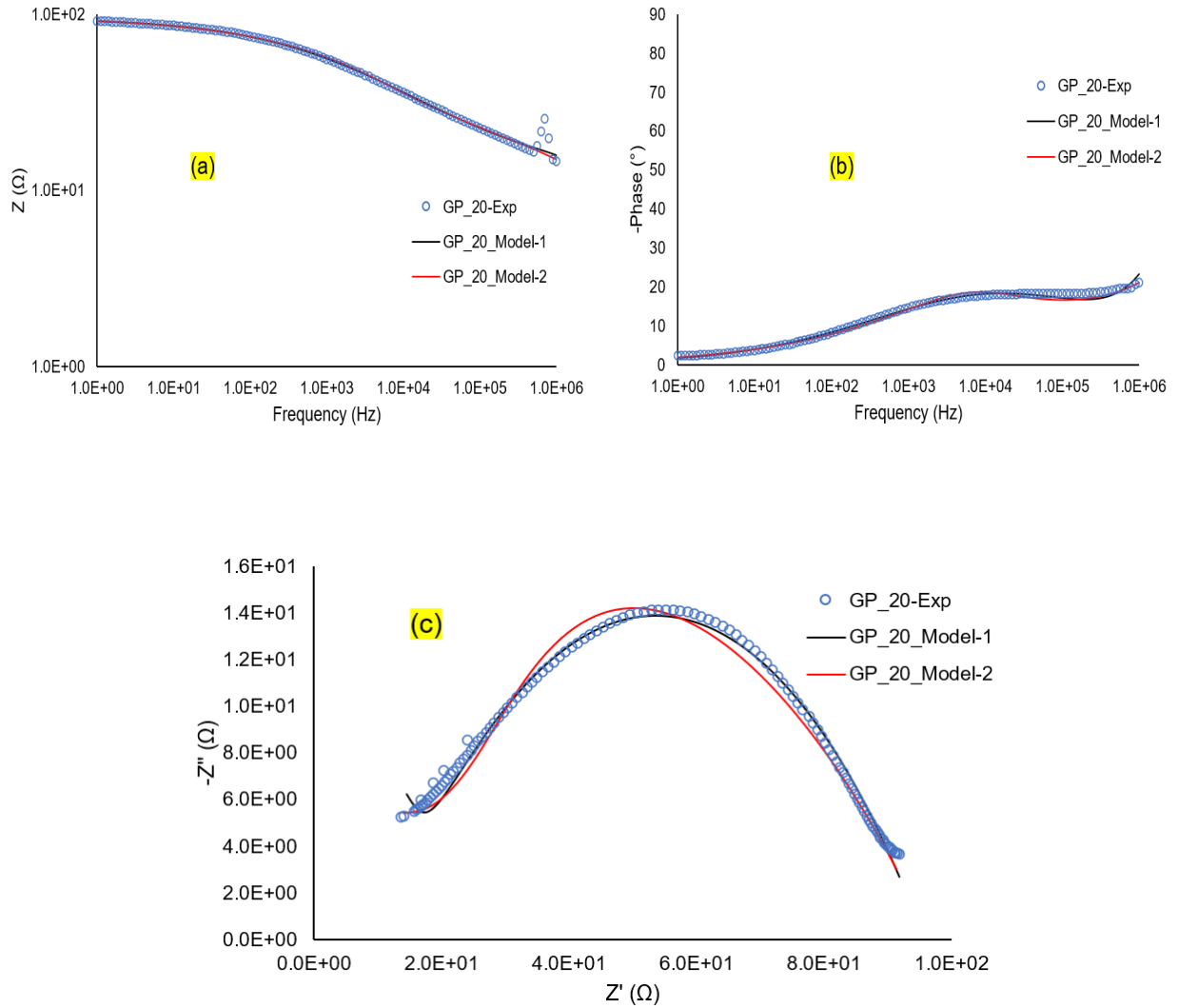


Figure 6.22: Comparison between experimental and equivalent circuit fit of Specimen with 20% graphite/control specimen at Wet Conditions (without fixing dry R_1 , R_2 , Q_2 , R_3 , Q_3 values in the model) (a) Bode Plot (b) Phase Angle (c) Nyquist Plot. (Solid lines represent the fitting data and symbols represent the experimental data).

Table 6.4: Summary of Equivalent Circuit Model-1 fitting results for Specimens at Wet Conditions (without fixing components values)

Component (Units)	Specimen with Graphite Content		
	GP_10	GP_15	GP_20
$R_1 (\Omega)$	13.2	4.394	0.1047×10^{-3}
$R_2 (\Omega)$	200.5	189	25.22×10^{-6}
$Q_2 (F. s^{(a-1)})$	41.32×10^{-6}	0.1231×10^{-3}	0.7468×10^{-3}
a_2	0.4957	0.4435	29.96×10^{-9}
$R_4 (\Omega)$	7498	194.6	11.41
$Q_4 (F. s^{(a-1)})$	0.509×10^{-3}	1.184×10^{-3}	4.662×10^{-9}
a_4	0.7322	0.9209	0.9983
$R_3 (\Omega)$	29.22	24.91	84.26
$Q_3 (F. s^{(a-1)})$	28.73×10^{-9}	29.8×10^{-6}	0.3315×10^{-3}
a_3	0.861	0.4406	0.4048

Table 6.5: Summary of Equivalent Circuit Model-2 fitting results for Specimens at Wet Conditions (without fixing components values)

Component (Units)	Specimen with Graphite Content		
	GP_10	GP_15	GP_20
$R_1 (\Omega)$	0.07119	0.9156	54.03
$R_2 (\Omega)$	241.5	397.8	44.64
$Q_2 (F. s^{(a-1)})$	64.64×10^{-9}	94.9×10^{-6}	6.653×10^{-6}
a_2	0.7434	0.357	0.7716
R_4	62.22	7.436×10^{-3}	0.737
$R_5 (\Omega)$	0.3782	86.24	6.321
$Q_5 (F. s^{(a-1)})$	0.9292×10^{-3}	21.58×10^{-9}	0.4416×10^{-6}
a_5	0.4864	0.6667	0.778
$R_6 (\Omega)$	0.1194×10^9	296.4	1740
$Q_6 (F. s^{(a-1)})$	24.94×10^{-6}	10.06×10^{-6}	0.398×10^{-3}
a_6	0.5076	0.636	0.3445
$R_3 (\Omega)$	5222	775.5	3.342
$Q_3 (F. s^{(a-1)})$	0.496×10^{-3}	2.425×10^{-3}	27.47×10^{-6}
a_3	0.7379	0.5905	0.516

It is evident from Figures 18, 19 and 20 that both models matched almost perfectly with the experimental data. Bode Plot, Phase angle, and Nyquist plot are obtained similar to the experimental plots. Both models can be used to represents the equivalent circuit for wet specimens. Between these two models, the first model is simpler and easy to simulate. In

contrast, the second model is a little complex but comprehends more microstructural behavior of conductive cement composite, especially when it is in wet conditions.

6.5 Conclusion

In this chapter, one electrical equivalent circuit model for dry specimens and two electrical equivalent circuit models for wet specimens are proposed. Fitted results obtained from all of the models for different graphite content specimens are extracted and then compared with the experimental data. It has been found that the model proposed for dry specimens fitted perfectly with the experimental data. In the case of wet specimens, both Model-1 and Model-2 give the best fitting with the experimental results. However, Model-2 represents very well the microstructure of wet conductive cement composite.

CHAPTER VII

CONCLUSION AND FUTURE WORK

7.1 Conclusion

In this research, electrical properties of conductive cement paste were investigated through three steps: 1) comparisons of two measurement methods including static (DC) measurement and AC impedance spectroscopy, 2) the effect of graphite content and moisture, and 3) construction of equivalent circuits. The conductive cement paste specimens were prepared using graphite powder (F-516 Flake type) through dry mixing. The graphite content varied from 0%, 5%, 10%, 15%, 20%, 25%, 30% by volume of cement paste. The findings are summarized as follows:

CHAPTER IV. Investigation on Electrical Properties Measurement Methods: Major findings from this chapter are:

- Due to the charging effect in DC measurement, the measured resistivity values were not consistent in the case of continuous monitoring. The discontinuous static (DC) measurement shows relatively consistent resistivity values over time. However, the magnitudes of static resistivity data vary with the devices and different trials. The variations were high when specimens contain lower concentrations of conductive fillers. In case of higher graphite content, both methods provide consistent resistivity values.

- It can be presumed that polarization (charging effects) causes the inconsistent static resistivity of conductive concrete. Notably, at continuous resistivity measurements, charging effects play a vital role and cause an increase in resistivity over time. Also, the voltage of the current source plays a significant role, and the resistivity is affected by its variation. The resistivity is observed to decrease with the increase in DC voltage. Therefore, the static resistivity measurements using DC are not fully capable of evaluating the electrical properties of conductive concrete, especially when the filler concentration is lower than forming a continuous conductive path.
- On the other hand, the Bode plots and Nyquist plots obtained by AC impedance spectroscopy showed consistent results when the moisture condition is identical. These results indicate that the electrical properties of the conductive concrete need to be measured by AC impedance spectroscopy. It can be used as an essential tool for getting repetitive electrical properties in concrete.

CHAPTER V. Electrical Characterization and Degrees of Saturation Effect Investigation:

Major findings from this chapter are:

- It has been found that the effect of graphite powder is noticeable for specimens in both dry and wet conditions.
- In dry specimens, both the impedance and the capacitance effect inside the cement paste are reduced with the increase of graphite powder content. The Nyquist plot tends to show a fixed resistance value for higher concentrated graphite content (20% or more) while changing a slight capacitance value.

- In the case of the wet specimens, the impedance was significantly lower than the dry specimens, and it decreases with the increase of graphite content in cement paste. However, the impedance reduction rate for the dry specimens is much higher than for the wet specimens. Moreover, there is always present the capacitance behavior inside the conductive cement paste in wet conditions even for higher concentrated graphite additives. The reason could be attributed to the presence of moisture.
- The results show that the percolation threshold for graphite added cement paste is between 15%-20% by cement paste volume for both wet and dry specimens.
- The results also show that moisture plays a significant role in concrete conductivity. For every test, Dry specimens show higher resistivity than wet specimens, as expected. The electrical resistivity increases with the decrease in DOS up to a certain level. For some specimens, that DOS level is observed as 20% or lower than that. Below this DOS, electrical resistivity started to decrease, and this can be attributed to the reduction in capacitance effect provided by moisture.

CHAPTER VI. Electrical Equivalent Circuit of Conductive Concrete: Major findings from this chapter are:

- In this study, one electrical equivalent circuit model for dry specimens and two distinguished equivalent circuit models for wet specimens are proposed. The simulation results obtained from all the models for different graphite content

specimens are compared with the experimental data. The results indicate that the proposed models successfully describe the electrical behaviors of conductive cement paste containing graphite additives.

- It has been found that the model proposed for dry specimens matches perfectly with the experimental data.
- In the case of wet specimens, both Model-1 and Model-2 show good agreements with the experimental results.

7.2 Recommendation for Future Work

Some possible recommendation for future work on electrical characterization of conductive concrete are listed below:

- The effect of temperature on the electrical properties of conductive cement-composite needs to be investigated using AC impedance Spectroscopy.
- For practically implementing graphite powder in cement concrete, the effects of graphite powders on mechanical strength of concrete needs to be investigated since graphite is a hydrophobic material which may cause some reduction in the strength of concrete.

REFERENCES

- AL-BAYATI, A. J., BUTROUNA, K. H., STEFFEN, R. E., SALMAN, B. and AL-QARALLEH, M. Utilizing Graphite Powder to Improve Concrete Conductivity, Compressive Strength, and Workability. Construction Research Congress 2020: Project Management and Controls, Materials, and Contracts, 2020. American Society of Civil Engineers Reston, VA, 881-888.
- AL-SALEH, M. H. and SUNDARARAJ, U. 2009. A review of vapor grown carbon nanofiber/polymer conductive composites. *Carbon*, 47, 2-22.
- BAEZA, F., CHUNG, D., ZORNOZA, E., ANDIÓN, L. and GARCÉS, P. 2010. Triple Percolation in Concrete Reinforced with Carbon Fiber. *ACI Materials Journal*, 107, 396-402.
- BAEZA, F. J., GALAO, O., ZORNOZA, E. and GARCÉS, P. 2013. Multifunctional Cement Composites Strain and Damage Sensors Applied on Reinforced Concrete (RC) Structural Elements. *Materials*, 6, 841-855.
- BALL, R. J., ALLEN, G. C., STARRS, G. and MCCARTER, W. J. 2011. Impedance spectroscopy measurements to study physio-chemical processes in lime-based composites. *Applied Physics A*, 105, 739-751.
- BANTHIA, N., DJERIDANE, S. and PIGEON, M. 1992. Electrical resistivity of carbon and steel micro-fiber reinforced cements. *Cement Concrete research*, 22, 804-814.
- BERROCAL, C. G., HORNBOSTEL, K., GEIKER, M. R., LÖFGREN, I., LUNDGREN, K. and BEKAS, D. G. 2018a. Electrical resistivity measurements in steel fibre reinforced cementitious materials. *Cement Concrete Composites*, 89, 216-229.
- BERROCAL, C. G., HORNBOSTEL, K., GEIKER, M. R., LÖFGREN, I., LUNDGREN, K. and BEKAS, D. G. 2018b. Electrical resistivity measurements in steel fibre reinforced cementitious materials. *Cement and Concrete Composites*, 89, 216-229.
- BERTOLINI, L., BOLZONI, F., PASTORE, T. and PEDEFERRI, P. 2004. Effectiveness of a conductive cementitious mortar anode for cathodic protection of steel in concrete. *Cement and Concrete Research*, 34, 681-694.

- BONTEA, D.-M., CHUNG, D. and LEE, G. 2000. Damage in carbon fiber-reinforced concrete, monitored by electrical resistance measurement. *Cement Concrete Research*, 30, 651-659.
- CABEZA, M., KEDDAM, M., NÓVOA, X. R., SÁNCHEZ, I. and TAKENOUTI, H. 2006. Impedance spectroscopy to characterize the pore structure during the hardening process of Portland cement paste. *Electrochimica Acta*, 51, 1831-1841.
- CABEZA, M., MERINO, P., MIRANDA, A., NÓVOA, X. R. and SANCHEZ, I. 2002. Impedance spectroscopy study of hardened Portland cement paste. *Cement and Concrete Research*, 32, 881-891.
- CAI, R., TIAN, Z., YE, H., HE, Z. and TANG, S. 2021. The role of metakaolin in pore structure evolution of Portland cement pastes revealed by an impedance approach. *Cement Concrete Composites*, 119, 103999.
- CAO, J. and CHUNG, D. 2004. Electric polarization and depolarization in cement-based materials, studied by apparent electrical resistance measurement. *Cement Concrete Research*, 34, 481-485.
- CAO, J., WEN, S. and CHUNG, D. 2001. Defect dynamics and damage of cement-based materials, studied by electrical resistance measurement. *Journal of materials science*, 36, 4351-4360.
- CAO, Y., YANG, X., ZHAO, R., CHEN, Y., LI, N. and AN, L. 2016. Giant piezoresistivity in polymer-derived amorphous SiAlCO ceramics. *Journal of materials science*, 51, 5646-5650.
- CEBECI, H., VILLORIA, R. G. D., HART, A. J. and WARDLE, B. L. 2009. Multifunctional properties of high volume fraction aligned carbon nanotube polymer composites with controlled morphology. *Composites Science and Technology*, 69, 2649-2656.
- CHEN, B., LIU, J. and WU, K. 2005. Electrical responses of carbon fiber reinforced cementitious composites to monotonic and cyclic loading. *Cement concrete Research*, 35, 2183-2191.
- CHEN, P.-W. and CHUNG, D. D. L. 1993. Carbon fiber reinforced concrete for smart structures capable of non-destructive flaw detection. *Smart Materials and Structures*, 2, 22-30.
- CHEN, P.-W. and CHUNG, D. D. L. 1994. Carbon Fiber Reinforced Concrete as an Intrinsically Smart Concrete for Damage Assessment During Dynamic Loading. *MRS Proceedings*, 360, 317.
- CHEN, P.-W. and CHUNG, D. D. L. 1995. Improving the electrical conductivity of composites comprised of short conducting fibers in a nonconducting matrix: The addition of a nonconducting particulate filler. *Journal of Electronic Materials*, 24, 47-51.

- CHEN, P.-W. and CHUNG, D. D. L. 1996. Concrete as a new strain/stress sensor. *Composites Part B: Engineering*, 27, 11-23.
- CHI, L., WANG, Z., LU, S., ZHAO, D. and YAO, Y. 2019. Development of mathematical models for predicting the compressive strength and hydration process using the EIS impedance of cementitious materials. *Construction Building Materials*, 208, 659-668.
- CHOLKER, A. K. and TANTRAY, M. A. 2019. Micro carbon fiber based concrete as a strain-damage sensing material. *Materials Today: Proceedings*, 19, 152-157.
- CHOU, T.-W., GAO, L., THOSTENSON, E. T., ZHANG, Z. and BYUN, J.-H. 2010. An assessment of the science and technology of carbon nanotube-based fibers and composites. *Composites Science and Technology*, 70, 1-19.
- CHRISTOPHER, Y. T. and SHERIF, Y. 2004. Evaluation of Electrically Conductive Concrete Containing Carbon Products for Deicing. *ACI Materials Journal*, 101.
- CHUNG, D. 2002a. Electrical conduction behavior of cement-matrix composites. *Journal of materials engineering performance*, 11, 194-204.
- CHUNG, D. 2002b. Piezoresistive cement-based materials for strain sensing. *Journal of Intelligent Material Systems Structures*, 13, 599-609.
- CHUNG, D. D. 2003a. Damage in cement-based materials, studied by electrical resistance measurement. *Materials Science Engineering: R: Reports*, 42, 1-40.
- CHUNG, D. D. L. 2002c. Electrical conduction behavior of cement-matrix composites. *Journal of Materials Engineering and Performance*, 11, 194-204.
- CHUNG, D. D. L. 2003b. Damage in cement-based materials, studied by electrical resistance measurement. *Materials Science and Engineering: R: Reports*, 42, 1-40.
- CHUNG, D. D. L. 2003c. *Multifunctional Cement-Based Materials*, Taylor and Francis.
- CHUNG, D. D. L. 2004. Electrically conductive cement-based materials. *Advanced Cement Research*, 16, 167-176.
- COPPOLA, L., BUOSO, A. and ARMOR, F. 2013. The influence of AC and DC electrical resistance and piezoresistivity measurements of CNTs / Cement composites. *The Boundaries of Structural Concrete*.
- CRUZ, J., FITA, I., SORIANO, L., PAYÁ, J. and BORRACHERO, M. 2013. The use of electrical impedance spectroscopy for monitoring the hydration products of Portland cement mortars with high percentage of pozzolans. *Cement Concrete Research*, 50, 51-61.

- DANOGLIDIS, P. A., KONSTA-GDOUTOS, M. S. and SHAH, S. P. 2019. Relationship between the carbon nanotube dispersion state, electrochemical impedance and capacitance and mechanical properties of percolative nanoreinforced OPC mortars. *Carbon*, 145, 218-228.
- DEHGHANPOUR, H. and YILMAZ, K. 2020a. Investigation of specimen size, geometry and temperature effects on resistivity of electrically conductive concretes. *Construction Building Materials*, 250, 118864.
- DEHGHANPOUR, H. and YILMAZ, K. 2020b. Investigation of specimen size, geometry and temperature effects on resistivity of electrically conductive concretes. *Construction and Building Materials*, 250, 118864.
- DEL MORAL, B., BAEZA, F. J., NAVARRO, R., GALAO, O., ZORNOZA, E., VERA, J., FARCAS, C. and GARCÉS, P. 2021. Temperature and humidity influence on the strain sensing performance of hybrid carbon nanotubes and graphite cement composites. *Construction and Building Materials*, 284, 122786.
- DEL MORAL, B., GALAO, O., ANTON, C., CLIMENT, M. A. and GARCÉS, P. 2013. Usability of cement paste containing carbon nanofibres as an anode in electrochemical chloride extraction from concrete (en). *Materiales de construcción (Madrid)*, Vol 63, 39-48.
- DEMIRCILIOĞLU, E., TEOMETE, E., SCHLANGEN, E. and BAEZA, F. J. 2019. Temperature and moisture effects on electrical resistance and strain sensitivity of smart concrete. *Construction Building Materials*, 224, 420-427.
- DING, S., RUAN, Y., YU, X., HAN, B. and NI, Y.-Q. 2019a. Self-monitoring of smart concrete column incorporating CNT/NCB composite fillers modified cementitious sensors. *Construction and Building Materials*, 201, 127-137.
- DING, Y., LIU, G., HUSSAIN, A., PACHECO-TORGAL, F. and ZHANG, Y. 2019b. Effect of steel fiber and carbon black on the self-sensing ability of concrete cracks under bending. *Construction and Building Materials*, 207, 630-639.
- DONG, B.-Q., QIU, Q.-W., XIANG, J.-Q., HUANG, C.-J., XING, F., HAN, N.-X. and LU, Y.-Y. 2014a. Electrochemical impedance measurement and modeling analysis of the carbonation behavior for cementitious materials. *Construction Building Materials*, 54, 558-565.
- DONG, B., GU, Z., QIU, Q., LIU, Y., DING, W., XING, F. and HONG, S. 2018. Electrochemical feature for chloride ion transportation in fly ash blended cementitious materials. *Construction Building Materials*, 161, 577-586.
- DONG, B., QIU, Q., GU, Z., XIANG, J., HUANG, C., FANG, Y., XING, F. and LIU, W. 2016a. Characterization of carbonation behavior of fly ash blended cement materials by the

- electrochemical impedance spectroscopy method. *Cement Concrete Composites*, 65, 118-127.
- DONG, B., QIU, Q., XIANG, J., HUANG, C., SUN, H., XING, F. and LIU, W. 2015. Electrochemical impedance interpretation of the carbonation behavior for fly ash–slag–cement materials. *Construction and Building Materials*, 93, 933-942.
- DONG, B., QIU, Q., XIANG, J., HUANG, C., XING, F. and HAN, N. 2014b. Study on the Carbonation Behavior of Cement Mortar by Electrochemical Impedance Spectroscopy. *Materials*, 7.
- DONG, B., ZHANG, J., LIU, Y., FANG, G., DING, Z. and XING, F. 2016b. Tracing hydration feature of aluminophosphate cementitious materials by means of electrochemical impedance method. *Construction Building Materials*, 113, 997-1006.
- DONG, S., DONG, X., ASHOUR, A., HAN, B. and OU, J. 2020a. Fracture and self-sensing characteristics of super-fine stainless wire reinforced reactive powder concrete. *Cement and Concrete Composites*, 105, 103427.
- DONG, W., HUANG, Y., LEHANE, B., ASLANI, F. and MA, G. 2021. Mechanical and electrical properties of concrete incorporating an iron-particle contained nano-graphite by-product. *Construction and Building Materials*, 270, 121377.
- DONG, W., LI, W., LONG, G., TAO, Z., LI, J. and WANG, K. 2019. Electrical resistivity and mechanical properties of cementitious composite incorporating conductive rubber fibres. *Smart Materials and Structures*, 28, 085013.
- DONG, W., LI, W., WANG, K., LUO, Z. and SHENG, D. 2020b. Self-sensing capabilities of cement-based sensor with layer-distributed conductive rubber fibres. *Sensors and Actuators A: Physical*, 301, 111763.
- EL-DIEB, A. S., EL-GHAREEB, M. A., ABDEL-RAHMAN, M. A. and EL SAYED, A. N. 2018. Multifunctional electrically conductive concrete using different fillers. *Journal of Building Engineering*, 15, 61-69.
- FAN, X., FANG, D., SUN, M. and LI, Z. 2011. Piezoresistivity of carbon fiber graphite cement-based composites with CCCW. *Journal of Wuhan University of Technology-Mater. Sci. Ed.*, 26, 339-343.
- FANECA, G., SEGURA, I., TORRENTS, J. and AGUADO, A. 2018. Development of conductive cementitious materials using recycled carbon fibres. *Cement Concrete Composites*, 92, 135-144.
- FU, X. and CHUNG, D. 1995. Contact electrical resistivity between cement and carbon fiber: its decrease with increasing bond strength and its increase during fiber pull-out. *Cement and concrete research*, 25, 1391-1396.

- FU, X. and CHUNG, D. 1997. Effect of curing age on the self-monitoring behavior of carbon fiber reinforced mortar. *Cement and concrete Research*, 27, 1313-1318.
- FU, X., LU, W. and CHUNG, D. 1998. Improving the strain-sensing ability of carbon fiber-reinforced cement by ozone treatment of the fibers. *Cement and concrete research*, 28, 183-187.
- FU, X., MA, E., CHUNG, D. and ANDERSON, W. 1997. Self-monitoring in carbon fiber reinforced mortar by reactance measurement. *Cement concrete research*, 27, 845-852.
- FULHAM-LEBRASSEUR, R., SORELLI, L. and CONCIATORI, D. 2020. Development of electrically conductive concrete and mortars with hybrid conductive inclusions. *Construction Building Materials*, 237, 117470.
- GU, P., XIE, P. and BEAUDOIN, J. J. 1993a. Impedance characterization of microcracking behaviour in fibre-reinforced cement composites. *Cement and Concrete Composites*, 15, 173-180.
- GU, P., XIE, P. and BEAUDOIN, J. J. 1993b. Microstructural characterization of the transition zone in cement systems by means of A.C. impedance spectroscopy. *Cement and Concrete Research*, 23, 581-591.
- GU, P., XU, Z., XIE, P. and BEAUDOIN, J. 1993c. An AC impedance spectroscopy study of micro-cracking in cement-based composites during compressive loading. *Cement concrete research*, 23, 675-682.
- GU, P., XU, Z., XIE, P. and BEAUDOIN, J. 1993d. Application of AC impedance techniques in studies of porous cementitious materials:(I): influence of solid phase and pore solution on high frequency resistance. *Cement Concrete Research*, 23, 531-540.
- HAN, B., DING, S. and YU, X. 2015. Intrinsic self-sensing concrete and structures: A review. *Measurement*, 59, 110-128.
- HAN, B., HAN, B. and OU, J. 2009a. Experimental study on use of nickel powder-filled Portland cement-based composite for fabrication of piezoresistive sensors with high sensitivity. *Sensors Actuators A: Physical*, 149, 51-55.
- HAN, B., HAN, B. and YU, X. 2009b. Experimental study on the contribution of the quantum tunneling effect to the improvement of the conductivity and piezoresistivity of a nickel powder-filled cement-based composite. *Smart materials structures*, 18, 065007.
- HAN, B., YU, X., KWON, E. and OU, J. 2011a. Effects of CNT concentration level and water/cement ratio on the piezoresistivity of CNT/cement composites. *Journal of Composite Materials*, 46, 19-25.

- HAN, B., YU, X. and OU, J. 2011b. Multifunctional and smart carbon nanotube reinforced cement-based materials. *Nanotechnology in civil infrastructure*. Springer.
- HAN, B., YU, X. and OU, J. 2014. *Self-sensing concrete in smart structures*, Elsevier Science.
- HAN, B., ZHANG, K., YU, X., KWON, E. and OU, J. 2012. Electrical characteristics and pressure-sensitive response measurements of carboxyl MWNT/cement composites. *Cement and Concrete Composites*, 34, 794-800.
- HAN, B., ZHANG, L. and OU, J. 2017. *Smart and multifunctional concrete toward sustainable infrastructures*, Springer.
- HE, H., ZHU, Y. and ZHOU, A. 2018a. Electrochemical impedance spectroscopy (EIS) used to evaluate influence of different external pressures, curing ages and self-healing environments on the self-healing behavior of engineered cementitious composites (ECC). *Construction Building Materials*, 188, 153-160.
- HE, H., ZHU, Y. and ZHOU, A. 2018b. Electrochemical impedance spectroscopy (EIS) used to evaluate influence of different external pressures, curing ages and self-healing environments on the self-healing behavior of engineered cementitious composites (ECC). *Construction and Building Materials*, 188, 153-160.
- HIXSON, A. D., WOO, L. Y., CAMPO, M. A. and MASON, T. O. 2003. The origin of nonlinear current–voltage behavior in fiber-reinforced cement composites. *Cement and Concrete Research*, 33, 835-840.
- HOU, J. and CHUNG, D. D. L. 1997. Cathodic protection of steel reinforced concrete facilitated by using carbon fiber reinforced mortar or concrete. *Cement and Concrete Research*, 27, 649-656.
- HOU, T.-C. and LYNCH, J. P. 2009. Electrical impedance tomographic methods for sensing strain fields and crack damage in cementitious structures. *Journal of intelligent material systems structures*, 20, 1363-1379.
- HUANG, Y., XIANG, B., MING, X., FU, X. and GE, Y. Conductive mechanism research based on pressure-sensitive conductive composite material for flexible tactile sensing. 2008 International Conference on Information and Automation, 2008. IEEE, 1614-1619.
- KALAITZIDOU, K., FUKUSHIMA, H. and DRZAL, L. T. 2007. Multifunctional polypropylene composites produced by incorporation of exfoliated graphite nanoplatelets. *Carbon*, 45, 1446-1452.
- KAMALI, M. and GHAREMANINEZHAD, A. 2015. Effect of glass powders on the mechanical and durability properties of cementitious materials. *Construction building materials*, 98, 407-416.

- KEDDAM, M., TAKENOUTI, H., NÓVOA, X. R., ANDRADE, C. and ALONSO, C. 1997. Impedance measurements on cement paste. *Cement and Concrete Research*, 27, 1191-1201.
- KIM, J.-K., KEE, S.-H., FUTALAN, C. M. and YEE, J.-J. 2020. Corrosion Monitoring of Reinforced Steel Embedded in Cement Mortar under Wet-And-Dry Cycles by Electrochemical Impedance Spectroscopy. *Sensors*, 20.
- KIM, Y.-J., CHA, J. Y., HAM, H., HUH, H., SO, D.-S. and KANG, I. 2011. Preparation of piezoresistive nano smart hybrid material based on graphene. *Current Applied Physics*, 11, S350-S352.
- KWON, H., PARK, Y. and KIM, C.-G. 2019. Strain sensing characteristics using piezoresistivity of semi-conductive silicon carbide fibers. *Smart Materials and Structures*, 28, 105035.
- LE, J.-L., DU, H. and PANG, S. D. 2014. Use of 2D Graphene Nanoplatelets (GNP) in cement composites for structural health evaluation. *Composites Part B: Engineering*, 67, 555-563.
- LI, H., XIAO, H.-G. and OU, J.-P. 2006. Effect of compressive strain on electrical resistivity of carbon black-filled cement-based composites. *Cement Concrete Composites*, 28, 824-828.
- LI, J., MA, P. C., CHOW, W. S., TO, C. K., TANG, B. Z. and KIM, J. K. 2007. Correlations between percolation threshold, dispersion state, and aspect ratio of carbon nanotubes. *Advanced Functional Materials*, 17, 3207-3215.
- LI, W.-W., JI, W.-M., FANG, G.-H., LIU, Y.-Q., XING, F., LIU, Y.-K. and DONG, B.-Q. 2016. Electrochemical impedance interpretation for the fracture toughness of carbon nanotube/cement composites. *Construction Building Materials*, 114, 499-505.
- LI, X. and LI, M. 2019. Multifunctional self-sensing and ductile cementitious materials. *Cement Concrete Research*, 123, 105714.
- LIU, G., ZHANG, Y., WU, M. and HUANG, R. 2017. Study of depassivation of carbon steel in simulated concrete pore solution using different equivalent circuits. *Construction and Building Materials*, 157, 357-362.
- MACPHEE, D. E., SINCLAIR, D. and STUBBS, S. 1996. Electrical characterization of pore reduced cement by impedance spectroscopy. *Journal of materials science letters*, 15, 1566-1568.
- MASON, T. O., CAMPO, M. A., HIXSON, A. D. and WOO, L. Y. 2002. Impedance spectroscopy of fiber-reinforced cement composites. *Cement and Concrete Composites*, 24, 457-465.

- MCCARTER, W. 1996. The ac impedance response of concrete during early hydration. *Journal of materials science*, 31, 6285-6292.
- MCCARTER, W., GARVIN, S. and BOUZID, N. 1988. Impedance measurements on cement paste. *Journal of materials science letters*, 7, 1056-1057.
- MCCARTER, W. J. 1995. Effects of temperature on conduction and polarization in Portland cement mortar. *Journal of the American Ceramic Society*, 78, 411-415.
- MCCARTER, W. J. and BROUSSEAU, R. 1990. The A.C. response of hardened cement paste. *Cement and Concrete Research*, 20, 891-900.
- MCCARTER, W. J., CHRISP, T., STARRS, G., ADAMSON, A., BASHEER, P., NANUKUTTAN, S., SRINIVASAN, S. and GREEN, C. 2013. Characterization of physio-chemical processes and hydration kinetics in concretes containing supplementary cementitious materials using electrical property measurements. *Cement concrete research*, 50, 26-33.
- MCCARTER, W. J., TAHA, H., SURYANTO, B. and STARRS, G. 2015. Two-point concrete resistivity measurements: interfacial phenomena at the electrode–concrete contact zone. *Measurement Science Technology*, 26, 085007.
- MEHTA, P. and MONTEIRO, P. 2006. *Concrete: microstructure, properties, and materials*, , McGraw-Hill, New York, USA.
- MELARA, E. K., MENDES, A. Z., ANDRECZEVECZ, N. C., BRAGANCA, M. O., CARRERA, G. T. and MEDEIROS-JUNIOR, R. A. 2020. Monitoring by electrochemical impedance spectroscopy of mortars subjected to ingress and extraction of chloride ions. *Construction Building Materials*, 242, 118001.
- MERCADO-MENDOZA, H., LORENTE, S. and BOURBON, X. 2014a. Ionic aqueous diffusion through unsaturated cementitious materials–A comparative study. *Construction Building Materials*, 51, 1-8.
- MERCADO-MENDOZA, H., LORENTE, S. and BOURBON, X. 2014b. Ionic aqueous diffusion through unsaturated cementitious materials – A comparative study. *Construction and Building Materials*, 51, 1-8.
- NEVERS, D., ZHAO, J., SOBOLEV, K. and HANSON, G. 2011. Investigation of strain-sensing materials based on EM surface wave propagation for steel bridge health monitoring. *Construction Building Materials*, 25, 3024-3029.
- NGUYEN, D.-L., KIM, D.-J. and THAI, D.-K. 2019. Enhancing Damage-Sensing Capacity of Strain-Hardening Macro-Steel Fiber-Reinforced Concrete by Adding Low Amount of Discrete Carbons. 12, 938.

- OSKOUYI, A. B., SUNDARARAJ, U. and MERTINY, P. 2014. Tunneling Conductivity and Piezoresistivity of Composites Containing Randomly Dispersed Conductive Nano-Platelets. 7, 2501-2521.
- PAPANIKOLAOU, I., LITINA, C., ZOMORODIAN, A. and AL-TABBAA, A. 2020. Effect of Natural Graphite Fineness on the Performance and Electrical Conductivity of Cement Paste Mixes for Self-Sensing Structures. *Materials* 13, 5833.
- PELED, A., TORRENTS, J. M., MASON, T. O., SHAH, S. P. and GARBOCZI, E. J. 2001. Electrical impedance spectra to monitor damage during tensile loading of cement composites. *ACI Materials Journal*, 98, 313-322.
- PÉREZ, A., CLIMENT, M. A. and GARCÉS, P. 2010. Electrochemical extraction of chlorides from reinforced concrete using a conductive cement paste as the anode. *Corrosion Science*, 52, 1576-1581.
- PU-WOEI, C. and CHUNG, D. D. L. 1996. Carbon Fiber Reinforced Concrete as an Intrinsically Smart Concrete for Damage Assessment during Static and Dynamic Loading. *ACI Materials Journal*, 93.
- QIU, J., ZHANG, C., WANG, B. and LIANG, R. 2007. Carbon nanotube integrated multifunctional multiscale composites. *Nanotechnology*, 18, 275708.
- RAVIKUMAR, D. and NEITHALATH, N. 2013. An electrical impedance investigation into the chloride ion transport resistance of alkali silicate powder activated slag concretes. *Cement Concrete Composites*, 44, 58-68.
- REN, J., ZHANG, J., WANG, X., LI, D., HAN, N. and XING, F. 2020. Electrochemical Impedance Spectroscopy: A potential approach for detecting the breakage rate of microcapsules for self-healing cementitious materials. *Cement and Concrete Composites*, 114, 103776.
- REZA, F., BATSON, G. B., YAMAMURO, J. A. and LEE, J. S. 2003. Resistance changes during compression of carbon fiber cement composites. *Journal of Materials in Civil Engineering*, 15, 476-483.
- SANDLER, J. K. W., KIRK, J. E., KINLOCH, I. A., SHAFFER, M. S. P. and WINDLE, A. H. 2003. Ultra-low electrical percolation threshold in carbon-nanotube-epoxy composites. *Polymer*, 44, 5893-5899.
- SASSANI, A., CEYLAN, H., KIM, S., GOPALAKRISHNAN, K., ARABZADEH, A. and TAYLOR, P. C. 2017. Influence of mix design variables on engineering properties of carbon fiber-modified electrically conductive concrete. *Construction Building Materials*, 152, 168-181.

- SEGURA, I., FANECA, G., TORRENTS, J. M. and AGUADO, A. 2019. Self-sensing concrete made from recycled carbon fibres. *Smart Materials and Structures*, 28, 105045.
- SONG, G. 2000. Equivalent circuit model for AC electrochemical impedance spectroscopy of concrete. *Cement and Concrete Research*, 30, 1723-1730.
- STAUFFER, D. and AHARONY, A. 1994. *Introduction to percolation theory*, CRC press.
- STEFANESCU, D. M. 2011. *Handbook of force transducers: principles and components*, Springer Science and Business Media.
- STEFANONI, M., ANGST, U. and ELSENER, B. 2020. The mechanism controlling corrosion of steel in carbonated cementitious materials in wetting and drying exposure. *Cement Concrete Composites*, 113, 103717.
- SUN, J., LIN, S., ZHANG, G., SUN, Y., ZHANG, J., CHEN, C., MORSY, A. M. and WANG, X. 2021. The effect of graphite and slag on electrical and mechanical properties of electrically conductive cementitious composites. *Construction and Building Materials*, 281, 122606.
- SUN, S., HAN, B., JIANG, S., YU, X., WANG, Y., LI, H. and OU, J. 2017. Nano graphite platelets-enabled piezoresistive cementitious composites for structural health monitoring. *Construction Building Materials*, 136, 314-328.
- SURYANTO, B., TAKAOKA, H., MCCATER, W. J., SARAIHEH, D. and TAHA, H. 2018. Impedance measurements on an engineered cementitious composite: A critical evaluation of testing protocols. *Measurement*, 129, 445-456.
- TANG, S. W., LI, Z., CHEN, E. and SHAO, H. Y. 2014. Impedance measurement to characterize the pore structure in Portland cement paste. *Construction Building Materials*, 51, 106-112.
- TEOMETE, E. and KOCYIGIT, O. I. 2013. Tensile strain sensitivity of steel fiber reinforced cement matrix composites tested by split tensile test. *Construction Building Materials*, 47, 962-968.
- TORRENTS, J. M., MASON, T. O. and GARBOCZI, E. J. 2000. Impedance spectra of fiber-reinforced cement-based composites: a modeling approach. *Cement and Concrete Research*, 30, 585-592.
- TORRENTS, J. M., MASON, T. O., PELED, A., SHAH, S. P. and GARBOCZI, E. J. 2001. Analysis of the impedance spectra of short conductive fiber-reinforced composites. *Journal of Materials Science*, 36, 4003-4012.
- TYSON, B. M., AL-RUB, R. K. A., YAZDANBAKHSI, A. and GRASLEY, Z. 2011. Carbon Nanotubes and Carbon Nanofibers for Enhancing the Mechanical Properties of

- Nanocomposite Cementitious Materials. *Journal of Materials in Civil Engineering*, 23, 1028-1035.
- VANCE, K., AGUAYO, M., DAKHANE, A., RAVIKUMAR, D., JAIN, J. and NEITHALATH, N. 2014. Microstructural, Mechanical, and Durability Related Similarities in Concretes Based on OPC and Alkali-Activated Slag Binders. *International Journal of Concrete Structures and Materials*, 8, 289-299.
- VILAPLANA, J. L., BAEZA, F. J., GALAO, O., ZORNOZA, E. and GARCÉS, P. 2013. Self-sensing properties of alkali activated blast furnace slag (BFS) composites reinforced with carbon fibers. *Materials Science and Engineering*, 6, 4776-4786.
- WANG, S. and CHUNG, D. 2006. Self-sensing of flexural strain and damage in carbon fiber polymer-matrix composite by electrical resistance measurement. *Carbon*, 44, 2739-2751.
- WANG, X., WANG, Y. and JIN, Z. 2002. Electrical conductivity characterization and variation of carbon fiber reinforced cement composite. *Journal of materials science*, 37, 223-227.
- WEN, S. and CHUNG, D. 2000. Damage monitoring of cement paste by electrical resistance measurement. *Cement Concrete Research*, 30, 1979-1982.
- WEN, S. and CHUNG, D. 2001a. Carbon fiber-reinforced cement as a strain-sensing coating. *Cement and Concrete Research*, 31, 665-667.
- WEN, S. and CHUNG, D. 2001b. Electric polarization in carbon fiber-reinforced cement. *Cement Concrete Research*, 31, 141-147.
- WEN, S. and CHUNG, D. D. L. 2005. Strain-Sensing Characteristics of Carbon Fiber-Reinforced Cement. *ACI Materials Journal*, 102, 244.
- WEN, S. and CHUNG, D. D. L. 2006. Model of piezoresistivity in carbon fiber cement. *Cement and Concrete Research*, 36, 1879-1885.
- WEN, S. and CHUNG, D. D. L. 2007. Electrical-resistance-based damage self-sensing in carbon fiber reinforced cement. *Carbon*, 45, 710-716.
- WU, J. and CHUNG, D. D. L. 2005. Pastes for electromagnetic interference shielding. *Journal of Electronic Materials*, 34, 1255-1258.
- WU, T., HUANG, R., CHI, M. and WENG, T. 2013. A study on electrical and thermal properties of conductive concrete. *Computers and Concrete*, 12, 337-349.
- YAO, W., CHEN, B. and WU, K. 2003. Smart behavior of carbon fiber reinforced cement-based composite. 19, 239-242.

- YE, L., LU, Y., SU, Z. and MENG, G. 2005. Functionalized composite structures for new generation airframes: a review. *Composites Science and Technology*, 65, 1436-1446.
- YOO, D.-Y., YOU, I. and LEE, S.-J. 2017. Electrical properties of cement-based composites with carbon nanotubes, graphene, and graphite nanofibers. *Sensors*, 17, 1064.
- ZHANG, L., DING, S., HAN, B., YU, X. and NI, Y.-Q. 2019. Effect of water content on the piezoresistive property of smart cement-based materials with carbon nanotube/nanocarbon black composite filler. *Composites Part A: Applied Science and Manufacturing*, 119, 8-20.
- ZHANG, Y. and KONG, X. 2014. Influences of superplasticizer, polymer latexes and asphalt emulsions on the pore structure and impermeability of hardened cementitious materials. *Construction Building Materials*, 53, 392-402.
- ZHU, S. and CHUNG, D. 2007. Analytical model of piezoresistivity for strain sensing in carbon fiber polymer–matrix structural composite under flexure. *Carbon*, 45, 1606-1613.
- ZHU, Y., ZHANG, H., ZHANG, Z., DONG, B. and LIAO, J. 2019. Monitoring the cracking behavior of engineered cementitious composites (ECC) and plain mortar by electrochemical impedance measurement. *Construction Building Materials*, 209, 195-201.
- ZHU, Y., ZHANG, H., ZHANG, Z. and YAO, Y. 2017. Electrochemical impedance spectroscopy (EIS) of hydration process and drying shrinkage for cement paste with W/C of 0.25 affected by high range water reducer. *Construction and Building Materials*, 131, 536-541.
- ZORNOZA, E., CATALÁ, G., JIMÉNEZ, F., ANDIÓN, L. G. and GARCÉS, P. 2010. Electromagnetic interference shielding with Portland cement paste containing carbon materials and processed fly ash. *Materiales de Construcción*, 60, 21-32.

BIOGRAPHICAL SKETCH

K I M Iqbal was born in Noakhali, Bangladesh, on 6th July 1992. He had completed his B.Sc. in Civil Engineering from Bangladesh University of Engineering and Technology (BUET) on 13th September 2017. Soon after graduation, Iqbal started working as Lecturer in the Department of Civil Engineering at Daffodil International University, Dhaka, Bangladesh. During his tenure at that University, he taught several theoretical courses and instructed some lab courses. He moved to the USA in January 2020 to pursue his M.Sc. in Civil Engineering with a full scholarship (Presidential Graduate Research Assistantship) from the graduate college of the University of Texas Rio Grande Valley (UTRGV). Iqbal worked as a graduate research assistant in his first academic year and a teaching assistant in the following year. During his master's study, he conducted research on multifunctional cement-based concrete. In addition to his own research, he also did some collaborative research with another team on removing hardness from water using conductive concrete. He has received the *Best Presenter Award* in Material/Physics *Oral Presentation* session at UTRGV COS Annual Research Conference, November 2020. He has published and presented three conference papers based on both his undergraduate and graduate research work. He has completed his Master of Science in Civil Engineering from the University of Texas Rio Grande Valley in August of 2021.

Kari Bari, Ward-02, Mirwarishpur, Begumgonj, Noakhali, Bangladesh-3823.

Email: Iqbal.buet11@gmail.com; kim.iqbal01@utrgv.edu.